A STUDY OF MACROPHAGES IN THE AGING LIVER AND IN THE HOST RESPONSE TO ENGINEERED LUNG SCAFFOLDS

by

Elizabeth C. Stahl

BS, University of Pittsburgh, 2013

Submitted to the Graduate Faculty of

the School of Medicine in partial fulfillment

of the requirements for the degree of

Doctor of Philosophy

University of Pittsburgh

2019

UNIVERSITY OF PITTSBURGH

SCHOOL OF MEDICINE

This dissertation was presented

by

Elizabeth C. Stahl

It was defended on

December 7, 2018

and approved by

Satdarshan P. Monga MD, Professor, Department of Pathology

Andrew Duncan PhD, Assistant Professor, Department of Pathology

Wendy Mars PhD, Associate Professor, Department of Pathology

Donna Stolz PhD, Associate Professor, Department of Cell Biology

William Wagner PhD, Professor, Department of Bioengineering

Dissertation Director: Bryan Brown PhD, Assistant Professor, Department of Bioengineering

A STUDY OF MACROPHAGES IN THE AGING LIVER AND IN THE HOST RESPONSE TO ENGINEERED LUNG SCAFFOLDS

Elizabeth C. Stahl, PhD

University of Pittsburgh, 2019

Macrophages are innate immune cells that contribute to tissue remodeling and homeostasis, respond to foreign antigens, and regulate the recruitment and activation of auxiliary immune cells. In chronic disease or a foreign body reaction, macrophages drive inflammation, leading to tissue damage and fibrosis. As such, understanding the developmental and phenotypic diversity of macrophages is of interest in both the pathobiology of disease as well as the design of novel therapeutics and materials. This dissertation examines macrophage biology in two contexts: the aging liver and the host response to engineered lung scaffolds.

The liver contains two subsets of macrophages: a stable population of embryonically-derived Kupffer cells and a transient population of monocyte-derived macrophages. The dynamics of hepatic macrophages during the process of aging is unknown and may influence the development of chronic liver disease. Studies presented here demonstrate an increase in hepatic macrophages from naturally aged (19-months-old) mice compared to young counterparts (3-months-old). Macrophages from aged livers express significantly greater amounts of CD11b surface antigen and upregulate arginase strongly after exposure to interleukin-4, suggesting monocytic origins and a predisposition towards an alternatively activated phenotype. Aged livers also exhibit increased triglycerides and pro-inflammatory signals, including monocyte

chemoattractant protein (MCP-1). Inhibiting MCP-1 signaling reduced lipids and inflammation but did not significantly alter the macrophage population. Additional methods to modulate hepatic macrophages remain to be studied in the context of age-associated pathologies.

Following implantation of biomaterials, macrophages are recruited and polarize to a classical or alternatively activated phenotype, which can influence the outcome of the foreign body response. A positive outcome is associated with reduced inflammation and is crucial for the success of animal-derived organs to be used for xenotransplantation. Studies presented herein demonstrate that the removal of the foreign Gal-epitope from decellularized porcine lung scaffolds improves the host response in non-human primates, in part by reducing CD86 expression on macrophages and preventing substantial adaptive immune recognition upon reimplantation.

Taken together, these studies further the understanding of macrophage biology in the aging liver and in the host response to Gal-epitopes and demonstrate novel strategies to reduce inflammation in chronic disease and tissue engineering contexts.

TABLE OF CONTENTS

LIST OF TABLES

LIST OF FIGURES

ACKNOWLEDGEMENTS

There are several people I would like to acknowledge who have guided my research and shaped my graduate school experience. First, I would like to thank my primary research advisor, Dr. Bryan Brown, who has given me every opportunity to explore my interests and passions in the lab, the freedom to design my own experiments, write funding proposals, attend national and international meetings, and pursue extracurricular activities. Thank you for a very productive graduate school experience and everything you have taught me. Second, I'd like to thank my co-mentor, Dr. Andy Duncan. I feel so blessed that your lab and office are located on our floor and we were able to form a strong collaboration and friendship between our research groups. I truly could not have completed this work without your intellectual contributions and guidance. Thank you for adopting me as a co-mentee, allowing me to present in your lab meetings, and always leading by example to help me to become a better thinker, writer, and scientist.

I am very thankful to the rest of my committee for their support, direction, and thoughtful comments that have led me to the completion of this work. Thank you to Dr. Donna Stolz and Dr. William Wagner for your creative and critical insights that have elevated the research in this dissertation. Thank you also to Dr. Wendy Mars for being an outstanding advocate for my personal and professional success. Thank you especially to Dr. Paul Monga, my committee chair, who has gone above and beyond expectations as a truly outstanding mentor from supporting my

research training by sponsoring proposals and welcoming me into a larger community of peers and scientists in the Department of Pathology and beyond.

Next, I need to thank my friends and peers who really made the day-to-day experience of graduate school so special. Thank you to Chelsea Merkel, Morgan Preziosi, Aliyah Weinstein, Mondraya Howard, Justin Wendzicki, Ali Nagle, Megan Sullivan for your support and friendship in graduate school and beyond. Thank you also to life-long friends I made in my BioE undergrad program, Marshall and Devin. Thank you especially to the members of the Brown lab family who have made every day an adventure: Aimon Iftikhar, Alexis Nolfi, Clint Skillen, Michael Buckenmeyer, Samuel LoPresti, Travis Prest, Marty Haschak, Tyler Meder, Branimir Popovich, and Elaine Becker, as well as past undergraduate students Brandon Burger and Andrea Hartman. Thank you to the members of the Duncan lab for your support and friendship: Evan Delgado, Patrick Wilkinson, Frances Alencastro, Nairita Roy, and Maddie Leek. I also would like to thank my past mentors and friends in the Badylak lab, especially Chris Medberry, Lisa Carey-Lohmueller, Jenna Dziki, and Lindsey Saldin. A big thank you to Dr. Badylak, Dr. Lisa Butterfield, Dr. Johnny Huard, Dr. Helena Kuivaniemi and members of their laboratories who supported my early scientific development and helped me to arrive here today.

Most importantly, I would like to thank my family for their unwavering support and encouragement throughout the past nine years. My parents, Karen and Barry, have always taken a sincere interest in my education and research. Thank you for teaching me at an early age how to be a leader and to persevere. I would not have done a PhD without your encouragement. I have so many additional family members to thank for their love and support, for always checking in on my progress, and sending me back to Pittsburgh with food and gifts. I certainly cannot fit everyone's name here, but I must give a special acknowledgement to my Grandma, my uncles

Rick, Eric, Tony, and John, aunts Laurie, Kelly, Barb, Mary, Cheryl, Patricia, and Elaine, and my cousins Nikole, Mark, Amanda, and Melissa. I can't wait to see where the future takes me next, but I know you will always be there to support and guide me.

1.0 INTRODUCTION

Chapter 1 is adapted from three published review articles:

Stahl EC[1], Brown BN[1]. Cell Therapy Strategies to Combat Immunosenescence. *Organogenesis*. 2015; 11(4):159-72.

Brown BN[1], Haschak MJ[1], LoPresti ST[1], Stahl EC[1]. Effects of age-related shifts in cellular function and local microenvironment upon the innate immune response to implants. *Seminars in Immunology.* 2017; 29:24-32.

Stahl EC[1], Haschak MJ[1], Popovich B[1], Brown BN[1]. Macrophages in the Aging Liver and Age-Related Liver Disease. *Frontiers in Immunology* (accepted Nov. 2018).

[1] McGowan Institute for Regenerative Medicine, Department of Bioengineering, Pittsburgh Liver Research Center, University of Pittsburgh, Pittsburgh, PA

1.1 THE MACROPHAGE

'Macrophage' is derived from the Greek word "large eater," named by Ilya Metchnikoff, the father of cellular immunity, in the late 1800s (Metchnikoff, 1891). Metchnikoff observed heavily vacuolated cells engulfing cellular debris, a process known as phagocytosis, and considered this the defining feature of the macrophage. The term 'macrophage' was thereafter used to describe several cell types including erythrophagocytes and histiocytes. Macrophages were later

reclassified under the reticulo-endothelial system by Ashhoff in 1924, to include several tissue-resident macrophage populations (Aschoff, 1924). It was not until the 1930s, that the monocyte was identified in the blood as the circulating precursor of the macrophage (Ebert, 1939). By the late 1960s, the understanding of the mononuclear phagocyte system was developed under the premise that all macrophages are derived from blood monocytes (van Furth et al., 1972).

Nearly 50 years later, with the advent of advanced lineage tracing technologies, several groups have determined that the origin of many tissue-resident macrophages are embryonic, and these populations can be maintained independently of monocytes under steady-state conditions (Ginhoux et al., 2010; Schulz et al., 2012; Yona et al., 2013). The revised mononuclear phagocyte system now encompasses three broad families of cells: embryonic-derived macrophages, monocyte-derived cells, and common dendritic cell precursor-derived cells (Guilliams et al., 2014). The function of the macrophage is also now understood to extend beyond phagocytosis and includes antigen presentation, cytokine signaling, and growth factor production (Murray & Wynn, 2011). Macrophages play important roles in tissue development, homeostasis, regeneration, wound healing, infection clearance, and disease that will be discussed further in this chapter.

1.1.1 Primitive and Definitive Development of Macrophages

Macrophage development begins in the extraembryonic yolk sac from erythro-myeloid progenitors, a process known as primitive hematopoiesis, prior to the appearance of hematopoietic stem cells or monocytic precursors (Dey, Allen, & Hankey-Giblin, 2014; van de Laar et al., 2016). After a transient wave of primitive hematopoiesis, hematopoietic stem cells appear in the aorto-gonado-mesonephric region and migrate to the fetal liver, marking the start of

definitive hematopoiesis and development of naïve macrophages through monocytic precursors (Dey et al., 2014). Definitive hematopoiesis remains in the fetal liver until approximately E18 in mice or 12 weeks post-conception in humans, after which hematopoietic stem cells migrate to the bone marrow niche, where they will remain throughout adulthood (L. D. Wang & Wagers, 2011) .

Macrophages can be subdivided into embryonic-derived or monocyte-derived populations. Embryonic-derived macrophages include Kupffer cells (liver), microglia (brain), and at various times during development alveolar macrophages (lungs), osteoclasts (bone), and Langerhans's cells (skin) (Murray & Wynn, 2011). Kupffer cells and microglia are colonized from a single developmental source (*i.e.* yolk sac macrophages), whereas Langerhans's cells are originally derived from yolk sac macrophages and are later replaced by fetal liver monocytes (Hoeffel et al., 2012; Yona et al., 2013). Resident tissue macrophages, including Kupffer cells, large peritoneal macrophages, and pleural macrophages, have been shown to undergo proliferation in response to Th2 cytokines, such as interleukin-4, and can be maintained independently of monocytic input (Jenkins et al., 2011).

Alternatively, macrophages residing in certain organs, such as the gut, spleen, and kidney, are replaced regularly by bone marrow derived monocytes (Scott et al., 2016; Yona et al., 2013). Infiltrating macrophages can be derived from either classical ($CD14^+CD16^-$ human, $Ly6C^{hi}$ mouse) or non-classical ($CD14^+CD16^+$ human, $Ly6C^{lo}$ mouse) monocytes, which extravasate into tissue sites under chemokine concentration gradient guidance (Dey et al., 2014; Ingersoll et al., 2010). Following extravasation, monocytes differentiate into macrophages whose functionality are largely based on the integration of the various signaling molecules present in the local microenvironment, reviewed here: (Lavin, Mortha, Rahman, & Merad, 2015).

Macrophages residing in a particular tissue maintain their phenotype through a process known as tissue imprinting, whereby epigenetic changes in the enhancer regions of the genome regulate gene expression (Amit, Winter, & Jung, 2016). Monocyte-derived macrophages have the capacity to take on a seemingly identical phenotype to Kupffer cells, including self-renewal, when the niche is made available through experimental manipulation (Scott et al., 2016); however, the physiological relevance of these depletion experiments remains unclear. The frequency of tissue resident macrophages varies considerably based on the tissue, and it has been reported that approximately 80% of total tissue resident macrophages are located in the liver (Kakinuma, Kimura, & Watanabe, 2017).

1.1.2 Polarization of Macrophages

In addition to developmental heterogeneity, macrophages are extraordinarily dynamic cells that exhibit various phenotypes ranging on a spectrum from a pro-inflammatory, classically activated "M1" polarization state to an anti-inflammatory, alternatively activated "M2" polarization state (Mills, Kincaid, Alt, Heilman, & Hill, 2000; Murray et al., 2014), as shown in **Figure 1** (adapted from (Stahl, Haschak, Popovic, & Brown, 2018) in accordance with the Creative Commons license).

The paradigm of macrophage polarization is thought to begin with a quiescent or patrolling "M0" cell, that may be derived from either circulating monocytes or tissue-resident populations. The transition from M0 to M1 can be stimulated by bacterial products, such as lipopolysaccharide (LPS), or from Th1 cytokines, such as interferon-gamma, resulting in a cell that has pro-inflammatory and anti-tumorigenic properties. The transition from M0 to M2 can be stimulated by Th2 cytokines, such as interleukin-4, resulting in a cell that has anti-inflammatory

or immunotolerant properties. Polarization to these extreme phenotypes can be stimulated *in vitro*, but the scenario *in vivo* is often more complex leading to a spectrum of phenotypes, which may concurrently express both pro and anti-inflammatory phenotypic traits (Martinez & Gordon, 2014; Murray et al., 2014).

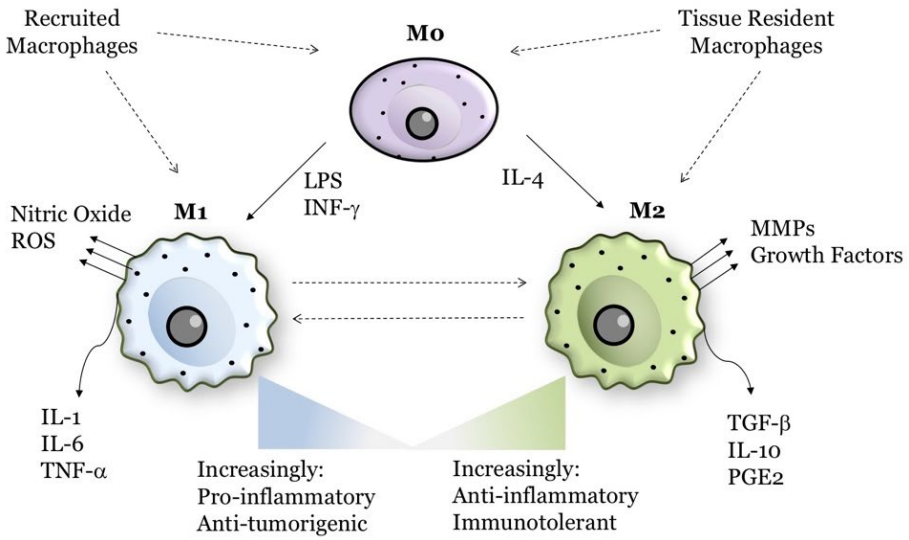

Figure 1. Macrophage Polarization.

In general, M1 polarization leads to production of canonical pro-inflammatory cytokines (IL-1, IL-6, IL-12, TNF, IL-23, IL-27), reactive oxygen species such as nitric oxide, and chemokines (CCL2, CCL5, CXCL9, CXCL10, CXCL11, IL-8), which are particularly important following injury or infection (Murray et al., 2014). The production of pro-inflammatory cytokines may be inflammasome-independent or dependent. Inflammasome formation is induced by damage-associated molecular patterns (DAMPs) and pathogen-associated molecular patterns (PAMPs) binding to nod-like receptors or to Pyrin receptor family members on the surface of macrophages (Schroder & Tschopp, 2010). Docking proteins assemble and recruit pro-caspase 1, where proximity-based autoproteolytic cleavage catalyzes the activation of caspase-1 (Kapetanovic,

Bokil, & Sweet, 2015; Sutterwala, Haasken, & Cassel, 2014) Caspase-1 activation subsequently catalyzes the cleavage of the pro-forms of IL-1β and IL-18 into activated forms (Winkler & Rosen-Wolff, 2015).

Alternatively, M2 macrophages appear from interaction with Th2 cytokines (IL-4, IL-5, IL-13, IL-25), which can occur following helminth infection and in the resolution phase of injury or infection. In an injury setting, M2-polarized macrophages typically appear following M1-polarized macrophages and serve as a counterbalance to resolve inflammation and promote tissue repair (Novak & Koh, 2013). The M2 polarization state leads to secretion of cytokines commonly associated with anti-inflammatory properties, such as IL-10, as well as various matrix-modulatory factors including transforming growth factor-β (TGF-β) and matrix metalloproteases (MMPs) (Sica, Erreni, Allavena, & Porta, 2015).

The overproduction of remodeling growth factors can lead to excessive deposition of matrix proteins (*i.e.* fibrosis), or excessive angiogenesis and immunosuppression in the case of tumor-associated macrophages (TAMs) (Liu & Cao, 2015). Therefore, the temporal regulation of the M1 and M2 macrophage response is extremely important for an appropriate outcome following injury and infection and often becomes dysregulated in disease.

1.1.3 Significance of Macrophages in Health and Disease

The routine role of the tissue-resident macrophage is to maintain homeostasis through surveillance of danger signals and the removal of dying cells through phagocytosis. Macrophages survey materials through engagement with pattern recognition receptors, including toll-like receptors (TLRs), C-type lectin receptors (CLRs), scavenger receptors, retinoic-acid inducible gene 1-like helicase receptors (RLRs), and NOD-like receptors (NLRs), which can

distinguish foreign substances and dead or dying cells from self (Murray & Wynn, 2011). Macrophages also express complement and Fc receptors that bind opsonin molecules, C3b, and antibodies to enhance phagocytosis. Dysregulation of macrophage surveillance and response properties have been associated with several autoimmune diseases including rheumatoid arthritis, systemic lupus erythromatosus, multiple sclerosis, and Sjogren's syndrome (Laria et al., 2016).

Macrophages are also important for normal tissue development. Mice deficient in PU.1, CSF1R, or CSF1 transcription factors required for primitive macrophage development displayed increased perinatal mortality, reduced postnatal survival, and stunted growth due to dysregulation of vascular growth and patterning (Epelman, Lavine, & Randolph, 2014). Depletion of osteoclasts specifically leads to defective long-bone formation, tooth eruption, and osteoporosis (Epelman, Lavine, & Randolph, 2014). Macrophages also play important protective roles during prenatal development and in adulthood against infectious pathogens as first responders to bacterial threats, reviewed here (Benoit, Desnues, & Mege, 2008).

In classic wound healing experiments, depletion of macrophages, but not neutrophils, resulted in impaired clearance of debris and disturbance in the healing process (Leibovich SJ, 1975). More recent studies have shown that depleting macrophages expressing lysozyme-M or CD11b causes a delay in wound closure and granulation tissue formation, as well as reduced angiogenesis and collagen synthesis (Koh & DiPietro, 2011). Macrophages also regulate the appropriate regeneration of liver and muscle following injury by clearing debris and secreting cytokines and growth factors that orchestrate repair (Wynn & Vannella, 2016). The removal of macrophages severely impairs these processes. Taken together, one can appreciate the important and diverse roles that macrophages play as innate immune cells in host defense, development,

wound healing, and in disease. The role of macrophages in the aging liver and the host response to engineered lung scaffolds is the main topic of this dissertation and will be discussed further.

1.2 THE HOST RESPONSE TO BIOMATERIALS

1.2.1 Implantable Biomaterials

A biomaterial is any substance designed to control or augment the biological environment within the body (Campoccia, Montanaro, & Arciola, 2013). First generation biomaterials (bone cement, stainless steel) were chosen for being mechanically stable and inert; these materials were functional but did not interface well with tissues. Second generation biomaterials were designed to be more closely integrated with the mechanical properties of the tissue they served to augment (titanium, bioglass, synthetic polymers) and evade immune detection (Fishman JM, 2015). However, more modern biomaterials are adapted for multiple tissue mechanics and implantation methods (injectable hydrogels, porous scaffolds, fibrous meshes, sponges, microspheres) and can be loaded with cargo to mediate specific biological effects, including manipulation of the immune system for desired outcomes (Badylak & Gilbert, 2008). Ultimately, the immunogenicity of a biomaterial is integral to its successful implementation (Fishman JM, 2015).

Biomaterials can be further classified as synthetic or natural. Synthetic biomaterials, as the name suggests, are composed of units that are chemically synthesized. Advantages of synthetic biomaterials are control over design and manufacturing and “off the shelf” availability (Fishman JM, 2015). However, depending on the material, there may be increased likelihood of

foreign body reaction and less compatibility with native tissue architecture and mechanics. Natural biomaterials are derived from organic sources, i.e. plants and animals. Several natural polymers have been studied as scaffolds for tissue engineering applications including alginate, gelatin, and collagen. Decellularizing tissues to expose "nature's template," the extracellular matrix, has been studied extensively in tissue engineering applications (Badylak & Gilbert, 2008).

1.2.2 Whole Organ Decellularization for Tissue Engineering

Decellularization is the removal of cellular material from organs and tissues, resulting in an acellular material composed of extracellular matrix (ECM). ECM scaffolds are advantageous biomaterials for tissue engineering applications as they have a low immunogenicity and retain bioactive signaling molecules that can direct site-appropriate repair (Gilbert, Sellaro, & Badylak, 2006).

The ECM itself is composed of proteins, glycosaminoglycans, proteoglycans and other molecules secreted by tissue resident cells that provide a physical and chemical microenvironment (Brown & Badylak, 2014). Cells interact with the matrix through an assortment of binding proteins including integrins, discoidin domain receptors, and syndecans, which transmit signals in a reciprocally dynamic way (Frantz, Stewart, & Weaver, 2010).

Currently, many acellular products composed of ECM are FDA approved and used in clinical applications such as tissue reconstruction, heart valve replacement, and hernia repair (Londono & Badylak, 2015). Once implanted, non-crosslinked acellular sheets or powders are degraded and replaced with cells from the host, acting as a scaffold to direct site-appropriate tissue remodeling (Brown & Badylak, 2014). More complex, three-dimensional ECM constructs

can be generated by whole organ decellularization, where the native vasculature is perfused with decellularization solutions (detergents, enzymes) generating "ghost organs" as shown in **Figure 2**. Animal derived tissues are a viable source for decellularized materials, particularly pig organs, because they are relatively easy to source, retain evolutionarily conserved proteins, and are of similar size to human organs (Ezzelarab, Ayares, & Cooper, 2005).

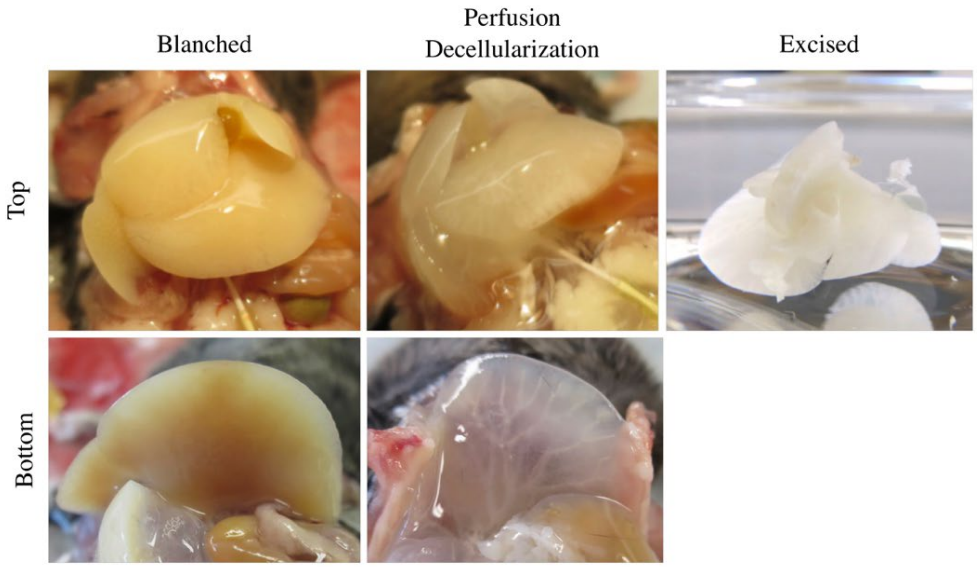

Figure 2. Whole Liver Decellularization.

Three-dimensional extracellular matrix constructs can be generated by whole organ decellularization. In this illustrative example, murine livers were perfused *in situ* with a saline solution to blanch the liver of blood (top: lateral, bottom: dorsal), followed by Triton-X detergent to remove cellular material over 1-3 hours, then excised as a proof of concept of whole organ decellularization.

Three-dimensional scaffolds would then be recellularized with autologous cells to generate a fully functional organ, which has shown preclinical success in animal models (Bonvillain et al., 2012; Faulk, Johnson, Zhang, & Badylak, 2014; Ott et al., 2010). However, several hurdles remain before tissue engineered organs are clinically adopted, including scaling up recellularization, maintaining cell survival and patency of blood vessels, and demonstrating

biocompatibility. Importantly, ECM sourced from pigs may retain non-conserved antigens, such as the alpha-Gal carbohydrate epitope. Humans and new world monkeys, which evolved with a mutation in the alpha-Gal depositing enzyme, respond to the antigen with a pro-inflammatory host response and poorer downstream outcomes.

1.2.3 The Alpha-Gal Antigen in Decellularized Biomaterials

Although decellularization techniques aim to remove cellular antigens, the presence of the porcine alpha-Gal epitope has been detected in acellular heart valves, anterior cruciate ligament, and small intestine submucosa implants used clinically (Konakci et al., 2005; McPherson, Liang, Record, & Badylak, 2000; Stone, Abdel-Motal, Walgenbach, Turek, & Galili, 2007). The Gal epitope is associated with glycoproteins and glycolipids and has been detected on ECM proteins including fibrinogen and laminin (Galili, Shohet, Kobrin, Stults, & Macher, 1988; Spiro & Bhoyroo, 1984; Thall & Galili, 1990; Towbin et al., 1987). The persistence of the Gal epitope in decellularized constructs have been suggested to result in long-term degeneration and calcification of heart valves in patients (Badylak & Gilbert, 2008; Konakci et al., 2005).

Once a biomaterial is implanted, a well-defined series of events are orchestrated, known as the host response. The host immune response to decellularized tissues from wild type and alpha-Gal knockout porcine tissues have been assessed in some applications (Daly et al., 2009; Helder et al., 2017; M. S. Kim, Lim, & Kim, 2016), but other applications remain to demonstrate the biocompatibility of these materials.

1.2.4 Macrophages in the Host Response to Acellular Scaffolds

The host immune response to implantable materials has been well studied over the last five decades. The foreign body reaction is now a well-recognized predictor of the downstream success or failure of implants, and has several conserved early stages, regardless of material type or downstream outcome (Brown, Ratner, Goodman, Amar, & Badylak, 2012).

Following implantation, all materials undergo some degree of protein adsorption, an early neutrophil response, and subsequent invasion of the implantation site by mononuclear phagocytes. While this represents an oversimplification of a complex process (which has been reviewed at length elsewhere (Anderson, 1988; Anderson, Rodriguez, & Chang, 2008; Klopfleisch & Jung, 2016), the view that these events that eventually lead to a negative inflammatory response at the implant surface has led to a number of approaches to evade the early host immune response. While some techniques have undoubtedly shown promise, prevention of long-term interaction of protein or cells with implants has yet to be demonstrated.

Recently, many studies have suggested that the interaction of host immune cells with implanted materials may be an integral and beneficial component of the response that leads to a positive remodeling outcome (Brown, Ratner, et al., 2012; Brown, Sicari, & Badylak, 2014). Just as macrophages have now been shown to be capable of affecting both beneficial and detrimental outcomes in the processes of wound healing and cancer (Mills, 2012; Murray & Wynn, 2011), it is now well recognized that macrophage populations that interact with implants also have heterogeneous phenotypes and functions which are predictive of downstream outcomes.

An early shift from an “M1” pro-inflammatory macrophage phenotype to a more “M2-like” anti-inflammatory phenotype is associated with improved implant integration and/or tissue regeneration, depending upon the type of implant and its intended purpose (i.e. permanent

implants versus regenerative medicine-based approaches to tissue reconstruction) (Brown, Londono, et al., 2012; Brown, Valentin, Stewart-Akers, McCabe, & Badylak, 2009; Guo, Merkel, Sterling, Davidson, & Guelcher, 2015; Hachim, LoPresti, Yates, & Brown, 2017; Keeney et al., 2013; Mokarram, Merchant, Mukhatyar, Patel, & Bellamkonda, 2012; Spiller et al., 2015; Sussman, Halpin, Muster, Moon, & Ratner, 2014).

ECM scaffolds initiate the foreign body response and have been shown to promote M2 macrophage polarization, in part dependent on Th2 cytokine response, leading to constructive tissue remodeling (Keane & Badylak, 2015). However, the biology of the host response in understudied groups, such as the elderly or patients with comorbidities, likely differs from the host response of young, healthy individuals. With aging, the immune system undergoes immunosenescence, an understudied area in the biology of macrophages in the host response and tissue homeostasis.

1.3 AGING AND THE IMMUNE SYSTEM

Aging has been shown to influence the functions of both innate and adaptive immune cells in scenarios such as wound healing, the response to pathogens, and vaccination: a process termed “immunosenescence”. Immunosenescence is associated with an increased susceptibility of elderly populations to develop infection, autoimmune disease, and cancer (Sebastián, Lloberas, & Celada, 2009). While the term ‘senescence’ typically refers to cells that have irreversibly exited the cell cycle (Hayflick, 1965; Williams, 1957), immunosenescence does not specifically refer to growth arrest. Immunosenescence manifests as altered numbers of circulating cells,

delayed migration of cells to sites of infection or injury, and disrupted effector responses, reviewed here (Aw, Silva, & Palmer, 2007; Stahl & Brown, 2015).

1.3.1 The Adaptive Immune System and Aging

The effector cells of the adaptive immune system, T-cells and B-cells, are derived from lymphoid progenitors in the bone marrow and mature in secondary lymphoid tissues, such as the spleen and thymus. The adaptive immune system provides acquired antigen-specific immunity, leading to highly effective cell destruction, immune regulation, and memory.

Generation of the adaptive immune system is robust in young, healthy individuals, establishing a diverse immune repertoire. However, lymphopoiesis is significantly diminished in elderly individuals, in part due to involution of the thymus and a skewing of hematopoietic progenitor cells towards the myeloid lineage (Linton & Dorshkind, 2004; Lynch et al., 2009; Rossi et al., 2005). As a result, the number of T-cell and B-cell progenitors in the bone marrow and thymus are markedly reduced with age (Johnson, Owen, & Witte, 2002; Miller & Allman, 2003; Min, Montecino-Rodriguez, & Dorshkind, 2004; Montecino-Rodriguez, Berent-Maoz, & Dorshkind, 2013).

Advanced age is specifically associated with low numbers of naïve T-cells, persistent memory T-cells, and reduced diversity of the T-cell receptor (TCR) repertoire, with a large proportion of TCRs directed towards persistent cytomegalovirus (CMV) infection (Blackman & Woodland, 2011; Cicin-Sain et al., 2012; Olsson et al., 2000; Wikby et al., 2002). Meanwhile, B-cell precursors do not proliferate as extensively in elderly mice as they do in young mice and undergo higher rates of apoptosis (Min, Montecino-Rodriguez, & Dorshkind, 2006). Changes in the bone marrow, including decreased secretion of interleukin-7 (IL-7) by stromal cells, have

been implicated in the reduction of B-cell development in aged individuals (Labrie, Sah, Allman, Cancro, & Gerstein, 2004; Stephan, Reilly, & Witte, 1998).

The functions of adaptive immune cells are also impaired with aging. T-cell activation occurs following interaction with antigen-presenting cells forming an immune synapse. Several defects in this synapse have been reported with aging, including glycosylation of costimulatory molecules, such as CD28, and changes in lipid membrane properties (Nguyen, Espinoza, & Taub, 2004; Weng, Akbar, & Goronzy, 2009). Perhaps the single most important consequence of synapse dysfunction with aging is reduced production of interleukin-2 (IL-2), as exogenous IL-2 has been shown to rescue many of the age-related deficits of T-cell activation (Haynes & Lefebvre, 2011; Haynes, Linton, Eaton, Tonkonogy, & Swain, 1999). The reduction in T helper 2 subsets also reduces the regenerative response seen during normal biomaterial remodeling in aged individuals (Sadtler et al., 2016). Similarly, B-cells exhibit impaired class switching with aging, limiting the specific phenotypes of antibody producing B-cells crucial for responding to invading pathogens (Frasca et al., 2008). These deficits in lymphocyte cell number and function are likely responsible for the reduced response to vaccination and ability to clear infections observed in elderly populations and are active areas of ongoing research.

1.3.2 The Innate Immune System and Aging

Innate immune cells include granulocytes (neutrophils, eosinophils, basophils, mast cells), innate lymphoid cells (natural killer cells), and antigen presenting cells (dendritic cells, macrophages) (Klose & Artis, 2016; Medzhitov & Janeway, 1997). Each of these innate immune cells provides a highly regulated, specific function that orchestrates tissue wound repair and response to foreign antigens with the ultimate goal of restoring tissue homeostasis.

Neutrophils are the first responders during injury, infection, and the foreign body reaction. While the number of neutrophils and their phagocytic capacity is reported to be largely preserved in the elderly, delays in migration and reduction of respiratory burst have been reported (Fulop et al., 2004). Growing evidence suggests that dendritic cell activation is impaired in aging, along with impaired capacity to cross tissue barriers, and to induce cytokine production from T-cells (Rhee, Zhong, Reizis, Cheong, & Veillette, 2014; Steinmann, Klaus, & Muller-Hermelink, 1985). With aging, natural killer cells have been reported to demonstrate diminished target binding leading to changes in effector function, such as release of granzyme, perforin, and other cytokines (Solana et al., 2012).

1.3.2.1 Macrophages and Monocytes

The process of aging has been more extensively studied on macrophage populations but is highly context and tissue specific, often resulting in conflicting reports in the literature. Although the output of immune cells from the bone marrow is weighted towards myeloid lineage with aging, the absolute numbers of monocytes are unchanged between young and aged individuals. (Hearps et al., 2012; Seidler, Zimmermann, Bartneck, Trautwein, & Tacke, 2010). An increased percentage of non-classical monocytes ($CD14^{+}$ $CD16^{++}$), and a reduction in classical monocytes ($CD14^{+}$ $CD16^{-}$) has been reported in aged humans (Hearps et al., 2012; Seidler et al., 2010). Like other innate immune cells, macrophage recruitment is delayed in aging, possibly due to a reduction in expression of the integrin very late antigen-4 (VLA-4) on monocytes, and vascular cell adhesion molecule-1 (VCAM-1) on endothelial cells (Ashcroft, Horan, & Ferguson, 1998).

Furthermore, a reduction in major histocompatibility complex (MHC-II) expression has been observed in both human and murine macrophages, leading to a reduction in antigen-presentation capacity and cross-talk with the adaptive immune system (Herrero et al., 2002; Zissel, Schlaak,

& Muller-Quernheim, 1999). Toll-like receptors, including TLR-1, TLR-2, and TLR-4, are reported to decrease on aged peritoneal and splenic macrophages, perhaps contributing to the susceptibility of the elderly to bacterial, mycotic, and viral infections (Boehmer, Meehan, Cutro, & Kovacs, 2005; van Duin et al., 2007).

Phagocytic clearance of extracellular pathogens tends to be attenuated in aged macrophage populations as well (Linehan et al., 2014). While no difference in phagocytic capacity was found between young and aged bone marrow derived macrophages, peritoneal macrophages exhibit an age-associated decline in phagocytic capacity and antigen presentation (Linehan et al., 2014). When young peritoneal macrophages were transplanted into aged peritoneal space, the young cells also exhibited reduced phagocytic and antigen presentation capabilities, suggesting cell extrinsic mechanisms (Linehan et al., 2014). Alveolar macrophages isolated from aged individuals have been shown to exhibit reduced phagocytic capacity as well as attenuated expression of genes associated with macrophage proliferation (C. K. Wong et al., 2017). This reduction both in cell number and phagocytic ability likely contributes to the age-related mortality risk following pathogen infection, such as in the case of an influenza lung infection model (C. K. Wong et al., 2017). In the liver, there have been mixed reports on the maintenance of Kupffer cell phagocytosis, where one study reported a deficit (Brouwer & Knook, 1983) and another reported an increase in phagocytosis with aging (Hilmer, Cogger, & Le Couteur, 2007).

Autophagy, or the intracellular degradation of damaged proteins and organelles in autophagosomes, is one such process which has been shown to become dysregulated with increasing age in macrophage populations (Stranks et al., 2015). Deletion of autophagy genes *Atg5* and *Atg7* in bone marrow-derived macrophages resulted in decreased antigen presentation

capacity, impaired maturation, altered mitochondrial metabolism, downregulation of surface receptors such as TLR-4, and increased secretion of pro-inflammatory cytokines (Rubinsztein, Marino, & Kroemer, 2011; Stranks et al., 2015). The phenotype of these autophagy deficient bone marrow macrophages closely mimics that of macrophages isolated from aged individuals (Stranks et al., 2015), which may be driven by the hypermethylation of autophagy associated genes (Khalil et al., 2016). It remains to be seen if restoring autophagic flux to aged macrophages can improve their function and polarization status, however caloric restriction has been shown to improve both longevity and autophagic capacity of cells in animal models (Trepanowski, Canale, Marshall, Kabir, & Bloomer, 2011).

The reduction in autophagosome activity prevents the degradation of both inflammasome components and damaged mitochondria and can thereby promote chronic activation of pro-inflammatory signals in aged cells (Rubinsztein et al., 2011). This phenomenon has been termed "inflamm-aging," one of the hallmarks of aging, and has been strongly correlated to morbidity (Puzianowska-Kuznicka et al., 2016). The release of radical oxygen species from damaged mitochondria or M1-polarized macrophages can then oxidize proteins, lipids, and DNA (Abais, Xia, Zhang, Boini, & Li, 2015; Cichoz-Lach & Michalak, 2014; Kapetanovic et al., 2015), further exacerbating inflammasome activation in aging and leading to systemic inflammation (Cecilio, Costa, Simioni, Gabriel, & Tamashiro, 2011; Dimitrijevic et al., 2013; Suchy, Labuzek, Buldak, Szkudlapski, & Okopien, 2014).

Bone marrow-derived macrophages isolated from aged murine and human donors have been shown to produce greater concentrations of nitric oxide and reactive oxidative species than macrophages isolated from young donors (Suchy et al., 2014). However, this upregulation in the secretion of reactive oxidative species was not observed following pro-inflammatory stimulation

of peritoneal macrophages (Cecilio et al., 2011; Dimitrijevic et al., 2013). Despite these increases in nitric oxide and reactive oxygen species, M2 macrophages have been found to accumulate in aged skeletal muscle and result in the detrimental replacement of muscle fibers with fibrotic tissue over time (Y. Wang, Wehling-Henricks, Samengo, & Tidball, 2015).

The gene signature of macrophages isolated from bone marrow and polarized to M1 or M2 phenotypes was mostly unchanged between young and aged mice, with the exception of increased Fizz-1 (M2 marker) expression on aged cells (Mahbub, Deburghgraeve, & Kovacs, 2012). However, macrophages isolated from mouse spleen had a reduction in both M1 and M2 gene expression patterns when stimulated with polarizing cytokines (Mahbub et al., 2012). Work from our group also demonstrates only marginal differences between young and aged bone marrow derived macrophages polarized *in vitro*, including a slight increase in nitric oxide production (Hachim, Wang, et al., 2017). However, when bone marrow derived macrophages are pre-exposed to degradation products from young and aged extracellular matrix or "tissue cues," differences in function arise following polarization with M1-inducing cytokines, again suggesting that cues in the microenvironment may be driving some of the cellular dysfunction (LoPresti & Brown, 2018).

Non-immune cell types can also contribute to the age-associated immune dysfunction. With age, increasingly large numbers of pre-adipocytes differentiate into mature adipocytes, with enhanced secretion of leptin, TNF-α, and IL-6, and reduced secretion of adiponectin, promoting M1 phenotypes (Garg, Delaney, Shi, & Yung, 2014; Tchkonia et al., 2010; Urs et al., 2004). Numerous DAMPs, which have been shown to promote inflammasome formation and activation, also have age-related increases in concentration, including cholesterol (Duewell et al., 2010), amyloid-β (Murphy, Grehan, & Lynch, 2014; K. Wang et al., 2017), hydroxyapatite crystals (Jin

et al., 2011), purine catabolic end products such as uric acid (Chen et al., 2006), and ATP (Mariathasan et al., 2006). More recently, the effect of the aging gut microbiome on macrophage function has been considered (Thevaranjan et al., 2017). Raising mice under germ-free conditions preserves the bactericidal capacity of alveolar macrophages and reduces secretion of IL-6 in old age, mediated by reduced dysbiosis and improved gut permeability (Thevaranjan et al., 2017). Finally, age-related alterations in the T cell compartment can shift the relative Th1 and Th2 cytokine concentrations and directly impact macrophage polarization (Onyema et al., 2015; van der Geest et al., 2014).

The morphology of macrophages can also be influenced by the aging process. Microglia have been shown to increase cell soma volume while reducing the length of cellular processes in aged brains (Hefendehl et al., 2014). These morphological changes reduce the capability of the microglia to interact with neural cells and perform routine surveillance of the local microenvironment (Hefendehl et al., 2014). While microglial population sizes increase to account for this reduction in cell process size (Dey et al., 2014), the population expansion tends to occur in a non-homogenous manner, disrupting the uniform microglial distributions commonly observed in young animals (Hefendehl et al., 2014). In addition, aged microglia exhibit enhanced secretion of reactive oxidative species following central nervous system injury through upregulation of NADPH oxidase 2 (von Leden, Khayrullina, Moritz, & Byrnes, 2017), and secrete more IL-1β, mediated by hypomethylation of CpG sites in the IL-1β proximal promoter (Cho et al., 2015).

The infiltration of monocyte-derived macrophages to multiple tissue sites has been observed in age-related diseases, including Alzheimer's disease (Malm, Koistinaho, Muona, Magga, & Koistinaho, 2010), which leads to increased inflammation and phagocytosis. In the

cardiovascular system, the tissue resident macrophage population (yolk-sac derived, M2-like) is replaced by bone marrow-derived macrophages over time in murine models (Epelman, Lavine, Beaudin, et al., 2014; Pinto et al., 2014). This shift in macrophage populations contributes to deleterious outcomes following cardiac injury, such as chronic inflammation, fibrotic scar deposition, and reduced re-vascularization of ischemic tissue following injury (Lavine et al., 2014; Pinto et al., 2014). Similarly, peritoneal macrophages derived from embryonic origins are replaced by circulating monocytes over time, which do not recapitulate expression of Tim-4 in murine models (Bain et al., 2016). Presently, the replacement of embryonic macrophage populations with monocyte-derived cells and consequences thereof are unknown in certain organs, including the liver.

1.3.2.2 Host Response to Synthetic Biomaterials

There are few, if any reports in the literature which have investigated the host response to implants in aged animals. However, a recent study from our group sought to elucidate the impacts of aging upon the host response to polypropylene mesh implanted into 8-week (young) and 18-month-old (aged) mice (Hachim, Wang, et al., 2017). The findings of the study suggested that the host macrophage response to polypropylene mesh implants was delayed, dysregulated, and unresolved in the aged animals as compared to the young.

Briefly, we observed decreased recruitment of macrophages to the site of subcutaneous implantation in the aged animals at 3- and 7-days post-implantation **(Figure 3a, b).** The population which was present in the aged animals was found to be expressing significantly more iNOS and less arginase than was observed in young animals, indicating a more M1 skewed response (**Figure 3c-f**).

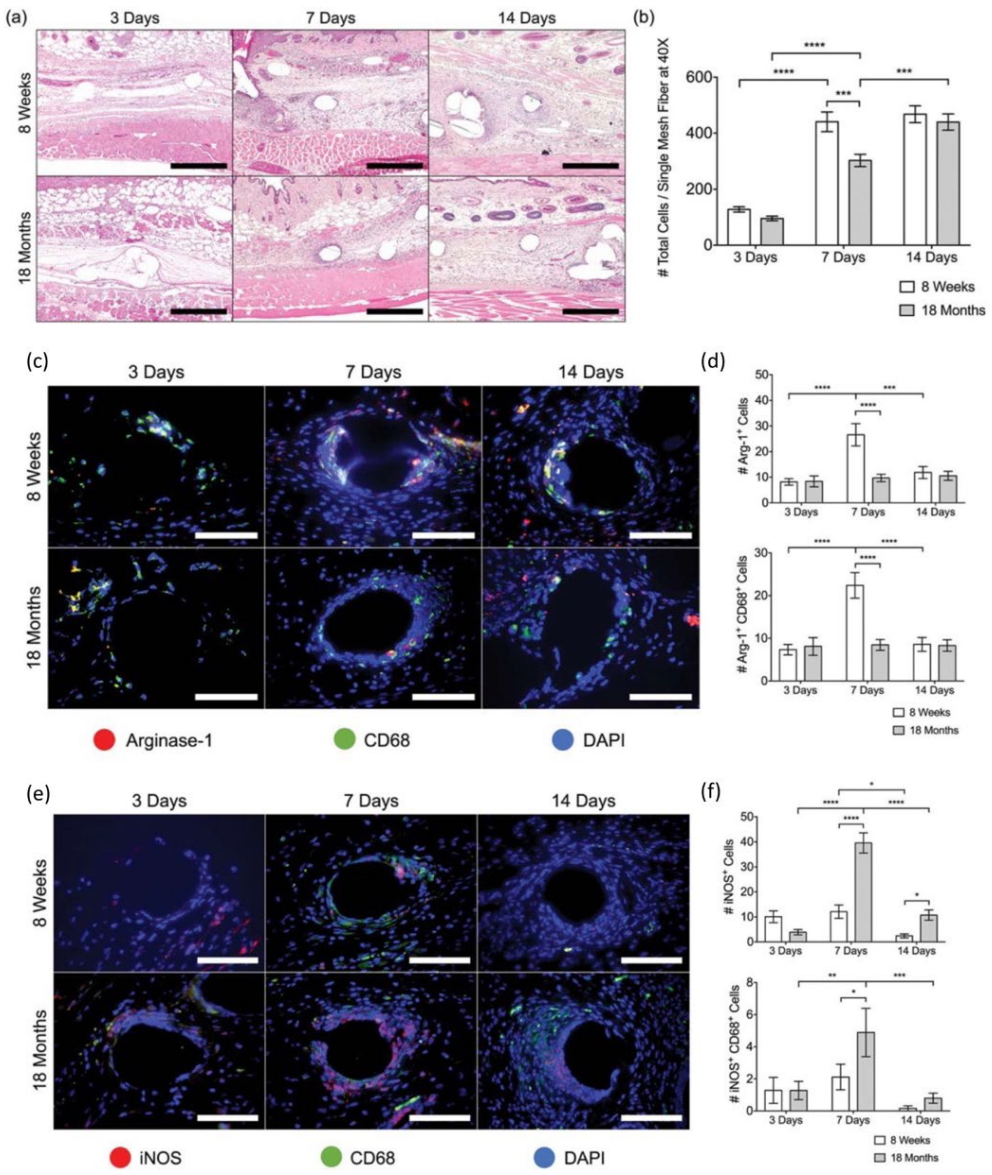

Figure 3. The Host Response to Polypropylene Mesh in Aged Mice

The early host response to implanted materials in young and aged C57BL/6 mice. (a) Images of H&E-stained tissue cross-sections and (b) total cell counts (DAPI) surrounding single mesh fibers at 3, 7, and 14 days. Scale bars represent 200 mm. Fluorescence microscopy images of (c) Arginase-1 (red) CD68 (green) co-immunolabeling and (e) iNOS (red) CD68 (green) co-immunolabeling at a single mesh fiber at 3, 7, and 14 days. Scale bars represent 50 mm. Cell count image analysis of (d) Arg-1^{+}, Arg-1^{+} CD68^{+} cells and (f) iNOS^{+}, iNOS^{+} CD68^{+} cells at 3, 7, and 14 days. Bars represent the mean ± SEM. Statistical significance as (*) $p < 0.05$, (**) $p < 0.01$, (***) $p < 0.001$, (****) $p < 0.0001$. All other differences are nonsignificant ($n = 7$).

Analysis of tissue remodeling outcomes at 90 days demonstrated similar composition and thickness of the tissue capsule surrounding the implants; however, 18-month-old animals were observed to have a significantly greater number of cells within the tissue capsule, suggesting an unresolved inflammatory response. These results correlate well with the findings of dysregulated, and unresolved host responses in studies of the response pathogen and in wound healing in aged individuals.

In summary, several age-related deficits have been identified in specific tissue-resident macrophage populations in a context dependent manner. Studies have largely focused on easily accessible sources of tissue-resident macrophages, such as bone marrow, peritoneal cavity, and alveolar macrophages. However, macrophages residing in the liver are less commonly studied, despite being the largest pool of tissue resident macrophages in the body. Future work directed at identifying changes in liver resident macrophages will be crucial for understanding the development of age-related liver disease and the host response to infection and implanted materials.

1.4 LIVER SPECIFIC MACROPHAGE POPULATIONS

The liver is an important immunological organ, serving as a surveillance system for gut-derived pathogens and producing several key immune components – complement, acute phase, and coagulation proteins (Crispe, 2009; Robinson, Harmon, & O'Farrelly, 2016). While hepatocytes and certain non-parenchymal cells possess some inherent immunological properties (see reviews (Zhou, Xu, & Gao, 2016) and (P. A. Knolle & Wohlleber, 2016)), multiple populations of $CD45^{+}$ immune cells are transiently or permanently located in the liver.

The healthy liver is home to several populations of lymphocytes, including natural killer (NK) cells, NK T-cells, B-cells, mucosal associated T-cells and γδ-T-cells (Doherty et al., 1999; Dusseaux et al., 2011; Kenna et al., 2004; Kenna et al., 2003). In humans, 40% of the resident lymphocyte population are composed of NK cells, while in mice 40% of the resident lymphocytes are NK T-cells. Innate immune cells also have a large presence in the liver. The majority of immune cells in the liver are myeloid derived cells, including dendritic cells and macrophages (Gao, Jeong, & Tian, 2008; Thomson & Knolle, 2010).

1.4.1 Hepatic Macrophages

Hepatic macrophages include both cells derived from circulating monocytes, which are present at various levels during homeostasis and inflammation, and the resident tissue macrophage, known as the Kupffer cell (KC) (Gomez Perdiguero et al., 2015; Schulz et al., 2012; Yona et al., 2013). KCs are the most highly represented immune cell, comprising nearly one-third of non-parenchymal cells in the liver (Bilzer, Roggel, & Gerbes, 2006).

1.4.1.1 Kupffer Cells

The KC is a primitive cell, appearing early during embryogenesis (E9.5-E12.5 in mice), derived primarily from the yolk sac (Gomez Perdiguero et al., 2015; Hoeffel et al., 2015; Mass et al., 2016). Importantly, the KC population is maintained through self-proliferation, with minimal input from circulating monocytes during homeostasis (Gomez Perdiguero et al., 2015; Jenkins et al., 2011; Schulz et al., 2012; Yona et al., 2013).

The Kupffer cell is the key detector of commensal or pathogenic microbial signals, danger signals, and tumor cells moving through the hepatic circulation (Bilzer et al., 2006; Kinoshita et

al., 2010; Movita et al., 2012). KCs are located along the hepatic sinusoids allowing for the low-pressure blood supply come into contact with both KCs and hepatocytes through the fenestrated endothelium (Robinson et al., 2016). KCs express the complement receptor CR1g, which binds complement fragments C3b and iC3b, allowing phagocytosis of complement C3-opsonized particles even under low-pressure blood flow (Helmy et al., 2006; Zeng et al., 2016). Bacterial clearance by KCs is crucial for host defense as 80% of blood-borne bacteria accumulate in the liver and are destroyed there (Bilzer et al., 2006; Kinoshita et al., 2010; Movita et al., 2012).

DAMPs and PAMPs are present in relatively high concentrations in blood entering the liver from the gut, via the portal vein, and engage with pattern recognition receptors, including Toll-like receptors, on the surface of macrophages and hepatocytes (Janeway, 1992; Kubes & Mehal, 2012; Takeuchi & Akira, 2010). With low levels of bacterial endotoxins, KCs promote immune tolerance by secreting anti-inflammatory factors including IL-10, TGF-β, and prostaglandin-E2 (PGE2), thereby inducing regulatory T-cells (Ju & Tacke, 2016; P. Knolle et al., 1995). In the presence of higher concentrations of damage or pathogen-associated signaling molecules, KCs can become polarized towards an M1 phenotype and produce a variety of inflammatory cytokines including IL-1, IL-6, IL-12, TNF-α (Bilzer et al., 2006; Kinoshita et al., 2010; Movita et al., 2012). Several liver diseases are influenced by KC activation and expansion, but their individual role has been difficult to dissect from more recently identified macrophage populations in the liver.

1.4.1.2 Infiltrating Monocyte Derived Macrophages

Within the past decade, the heterogeneity of hepatic macrophages, *i.e.* Kupffer cells and monocyte-derived macrophages, has become an emerging topic in hepatology. Fate tracing

experiments in the brain first determined that resident microglia are established prenatally and maintained independently from monocyte input, which was later translated to the liver (Ginhoux et al., 2010). Holt et al. were among the first to identify two populations of macrophages in the liver (Holt, Cheng, & Ju, 2008). Through bone marrow chimera experiments, cells expressing $F4/80^{hi}CD11b^{lo}$ were identified as KCs, while cells expressing $F4/80^{lo}CD11b^{hi}$ were found to be derived from circulating monocytic progenitors (Holt et al., 2008). Shortly after, Klein et al. classified two macrophage populations in the liver: KCs as immobile, "sessile" macrophages and monocyte-derived macrophages as motile cells (Klein et al., 2007).

In most cases, murine monocyte-derived macrophages in the liver are derived from an influx of bone marrow derived, $Ly6C^{hi}$ monocytes, primarily driven by monocyte chemoattractant protein, which can be produced by KCs, stellate cells, or hepatocytes (also known as CCR2-CCL2 interactions) (Dal-Secco et al., 2015; Mossanen et al., 2016). Secondary pathways of monocyte recruitment to the liver are CXCR3-CXCL10, CCR1-CCL5, and CCR8-CCL1 dependent (Heymann et al., 2012; Seki, De Minicis, Gwak, et al., 2009; Zhang et al., 2016). Murine monocyte-derived macrophages may also be derived from $Ly6C^{lo}$ monocytes trafficking from the spleen, which express CD11b, but are thought to take on a more patrolling or regulatory macrophage phenotype (Swirski et al., 2009). Phagocytes from the peritoneal cavity, which express F4/80, CD11b, and GATA6, have been shown to cross into the liver after subcapsular liver lesion (J. Wang & Kubes, 2016), but it remains unclear if this infiltration occurs in other liver injury settings.

1.4.1.3 Roles in Health and Disease

Kinoshita et al. determined that murine monocyte-derived macrophages and KCs could be distinguished by CD11b and CD68 expression, respectively (Kinoshita et al., 2010). The

CD11b^{hi} monocyte-derived macrophages were radiosensitive and particularly efficient at producing IL-12, protecting the host against tumor xenografts, while the CD68^{hi} KCs were radioresistant and highly efficient at phagocytosis, protecting the host against bacterial challenge (Kinoshita et al., 2010). The use of these differentiating markers has been expanded to several disease models, identifying a damaging role of TNF/FasL production by CD11b^{+} monocyte-derived macrophages in carbon-tetrachloride acute liver injury and hepatitis in hypercholesterolemic mice (Nakashima et al., 2013; Sato et al., 2014). The CD11b^{+} monocyte-derived macrophages were also found to accumulate in the liver following repeated lipopolysaccharide injections, but suppressed TNF efflux into the systemic circulation, thereby reducing lethal septicemia (Kinoshita et al., 2017). In addition, the CD11b^{+} monocyte-derived macrophages were recruited during diet-induced steatohepatitis in FGF5 deficient mice and following partial hepatectomy, where they were crucial for liver regeneration (Nakashima et al., 2016; Nishiyama et al., 2015). Others have observed that monocyte derived cells protect the liver from iron toxicity in hemolytic anemia by ingesting senescent and dying erythrocytes (Theurl et al., 2016).

More recently, the C-type lectin, Clec4f, has been identified as a selective murine KC marker (Scott et al., 2016). Interesting, ablating KCs via Clec4f-driven diphtheria toxin causes an influx of monocyte-derived macrophages, which can differentiate into nearly identical KCs when this "niche" is made available. Only 12 genes remained differentially expressed between monocyte derived KCs and embryonically derived KCs, including *CD209f, CD163, C2, CCR3, Timd4,* and *Snrpn* at the time points examined (Scott et al., 2016).

Taken together, KCs and monocyte-derived macrophages play heterogenous roles in various liver disease states and cannot be considered wholly harmful or beneficial without deciphering

the given context. Importantly, infiltrating monocytes may also differentiate into dendritic cells, which play distinct immunostimulatory and antigen presentation roles in the liver (Kingham et al., 2007). The heterogeneity of hepatic macrophages is less well defined in humans as compared to murine animal models. The role of these diverse hepatic macrophage populations in a given disease context is just beginning to be understood and has not yet been examined in the natural aging process, a major risk factor for several chronic liver diseases.

1.4.2 Effects of Aging on Liver Parenchymal and Non-Parenchymal Cells

The process of aging is closely associated with a number of degenerative modifications in the liver, where hepatic structure and cell function are observed to decline. Both hepatocytes and macrophages exhibit deficits in mitochondrial function, linked to a decline in autophagy and production of pro-inflammatory molecules (I. H. Kim, Kisseleva, & Brenner, 2015; Salminen, Kaarniranta, & Kauppinen, 2012). While the effects of aging on hepatic macrophages have not been well characterized on a cellular and molecular level, several studies have examined macrophages from alternative tissue sources and may offer some insight about hepatic macrophages (see section 1.3.2.1, **page 16**).

Several studies have shown that the volume of blood in the liver decreases in elderly individuals, leading to a total volume loss of 20%-40% (Zeeh & Platt, 2002). In addition, the thickness of liver sinusoidal endothelial cells fenestrations increases, limiting the exchange of molecules to and from the liver (McLean et al., 2003). At the serum level, aging is associated with reductions in albumin and bilirubin, increases in alkaline phosphatase, and minimal changes in aminotransferase levels (Tietz, Shuey, & Wekstein, 1992). The metabolism of cholesterol in the liver also decreases, leading to increased blood cholesterol and neutral fat levels over time

(Tietz et al., 1992). However, more recent investigations suggest the most essential change in liver aging is loss of the functional liver cell mass (Wakabayashi, Nishiyama, Ushiyama, Maeba, & Maeta, 2002).

Changes in the morphology of hepatocytes may be related to increased polyploidy, accumulation of lipofuscin in the cytoplasm, and declining surface area of endoplasmic reticulum and number of mitochondria, ultimately negatively affecting the function of hepatocytes (Hohn & Grune, 2013; I. H. Kim et al., 2015; Sastre et al., 1996). The oxidative capacity of the liver declines with aging, reducing the capacity to metabolize certain drugs such as benzodiazepines (American Geriatrics Society Beers Criteria Update Expert, 2012). The decline in hepatocyte mitochondrial function has been suggested to enhance the vulnerability of aged livers to acute injury and to cause delays in liver regeneration (Poulose & Raju, 2014). In addition, aging livers are known to accumulate a multiprotein complex (C/EBPalpha-Brm-HDAC1) that silences elongation factor 2 (E2F)-dependent promoters, thereby reducing proliferation and regenerative capacity of hepatocytes (G. L. Wang et al., 2008).

The reduction in proliferation of aged hepatocytes may also be related to an increase in senescent cells with aging. Senescent cells accumulate in the liver during aging and in chronic liver disease; and may include hepatocytes, cholangiocytes, stellate cells, and immune cells (reviewed here: (A. D. Aravinthan & Alexander, 2016)). Cells become senescent as a result of replicative exhaustion (telomere shortening), DNA damage, or oxidative stress, among other mechanisms (Ben-Porath & Weinberg, 2005). Senescent cells are characterized by the expression of cell cycle inhibitors p21, p16, and p53, which prevent replication and apoptosis, as well as secretion of pro-inflammatory cytokines that signal for their removal but can lead to tissue damage when chronically expressed (Campisi, 1996; Coppe et al., 2008). Senescent

hepatocytes accumulate with age and appear as an almost “universal phenomenon” in chronic liver diseases including hepatitis B and C infection, alcoholic and non-alcoholic liver disease, and genetic haemochromatosis (A. D. Aravinthan & Alexander, 2016). Furthermore, senescent hepatocytes undergo metabolic changes, such as increased transport of conjugated bilirubin into the hepatic sinusoids and insulin resistance through dysregulated glucose transporter expression and Akt signaling among others (A. Aravinthan et al., 2015). Interestingly, the length of telomeres was found to be conserved in aged hepatocytes and bile duct cholangiocytes but decreased in aged Kupffer cells and stellate cells, suggesting cell-specific mechanisms of senescent phenotype acquisition in the liver (Verma et al., 2012).

Overall, the effects of aging on non-parenchymal cell subsets, particularly hepatic macrophages, is an understudied area. Hilmer et al. determined that the number and basal activity of Kupffer cells was increased with old age in a rat model (Hilmer et al., 2007), however this work was performed before the heterogeneity of liver macrophages was fully understood. Similarly, Singh et al. identified a change in liver macrophage distribution with aging, where old mice had more F4/80^{+} macrophages located in large lymphoid structures (also containing T-cells and B-cells), and a reduction in the number of spindle shaped macrophages throughout the parenchyma (Singh et al., 2008).

Recent work by Maeso-Diaz et. al characterized molecular changes in LSECs, stellate cells, and hepatic macrophages in the livers of aged rats (Maeso-Diaz et al., 2018). The authors identified a significant deregulation of LSEC phenotype with aging as demonstrated by downregulation of vasodilatory pathways (nitric oxide, heme oxygenase), increase in oxidative stress, and decrease in angiocrine markers (stabilin-2, CD32b, and VEGFR2) (Maeso-Diaz et al., 2018). Aged stellate cells had increased markers of activation (alpha smooth muscle actin and

collagen I), increased intracellular lipid stores, and alterations in retinoid metabolism (Maeso-Diaz et al., 2018). Finally, the authors noted an increase in recruitment of proinflammatory cells in aged livers, including increased IL-6 expression in isolated hepatic macrophages, but no change in the traditional macrophage polarization markers (Maeso-Diaz et al., 2018). Human livers showed similar trends in downregulation of endothelial markers, but substantial work remains to extend and decode these findings in both aged murine and human systems.

1.4.3 Aging and Fatty Liver Disease

Aging is a major risk factor for the development and prognosis of several chronic liver diseases and conditions, including nonalcoholic fatty liver disease, alcoholic liver disease, hepatitis C, and an increased susceptibility to develop fibrosis and cirrhosis (Sheedfar, Di Biase, Koonen, & Vinciguerra, 2013). The reduced capacity of aged livers to regenerate and to tolerate transplantation leads to increased risk of mortality from chronic liver diseases, as demonstrated in **Figure 4** (adapted from (Stahl et al., 2018) in accordance with the Creative Commons license).

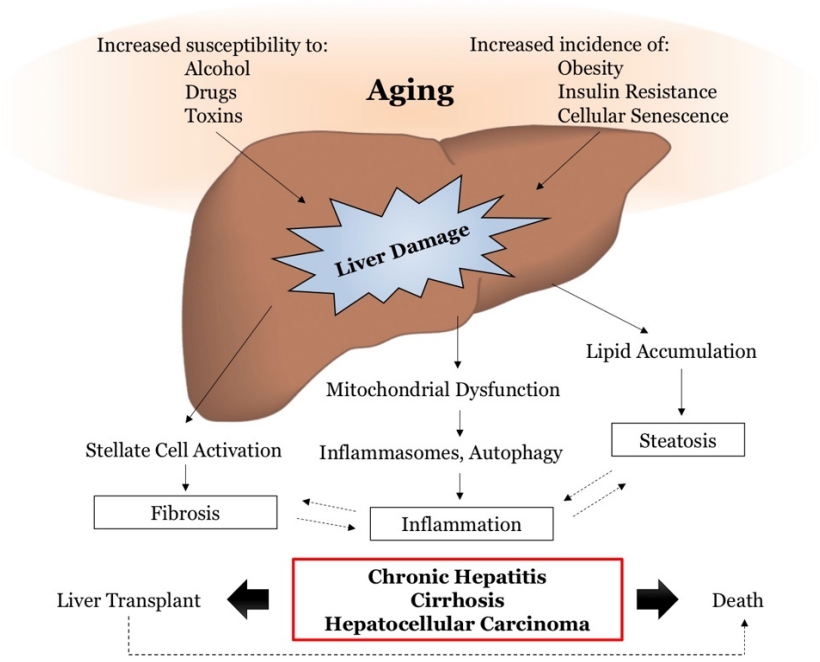

Figure 4. Aging and Mechanisms of Liver Disease.

In the context of this dissertation, steatosis associated with non-alcoholic fatty liver disease is the most relevant chronic liver disease associated with aging and inflammation. Non-alcoholic fatty liver disease (NAFLD) and non-alcoholic steatohepatitis (NASH) are leading causes of chronic liver disease globally and are projected to become the leading indication for liver transplantation in the United States (Mikolasevic et al., 2018; R. J. Wong et al., 2015; Younossi et al., 2016). NAFLD often presents with metabolic syndrome, such as obesity and excessive visceral fat, hyperlipidemia, hypertension, insulin resistance and an increased secretion of pro-inflammatory cytokines (Barzilai, Huffman, Muzumdar, & Bartke, 2012). All of these components of metabolic syndrome are generally observed in elderly populations and many studies find increased rates of NAFLD among elderly people compared with their younger counterparts (Frith, Day, Henderson, Burt, & Newton, 2009; Koehler et al., 2012; Noureddin et al., 2013).

The mechanism for developing age-related steatosis is not fully understood but has been attributed to hepatocyte senescence driving a reduction in mitochondrial metabolism (Ogrodnik et al., 2017), decreased transport of insulin across the sinusoidal endothelium (Mohamad et al., 2016), reduction in autophagic flux (Gonzalez-Rodriguez et al., 2014), or chronic low-level inflammation (Duval et al., 2010; Kumar et al., 2013), leading to the build-up of toxic free fatty acids in the liver. Lifestyle choices, such as high fat diet (HFD), may also lead to the development of NAFLD in aged individuals. Work by Fontana et. al showed that mice were equally susceptible to steatosis following HFD regardless of age. However, the older mice exhibited more severe hepatocellular injury and inflammation following administration of HFD that was attributed to increased M1 macrophage polarization in both the liver and white adipose tissues (Fontana et al., 2013).

As in other chronic liver diseases, macrophages accumulate in the livers of NAFLD patients (Wan et al., 2014). Experimental mouse models have shown an accumulation of $Ly6C^{+}$ monocytes is a critical step in the development of progressive fibrosis from steatohepatitis in a CCL2-dependent mechanism (Tacke, 2017). In addition, lipids and free fatty acids contribute to DAMP-induced Kupffer cell activation (Reid et al., 2016). Patients with low-grade steatosis were found to have higher mRNA expression of M2 markers, CD206 and CD163, compared to patients with advanced steatosis. The M2 macrophages were hypothesized to promote apoptosis of M1 polarized hepatic macrophages and protect against disease progression of NAFLD or alcoholic hepatitis (Wan et al., 2014). Interestingly, soluble CD163 (sCD163), a marker of M1 macrophage polarization, increases systemically with severity of NAFLD in human patients (Kazankov et al., 2015), again suggesting that M1 polarization is associated with more advanced stages of the disease.

Both Kupffer cells and infiltrating monocytes are implicated to various levels in the etiology of chronic liver disease, however the distinction between these two cell populations is less clear in human clinical liver samples compared to animal studies. Importantly, most models of chronic liver disease are induced in young, healthy animals through genetic manipulation or by administering specific diets or chemical toxins. Findings from these animal studies are important to identify novel mechanisms regulating liver disease but may not prove relevant or all-encompassing when translating the findings to older, human populations, as evidenced by the moderate success of several anti-fibrotic therapies in clinical trials (Cohen-Naftaly & Friedman, 2011). Distinguishing between the biology of aging and age-associated pathologies can be a difficult task but is an important effort in the field of hepatology. Additional studies are needed to assess the effect of aging on the liver prior to the onset of age-associated pathologies in order to dissect mechanisms of aging from the manifestation of the pathology itself.

2.0 A STUDY OF MACROPHAGES IN THE AGING LIVER

Chapter 2 is adapted from one primary research article, presently in under revision at the time of submission of this dissertation:

Stahl EC[1], Delgado ER[1,2], Alencastro F[1,2], LoPresti ST[1,3], Wilkinson PD[1,2], Roy N[1,2], Haschak MJ[1,3], Monga SP[1,2,4], Duncan AW[1,2,4], Brown BN[*1,2,3,4]. (2018) Inflammation and ectopic fat deposition in the aging murine liver is influenced by CCR2. ***(submitted October 2018).***

[1]McGowan Institute for Regenerative Medicine, [2]Department of Pathology, [3]Department of Bioengineering, [4]Pittsburgh Liver Research Center, University of Pittsburgh, Pittsburgh, PA

2.1 INTRODUCTION

Non-alcoholic steatohepatitis (NASH) is the leading causes of chronic liver disease in the world and is currently the second leading indication for liver transplantation in the United States (Mikolasevic et al., 2018; R. J. Wong et al., 2015; Younossi et al., 2016). Importantly, the prevalence of the non-alcoholic fatty liver disease (NAFLD) including NASH increases with age (Mikolasevic et al., 2018). Individuals over the age of 60 exhibit a 200% increase in liver triglyceride content compared to young individuals when matched for body mass index, fat percentage, physical activity, smoking, and medical history (K. F. Petersen et al., 2003). With an

aging population, the number of individuals requiring a liver transplant is expected to increase, while the number of healthy donor organs available for transplant is anticipated to decrease as hepatic steatosis risk factors, *e.g.* obesity and type-two diabetes mellitus, continue to rise, further exacerbating the disparities in liver transplantation (Mikolasevic et al., 2018).

The mechanism for developing age-related steatosis is not fully understood but was recently attributed to hepatocyte senescence driving a reduction in mitochondrial fatty acid metabolism (Ogrodnik et al., 2017). Progression of NAFLD/NASH in aged individuals may also be related to decreased transport of insulin across the sinusoidal endothelium (Mohamad et al., 2016), reduction in autophagic flux (Gonzalez-Rodriguez et al., 2014), or chronic low-level inflammation originating from adipose tissue or local immune cells (Duval et al., 2010; Kumar et al., 2013), leading to the build-up of toxic free fatty acids in the liver.

Hepatic macrophages are strongly implicated in the development and progression of NAFLD/NASH (Bieghs, Rensen, Hofker, & Shiri-Sverdlov, 2012; Lanthier, 2015; Tacke & Zimmermann, 2014). Liver-resident macrophages, known as Kupffer cells (KCs), are the largest population of immune cells in the liver, comprising up to one-third of the non-parenchymal cell population. KCs are derived from the embryonic yolk sac and are maintained by self-renewal. Alternatively, monocyte-derived macrophages have been found to hone to the liver under chemotactic stimulus (Ju & Tacke, 2016). When mice were fed a high-fat or high-cholesterol diet, the balance of hepatic macrophages was found to shift toward monocyte-derived cells ($F4/80^{lo}CD68^{-}CD11b^{hi}$) and away from the resident KC population ($F4/80^{hi}CD68^{+}CD11b^{lo}$) (Nakashima et al., 2016). Hepatic macrophages are known to secrete IL-1β, TNFα, and CCL5 during steatosis, which may promote apoptosis of hepatocytes, as well as CCL2 (MCP-1), which can also be produced by hepatocytes to recruit monocytes (Tacke, 2017). The production of

CCL2 is regulated by the canonical NFκB signaling pathway and is inversely correlated to LXR-RXR signaling in both macrophages and hepatocytes (Chinenov, Gupte, & Rogatsky, 2013).

The present study characterizes hepatic steatosis in aged mice and identifies phenotypical and functional changes in the liver macrophage compartment, toward a better understanding of mechanisms underlying the development of fatty liver disease and inflammation in the natural aging process.

2.2 METHODS

Animal Models. The Institutional Care and Use Committee (IACUC) of the University of Pittsburgh approved all mouse experiments. C57BL/6 wild-type (WT) mice were obtained at 2-months and 18-months of age from the National Institute of Aging (NIA) Rodent Colony (Charles River Laboratories, Wilmington, MA), where they were maintained on NIH 31 diet (Ziegler Bros, Inc. Garners, PA) and used for experiments one month after arrival. CCR2 knockout mice (B6.129S4-CCr2<tm1lfc>) or WT controls were obtained from The Jackson Laboratory (Bar Harbor, ME), where they were maintained on JL Rat and Mouse Auto 6F 5K52 feed (LabDiet, St. Louis, MO) as retired breeders (7-8 months of age), and were then aged in-house at the University of Pittsburgh for an additional 11-12 months, where they were maintained on Prolab Isopro RMH 3000 feed (LabDiet).

Female mice were included exclusively in this study, as sex-specific differences in the age of onset of NAFLD/NASH have been noted in the literature and (Ballestri et al., 2017). Females are more likely to develop NAFLD/NASH with aging and post-menopause, while males are less well associated with age as a risk factor for developing NAFLD/NASH (Ballestri et al.,

2017). Mice were maintained on a standard 12-hour light and 12-hour dark system at the University of Pittsburgh specific-pathogen free animal facility. Mice were housed in Optimice cages (AnimalCare Systems, Centennial, CO) with Sani-Chip Coarse bedding (P. J. Murphy, Montville, NJ) and provided *ad libitum* access to water and standard mouse chow (LabDiet, St. Louis, MO, Purina ISO Pro Rodent 3000). Mice were provided huts and running wheels for enrichment.

Harvest of liver tissues. Mice were weighed and sacrificed by CO_2 inhalation followed by cervical dislocation, in accordance with University of Pittsburgh IACUC standards. Livers were excised and rinsed in PBS. Liver mass was recorded. Small pieces of liver were dissected and (a) fixed in 2% paraformaldehyde (Acros Organics, Fisher Scientific, Pittsburgh, PA) for 2 hours, followed by 60% sucrose (Fisher Scientific, Pittsburgh, PA) overnight, then embedded in Optimal Cutting Temperature (Fisher Scientific, Pittsburgh, PA), or (b) fixed in 10% neutral buffered formalin (Fisher Scientific, Pittsburgh, PA) and embedded into paraffin blocks by the McGowan Institute for Regenerative Medicine histology core, or (c) snap frozen in liquid nitrogen and stored at -80 degrees Celsius for later analysis of RNA, protein, or lipids.

Primary liver cell isolation. Primary hepatocytes were isolated using a two-step collagenase perfusion (Overturf et al., 1996). Briefly, following general anesthesia induction, a catheter was inserted into the portal vein or inferior vena cava and 0.3 mg/ml collagenase II (Worthington, Lakewood, NJ) was circulated through the liver. Digested livers were placed in Dulbecco's modified Eagle's medium (DMEM) with 10% fetal bovine serum (Corning, Tewksburg, MA) passed through 100 and 70μm cell strainers and washed twice using low-speed centrifugation (50xg for 3 min) to remove non-parenchymal cells (NPCs). Hepatocyte viability, determined by trypan blue staining, was typically >80%, with purity >90%. Hepatocytes were

stored in RNA-later (Fisher Scientific, Pittsburgh, PA) or radioimmunoprecipitation assay buffer (RIPA, 1% IgePAL, 0.5% sodium deoxycholate, 0.1% SDS, Sigma-Aldrich, St. Louis, MO, with Pierce protease and phosphatase inhibitor mini tablet, ThermoScientific, Waltham, MA) at -20 degrees Celsius for RNA/protein analysis at a later time. NPCs were used for flow cytometry (see supporting methods) or were further purified to collect hepatic macrophages. Briefly, NPCs were blocked with Fc receptor (1:100, rat anti-mouse CD16/32, BD Biosciences, San Jose, CA), stained with F4/80-PE (1:20, rat anti-mouse (BM8), eBioscience, ThermoFisher Scientific, Waltham, MA), and incubated with anti-PE microbeads (1:10, Miltenyi Biotec, Auburn, CA). Cells were applied to LS columns on the QuadroMACS separator (Miltenyi Biotec, Auburn, CA) and washed three times to remove non-tagged NPCs. $F4/80^+$ cells were eluted and counted. Viability of collected $F4/80^+$ cells was typically >85%, with purity >95%.

Statistical analysis. When comparing young and aged samples (WT or KO), a two-tailed Student's t-test was used, unless otherwise stated. One-way ANOVA was used to compare polarization of macrophages, with Tukey's multiple comparisons, unless otherwise stated. Two-way ANOVA was used to detect differences in the proportions of CD11b and CD68 populations between young and aged mice, with Sidak's multiple comparisons test. P values < 0.05 were considered significant.

Additional methods can be found **Appendix A (page 110)**.

2.3 RESULTS

Aged mice exhibit increased body weight, liver weight, and elevated serum ALT levels

Aged female mice (19-months-old) obtained from the National Institute of Aging animal repository showed a 1.3-fold increase in total body weight and liver weight compared to young female mice (3-months-old) (Table 1). The liver to body weight ratio remained proportional between the age groups (4.7 – 5.0% total body mass).

To evaluate hepatic injury and function, serum levels of alanine aminotransferase (ALT), aspartate aminotransferase (AST), bilirubin, and albumin were measured in the aging female mice (Table 1). There were marginal but significant increases in serum ALT and AST while serum albumin and bilirubin were unchanged, suggesting some level of hepatocyte injury. Furthermore, serum cholesterol was increased significantly while serum triglyceride levels were unchanged.

Table 1. Body Weight, Liver Biochemistry, and Serum Lipids in Young and Aged WT Mice (NIA)

	Young (3 mo., n=5-7)	**Aged** (19 mo., n=5-6)	**Significance**
Body weight (grams)	22.0 ± 1.4	29.2 ± 4.0	***p<0.01***
Liver weight (grams)	1.04 ± 0.2	1.33 ± 0.2	***p<0.05***
Liver:Body weight ratio	4.72 ± 0.9	4.98 ± 0.4	*p=0.62*
Serum Alanine Aminotransferase (IU/L)	23.0 ± 5.5	45.3 ± 24	***p<0.01***
Serum Aspartate Aminotransferase (IU/L)	40.3 ± 7.6	62.0 ± 27	***p=0.05***
Serum Bilirubin (mg/dL)	0.21 ± 0.1	0.17 ± 0.1	*p=0.22*
Serum Albumin (g/dL)	2.50 ± 0.3	2.48 ± 0.2	*p=0.78*
Serum Cholesterol (mg/dL)	59.6 ± 11	78.8 ± 28	***p=0.05***
Serum Triglycerides (mg/dL)	69.6 ± 28	66.7 ± 20	*p=0.88*

Livers from aged mice show signs of steatosis in the absence of injury

Macroscopically, livers from 19-month-old mice appear similar to those from 3-month-old mice, with no evidence of gross tumor, fibrosis or cirrhosis, although aged livers are larger with slight pallor (Figure 5A). Microscopically, the aged livers showed modest microvesicular steatosis both by Oil Red O staining and by H&E (Figure 5B).

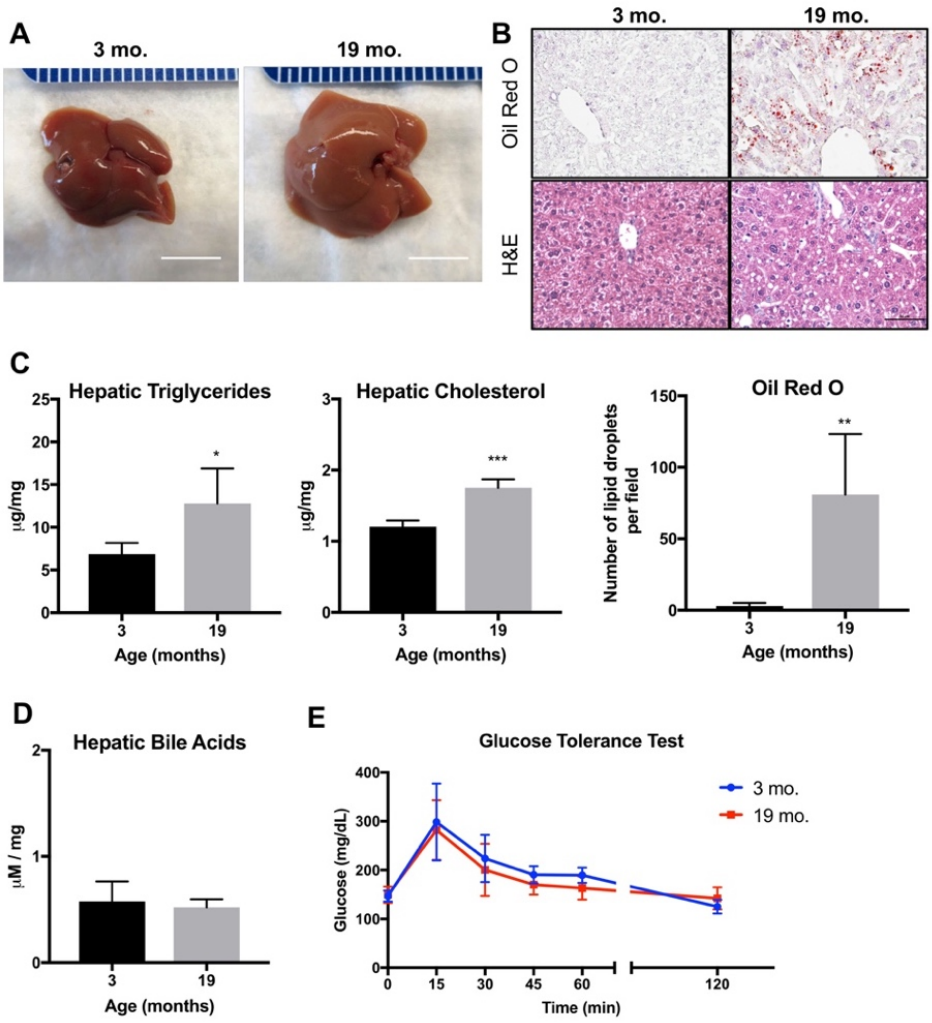

Figure 5. Aged livers exhibit signs of steatosis.

(A) Representative photos of 3-month-old and 19-month-old livers, scale bar: 1cm. (B) Representative images of Oil Red O and H&E staining demonstrate an increase in hepatic lipids in 19-month-old livers (quantification bottom, n=4-5, ** $p<0.01$, scale bar: 50µm). (C) Quantification of hepatic triglycerides and cholesterol per milligram of liver tissue (n=4, *$p<0.05$, *** $p<0.001$). (D) Quantification of total hepatic bile acids (n=3). (E) Glucose tolerance test (n=4) showed no change in fasting glucose levels or blood glucose over time Data are displayed as mean ± standard deviation.

To further investigate the lipid content in the aged livers, the amount of total cholesterol and triglycerides were measured in mice fasted for six hours to control for dietary intake. Aged livers showed a 1.5-fold and a significant increase in cholesterol content per milligram of liver weight and a 1.9-fold and a significant increase in triglyceride content per milligram of liver tissue when compared to the young livers (Figure 5C). The types of fatty acids composing the triglycerides and their relative proportions were unchanged between the age groups (Table 2). In addition, the concentration of total bile acids in the livers was similar between the two age groups, suggesting no deficits in bile acid production and metabolism or signs of cholestasis (Figure 5D). TUNEL staining showed minimal apoptotic hepatocytes or non-parenchymal cells, and picrosirius red staining also showed lack of any fibrosis in either young or aged liver samples (Figure 6).

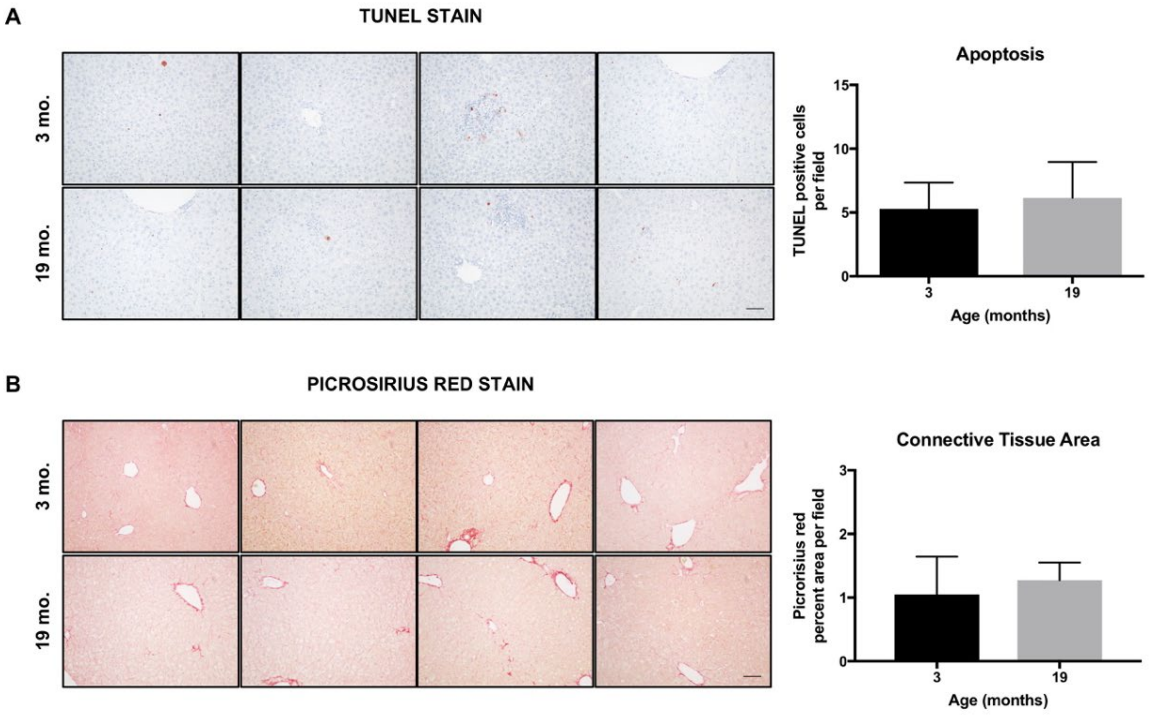

Figure 6. Apoptosis and fibrosis in young and aged livers.

(A) Representative images of TUNEL staining for apoptosis (red) counterstained with hematoxylin (blue) to visualize nuclei. Cells undergoing apoptosis were identified in both young and aged livers at similar frequencies and in a variety of cell populations including hepatocytes, non-parenchymal cells, and clusters of immune cells (n=5). (B) Representative images of Picrosirius red staining for connective tissue (red). Most connective tissue was identified around large vasculature with no quantitative difference between the young and aged livers (n=4). Scale bar = 50 μm. Data are displayed as mean ± standard deviation.

In order to assess potential confounding effects of metabolic syndrome on lipid storage in the liver, an intraperitoneal glucose tolerance test was performed on the 3-month-old and 19-month-old mice after fasting for six hours. Basal glucose concentrations were similar between the age groups and both age groups metabolized glucose comparably, suggesting preserved glucose tolerance (Figure 5E). Overall, these studies demonstrate basal hepatic steatosis in the unmanipulated, aged mice without notable differences in bile acid and glucose homeostasis.

Table 2. Fatty Acid Profile of Triglycerides in Young and Aged Livers

Fatty Acids	**3 mo.** (% total)	**19 mo.** (% total)	**Significance**
14:0	0.62 ± 0.05	0.53 ± 0.04	***p<0.05***
16:0	24.65 ± 1.34	23.73 ± 1.75	p=0.44
16:1	2.20 ± 0.37	2.22 ± 0.35	p=0.94
18:0	3.35 ± 0.36	3.34 ± 0.49	p=0.98
18:1ω9	35.59 ± 1.66	36.62 ± 1.80	p=0.43
18:1ω7	2.04 ± 0.15	1.87 ± 0.13	p=0.13
18:2	20.17 ± 1.26	21.45 ± 1.35	p=0.21
18:3ω6	0.39 ± 0.06	0.49 ± 0.07	p=0.07
18:3ω3	0.84 ± 0.10	0.87 ± 0.14	p=0.76
20:3ω6	0.74 ± 0.11	0.64 ± 0.04	p=0.10
20:4	1.58 ± 0.13	1.67 ± 0.36	p=0.65
20:5	0.67 ± 0.14	0.79 ± 0.21	p=0.38
22:4ω6	0.48 ± 0.04	0.51 ± 0.11	p=0.61
22:5ω6	0.21 ± 0.04	0.15 ± 0.04	p=0.13
22:5ω3	1.11 ± 0.19	0.84 ± 0.18	p=0.09
22:6	5.44 ± 0.89	4.35 ± 0.47	p=0.07

Livers from aged mice show signs of spontaneous inflammation in the absence of injury

We next assessed the aging livers for the presence of any inflammation. Whole liver tissue, hepatocytes, and hepatic macrophages were isolated from the 3-month-old and 19-month-old mice. qRT-PCR showed an increase in the chemokine CCL2 in aged whole liver samples (+3-fold) and aged hepatocytes (+10-fold), but no change in aged $F480^{+}$ hepatic macrophages compared to young samples (Figure 7A).

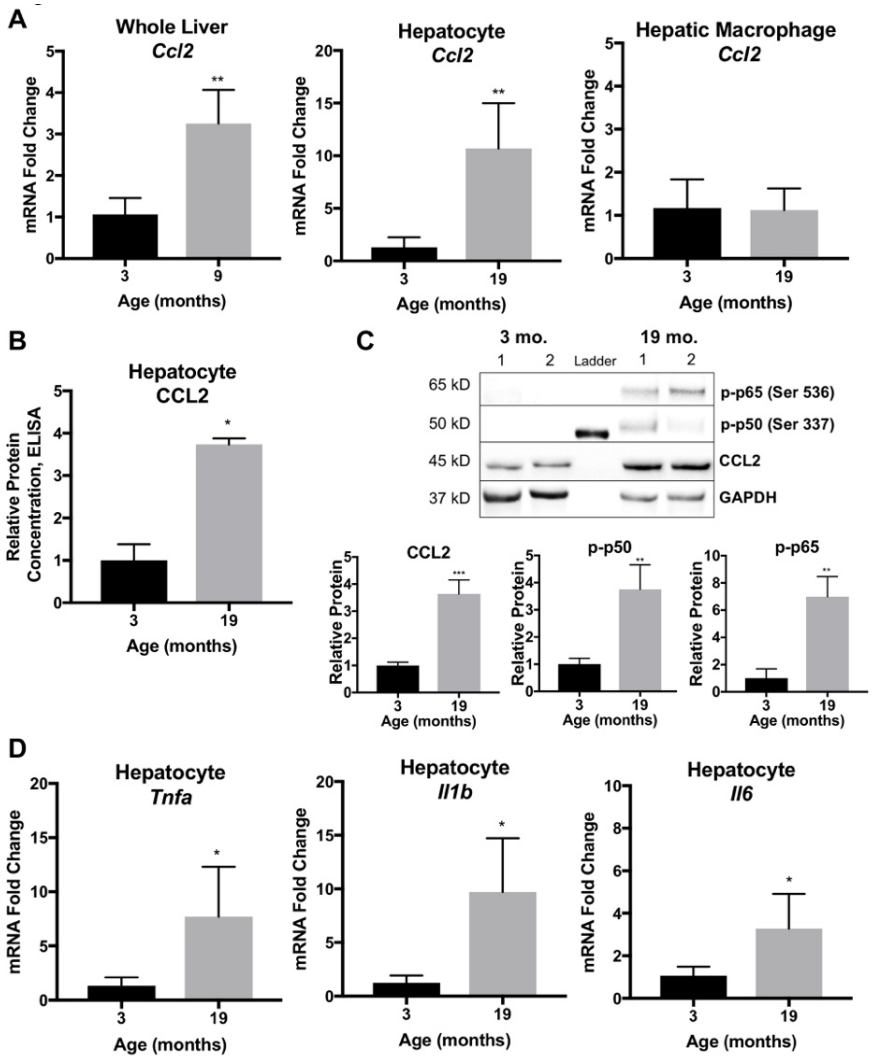

Figure 7. Aged livers have robust inflammatory signatures.

(A) Significant increase in mRNA levels of CCL2 were detected in 19-month-old whole livers and hepatocytes, but not hepatic macrophages, normalized to beta-actin housekeeping gene and 3-month-old controls (n=3-4, **p<0.01) (B) ELISA for CCL2 in hepatocyte protein lysates normalized to 3-month-old controls (n=3, **p<0.01) (C) Representative western blot and quantification for phosphorylated p65 (Ser 536), phosphorylated p50 (Ser 337), CCL2, and GADPH normalized to 3-month-old controls (n=3, **p<0.01, *** p<0.001) (D) Significant increases in mRNA levels of TNF-alpha, interleukin-1 beta, and interleukin-6, were detected in 19-month-old hepatocyte cell fractions, normalized to beta-actin housekeeping gene and 3-month-old controls (n=6, *p<0.05). Data are displayed as mean ± standard deviation.

Western blot and ELISA confirmed an increase in protein levels of CCL2 (+3.6-fold) from aged hepatocyte fraction lysates, as well as phosphorylated members of the NFκB canonical signaling pathway (p-p65 Ser 536, +6.9-fold and p-p50 Ser 337, +3.7-fold), suggesting activation of inflammatory gene signatures in hepatocytes (Figure 7B,C). Additional inflammatory genes were found to be upregulated in the aged samples, including TNFα, IL-1β, and IL-6 (Figure 7D). Taken together, inflammatory chemokines and cytokines were detected in the aged liver hepatocyte cell fractions at both the protein and RNA levels.

Macrophages increase in the aged liver and retain polarization and phagocytic capacity in vitro

The increase of chemokine CCL2 levels prompted a closer look at the macrophage content of the aged livers. Flow cytometry of the non-parenchymal cell fraction revealed a significant increase in F4/80^{+} macrophages in the aged liver (Figure 8A), which was confirmed by histological staining (Figure 8B). A time course of F4/80^{+} cell content showed stable levels of hepatic macrophages at 3, 7, and 15 months of age, a significant increase at 19 months, and further elevation at 24 months of age (Figure 9). By 24 months of age, the majority of mice developed either tumors or extensive NASH and were thus were excluded from further investigation as part of the current study.

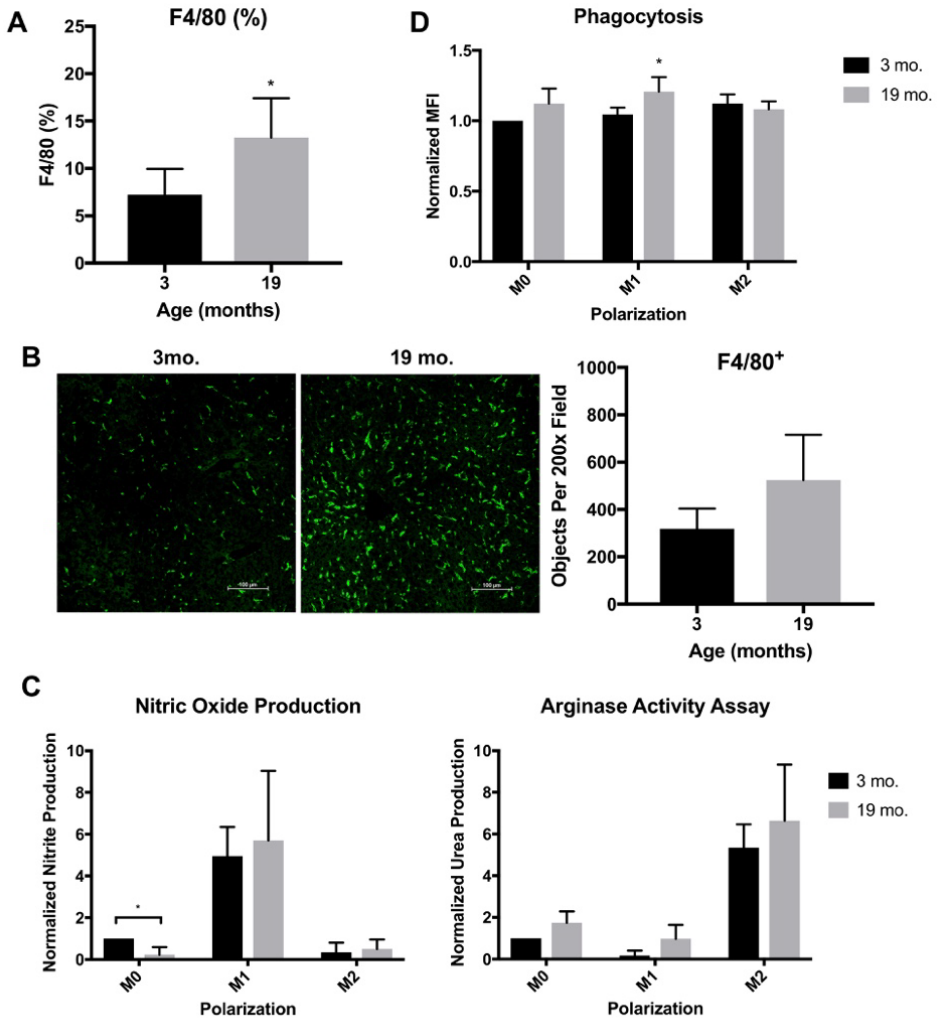

Figure 8. Macrophages accumulate in the uninjured, aged liver and exhibit similar polarization capacity.

(A) Percentage of total F4/80$^+$ cells in the non-parenchymal cell fraction determined by flow cytometry (n=5, *p<0.01). Gating strategy is available in Supporting Figure S2. (B) Histological immunostaining for F4/80 (green) further demonstrated increase in macrophages across 19-month-old liver sections (n=5), scale bar: 100μm (C) F4/80$^+$ cells isolated from 3-month-old and 19-month-old livers were treated with "M1" stimulus (20 ng/ml IFNγ and 100 ng/ml LPS) or "M2" stimulus (20 ng/ml IL-4) and showed effective polarization. Aged M0 cells produced less nitrite than young M0 (n=4-5, *p<0.01), normalized for nuclei count, while M2 polarization was preserved in all treatments and age groups (D) Phagocytosis of FITC-labeled *e.coli* particles was preserved with aging, where aged M1 was significantly greater than aged M2 (n=3, *p<0.05) and young M1 (p=0.054). Data are displayed as mean ± standard deviation.

Macrophages can polarize to a spectrum of phenotypes, which exhibit specific cellular functions. Proinflammatory macrophages are commonly referred to as classically activated or "M1" polarized cells, whereas anti-inflammatory or pro-regenerative macrophages are referred to as alternatively activated or "M2" polarized cells, both derived from an "M0" inactive state (Murray et al., 2014). The $F4/80^+$ hepatic macrophages isolated from 3-month-old and 19-month-old mice were cultured and stimulated *in vitro* with M1-polarizing stimuli (IFNγ and LPS) or M2-polarizing stimuli (IL-4) to evaluate the ability of the cells to effectively transition to a variety of phenotypes. After treatment with the polarizing cytokines for 12 hours, both young and aged $F4/80^+$ cells were able to polarize effectively, as measured by nitric oxide production for M1 polarization and urea production by arginase-1 enzyme activity for M2 polarization (Figure 8C). The baseline production of nitric oxide was significantly lower in the aged M0 group compared to young M0 group. The $F4/80^+$ cells from young and aged livers were able to phagocytose FITC-labeled *e. coli* particles to a similar extent in both M0 and M2 treatments, with a slight increase in the aged M1 group (Figure 8D).

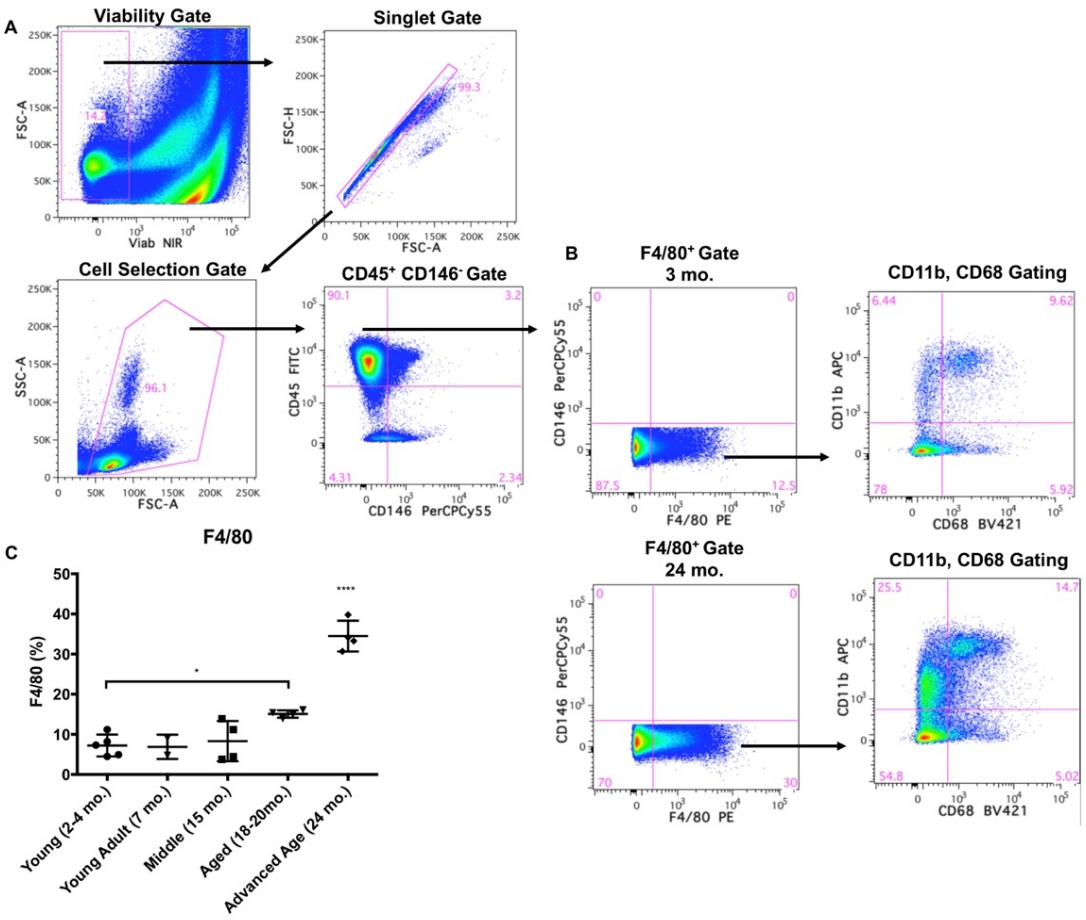

Figure 9. Gating strategy and time course of F4/80^{+} flow cytometry.

(A) Gating strategy for flow analysis was performed in FlowJo. The viable cell population was selected by exclusion of fixable live-dead near-IR viability dye and single cells were selected on the axis of FSC-H vs. FSC-A. Debris was excluded then CD45^{+}CD146^{-} immune cells were selected (further excluding LSECs and stellate cells). (B) The proportion of F4/80^{+} cells were measured from live, single, CD45^{+}CD146^{-} events and stratified by CD11b and CD68 expression on the fixed, permeabilized cells for 3-month-old and 19-month-old samples. (C) Time course of F4/80^{+} expression measured by flow cytometry.

In addition, the mean fluorescence intensity of liver arginase staining was dramatically increased in the aged M2-polarized macrophages compared to young M2-polarized macrophages, while staining for inducible nitric oxide (iNOS) was dim in all samples regardless

of treatment (Figure 10). Thus overall, the aged hepatic macrophages retained polarization and phagocytosis function *in vitro*, with a predisposition toward M2 polarization characteristics.

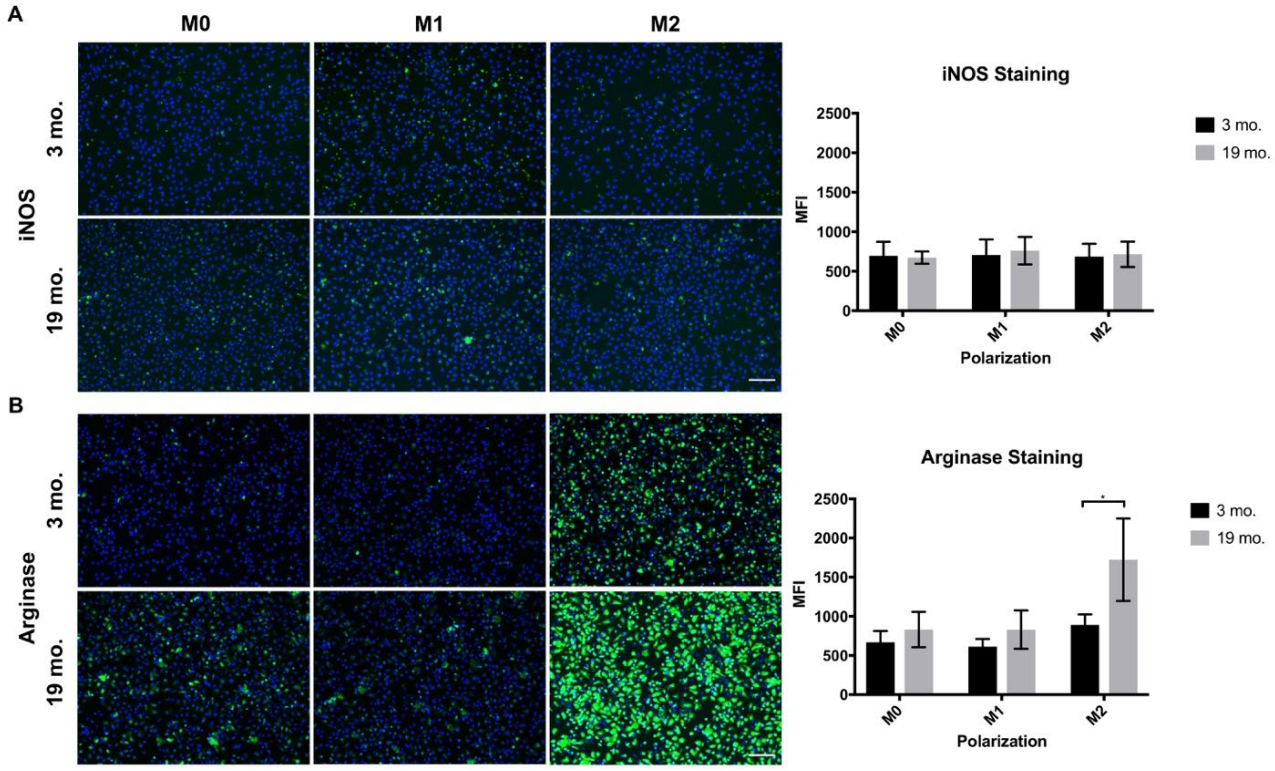

Figure 10. Macrophage polarization staining in vitro.

(A) iNOS staining on cultured hepatic macrophages (F4/80^{+} non-parenchymal cells) after 12-hour treatment with media (M0: RPMI + 10% fetal bovine serum + 1% pen-strep), or media supplemented with polarization cytokines (M1: LPS 100 ng/ml, IFNγ 20 ng/ml or M2: IL-4 20 ng/ml). No significant difference was detected in the mean intensive fluorescence (MFI) for iNOS (n=4). (B) Liver arginase staining on cultured hepatic macrophages that received treatment with media (M0: RPMI + 10% fetal bovine serum + 1% pennstrep), or media supplemented with polarization cytokines (M1: LPS 100 ng/ml, IFNγ 20 ng/ml or M2: IL-4 20 ng/ml). The MFI of arginase was significantly increased in M2-treated hepatic macrophages from 19-month-old mice compared to those from 3-month-old mice (n=4). Scale bar = 100 μm.

Livers from aged mice have increases in CD11b$^+$ macrophage populations

In order to further profile the aged liver macrophage compartment, expression levels of CD11b and CD68 were examined by flow cytometry, as these markers have been used as indicators of macrophage origin from bone marrow or tissue respectively (Holt et al., 2008; Kinoshita et al., 2010). Aged livers had a significant increase in the CD68$^-$CD11b$^+$ monocyte-derived population, in both percentage and absolute number of F4/80$^+$ cells (Figure 11A). No change was observed in the CD68$^+$CD11b$^-$ population, reported by others to be Kupffer cells, while there was a marginal but insignificant increase in the CD68$^+$CD11b$^+$ population. The increase in F4/80$^+$CD11b$^+$ hepatic macrophages, but not F4/80$^+$CD68$^+$ Kupffer cells, in aged livers was also confirmed by histological staining (Figure 11B).

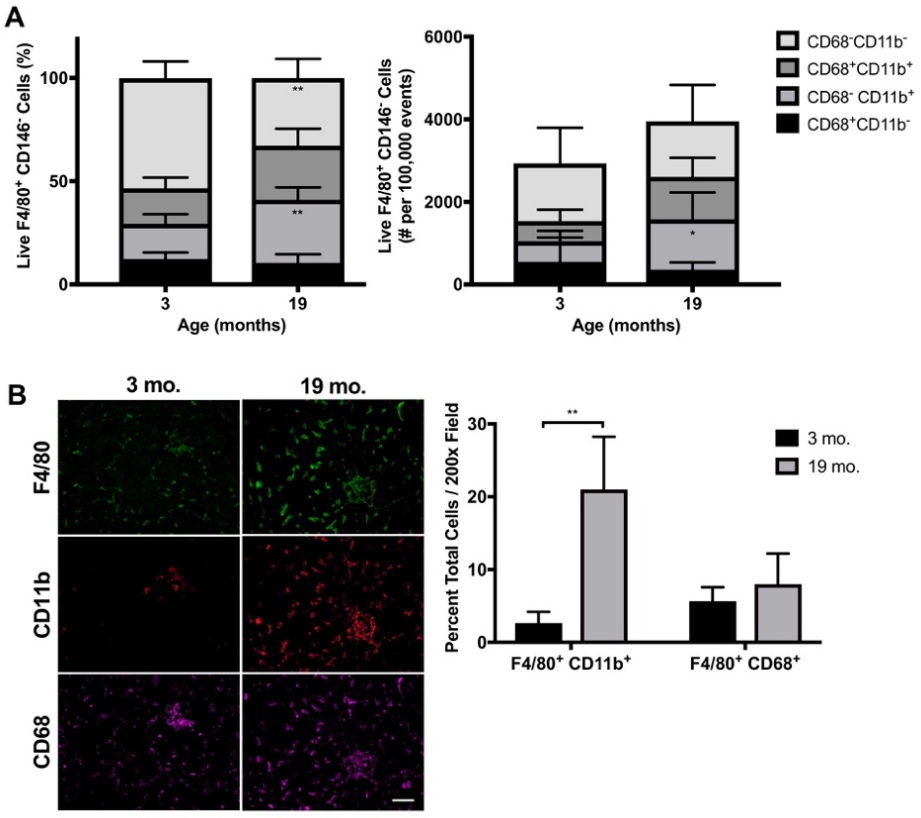

Figure 11. Macrophages in aged livers have increased CD11b$^+$ subsets.

(A) Proportion and number of CD11b and CD68-expressing F4/80$^+$ cells detected by flow cytometry showed an increase in CD11b$^+$ macrophages in 19-month-old livers (n=5, *p<0.05, **p<0.01). Gating strategy is available in Supporting Figure S2. (B) Increases in F4/80$^+$ CD11b$^+$ macrophages were confirmed with histological immunostaining (n=5, *p<0.05, **p<0.01), scale bar: 50μm. Data are displayed as mean ± standard deviation.

Altogether, these data suggest that the increase in hepatic macrophages in aged livers is derived primarily from infiltrating monocytes and not due to an expanding resident Kupffer cell population, consistent with the detected increase in monocyte chemoattractant protein (CCL2) and the observations of others in models of steatosis (Nakashima et al., 2016).

CCL2-CCR2 inhibition reduces inflammation and steatosis in aged livers, but does not prevent accumulation of CD11b^{+} macrophages

To test the hypothesis that inhibiting CCL2 signaling would reduce inflammation and steatosis in aging livers, female mice with global CCR2 knockout (KO) or wild-type (WT) controls were obtained from Jackson Laboratories and aged in-house. The aged WT mice had a 1.6-fold increase in body weight compared to their young controls (Table 3), while the aged KO mice had a 1.2-fold increase in body weight compared to their young controls (Table 4). In addition, the aged KO mice had elevated serum cholesterol levels compared to the young KO mice. Levels of serum ALT, AST, albumin, and triglycerides were similar between the groups.

Table 3. Body Weight, Liver Biochemistry, and Serum Lipids in Young and Aged WT Mice (JAX)

	Young WT (3 mo., n=5)	**Aged WT** (19 mo., n=8)	**Significance**
Body weight (grams)	21.4 ± 1.8	33.2 ± 6.9	***p<0.01***
Serum Alanine Aminotransferase (IU/L)	21.2 ± 8.4	31.8 ± 10	*p=0.09*
Serum Aspartate Aminotransferase (IU/L)	43.8 ± 10	55.1 ± 22	*p=0.31*
Serum Albumin (g/dL)	2.68 ± 0.2	2.47 ± 0.1	*p=0.17*
Serum Cholesterol (mg/dL)	75.0 ± 0.5	63.0 ± 8.0	*p=0.13*
Serum Triglycerides (mg/dL)	63.0 ± 16	57.8 ± 32	*p=0.76*

Of note, three mice in the aged WT cohort were excluded from study: one showed advanced fatty liver disease with hepatocyte ballooning characteristic of NASH, another had extensive tumorigenesis, and one died prematurely. No mice in the aged KO group exhibited these pathological signs.

Table 4. Body Weight, Liver Biochemistry, and Serum Lipids in Young and Aged CCR2 KO Mice (JAX)

	Young KO (3 mo., n=4)	**Aged KO** (19 mo., n=10)	**Significance**
Body weight (grams)	23.4 ± 2.2	27.3 ± 3.2	***p<0.05***
Serum Alanine Aminotransferase (IU/L)	24.5 ± 10	23.3 ± 5.6	*p=0.77*
Serum Aspartate Aminotransferase (IU/L)	46.0 ± 18	48.6 ± 13	*p=0.77*
Serum Albumin (g/dL)	2.47 ± 0.1	2.50 ± 0.1	*P=0.72*
Serum Cholesterol (mg/dL)	53.0 ± 2.8	70.7 ± 2.9	***p<0.01***
Serum Triglycerides (mg/dL)	46.3 ± 12	46.2 ± 17	*p=0.99*

Both 19-month-old WT and KO cohorts had increases in lipid accumulation compared to their respective 3-month-old control, as shown by H&E and Oil Red O staining, however fat accumulation was notably less pronounced in the aged KO group when compared to the aged WT (Figure 12A). The concentration of hepatic lipids was measured in the 3-month-old and 19-month-old WT and KO mice after fasting mice for six hours. The 19-month-old WT mice had a significant and a 1.5-fold increase in the triglyceride content compared to the 3-month-old WT mice, whereas the KO groups were not significantly different (Figure 12B, top). Intriguingly, no differences in cholesterol content was detected between the young and old groups in both the WT and KO in this strain of mice (Figure 12B, bottom).

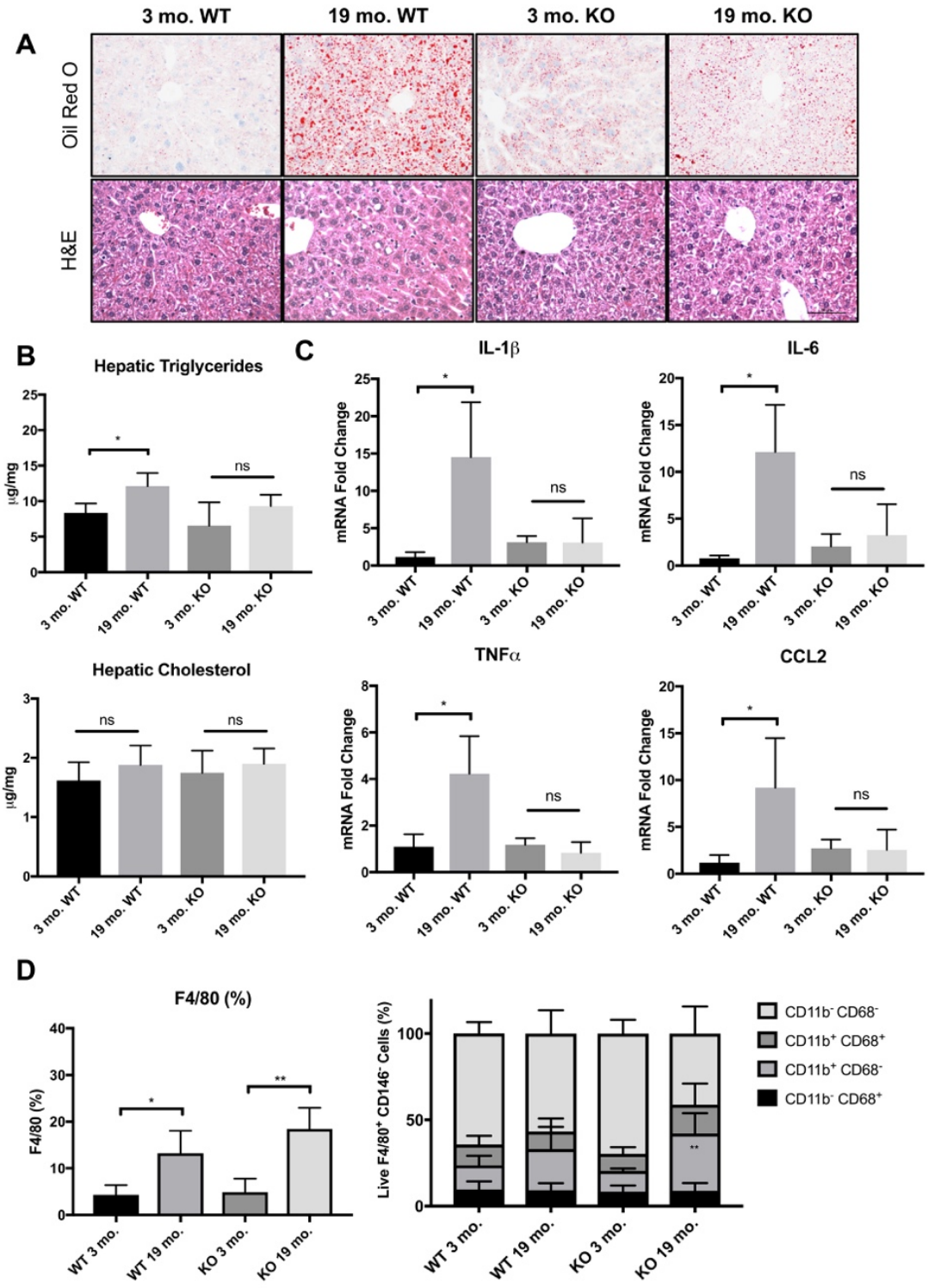

Figure 12. Aged CCR2 knockout mice exhibit reduced steatosis and inflammation, but no change in accumulated macrophage populations.

(A) Representative images of Oil Red O and H&E staining, scale bar: 50μm. (B) Quantification of hepatic triglycerides and cholesterol per milligram of liver tissue (n=4-5, *p<0.05). (C) Significant increases in mRNA levels of interleukin-1 beta, interleukin-6, TNF-alpha, and CCL2 in aged WT compared to young WT normalized to beta-actin housekeeping gene (n=4-5, *p<0.05, ** p<0.01). (D) Percentage of total F4/80, CD11b, and CD68-expressing cells in the non-parenchymal cell fraction determined by flow cytometry (n=4-5, *p<0.05, **p<0.01).

The inflammatory gene signature of hepatocyte cell fractions isolated from 3-month-old and 19-month-old WT and KO mice was evaluated by qRT-PCR. The 19-month-old WT cells had a significant increase in *Il1β, Il6, Tnfα, and Ccl2* transcripts compared to the 3-month-old WT group, while there were no changes in inflammatory gene expression between the 3-month-old and 19-month-old KOs (Figure 12C). Despite the reduction in the inflammatory gene signature by hepatocytes from aged CCR2 knockout mice, the levels of $F4/80^+$ cells and specifically $F4/80^+CD11b^+$ macrophage subsets were elevated in both WT and KO 19-month-old livers, compared to their 3-month-old counterparts, as determined by flow cytometry (Figure 12D). Taken together, these data suggest that inhibiting CCR2 signaling is sufficient to reduce hepatic triglyceride content and inflammatory gene expression but did not prevent the accumulation of $CD11b^+$ macrophages in the aging liver.

Since inhibiting CCL2-CCR2 was insufficient to prevent macrophage accumulation in aged livers, levels of endotoxin and bacterial DNA for 16s rRNA in hepatic blood were measured to test for "leaky gut syndrome," as this has been implicated in the acquisition of age-related inflammation (Thevaranjan et al., 2017). However, no differences in serum endotoxin or 16s rRNA were detected in hepatic blood (Figure 13).

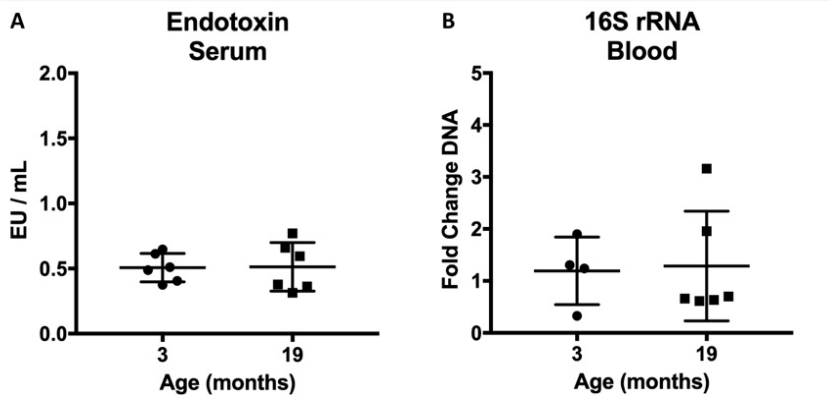

Figure 13. Endotoxin and 16S rRNA levels in aged hepatic blood.

(A) Concentration of bacterial endotoxin in serum isolated from coagulated blood drawn sterilely from the inferior vena cava and portal vein from young and aged mice showed no difference (n=6). (B) qPCR was performed on DNA isolated from non-coagulated blood drawn sterilely from the inferior vena cava and portal vein and showed no differences in 16S rRNA between young and aged mice (n=4-6).

RNA-Seq analysis demonstrates robust inflammatory and metabolic changes in aged livers beyond the CCL2-CCR2 signaling paradigm

Finally, RNA-Seq was performed as an unbiased screen to further elucidate mechanisms underlying the onset of inflammation and steatosis in aged livers. Independent samples of hepatocytes were enriched from 3-month-old and 19-month-old wild-type mice (National Institutes of Aging, n=3) by two-step collagenase perfusion after fasting for six hours. Albumin was detected as the most highly expressed transcript across all samples, demonstrating hepatocyte specificity.

In total, 296 genes were differentially upregulated, and 74 genes were differentially downregulated between the 3-month-old and 19-month-old samples (fold change ±2, false discovery rate p-value <0.05, Figure 14A). Among the most highly differentially expressed genes were chemokines *Cxcl7* (+34.5-fold), *Cxcl13* (+8.1-fold), *Ccl22* (+6.8-fold), *Ccl5* (+6.3-

fold), and *Ccl6* (+2.1 fold). Other chemokines that were upregulated, however insignificantly, included *Ccl3* (+16.7-fold, *p=0.1*) and *Ccl2* (+2.4-fold, *p=0.15*). While an increase in the proliferation/ploidy gene *E2f7* (+9.5-fold) was detected, no changes in senescence associated genes (*p16, p21, p53*) were found. A complete list of differentially expressed genes can be found in **Appendix B (page 117)**.

A

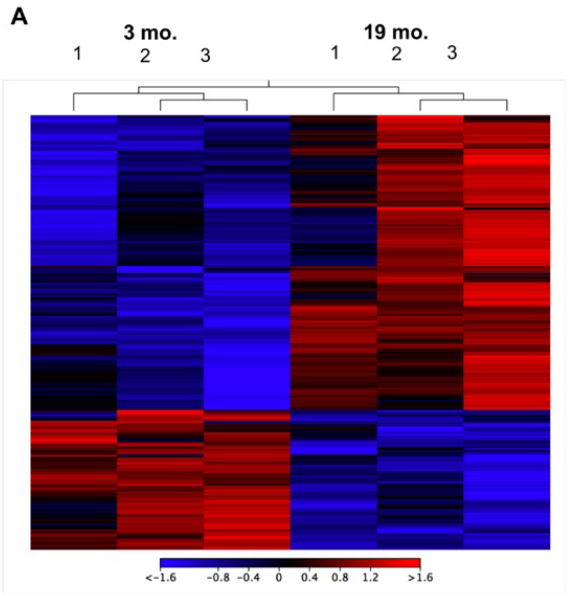

B

Pathway Name	Activation	Overlap	P-value
Melatonin Degradation I	Down	24.4% (10/41)	1.97E-07
Granulocyte Adhesion and Diapedesis	Undet.	15.6% (14/90)	2.96E-07
Superpathway of Melatonin Degradation	Down	22.7% (10/44)	4.03E-07
Nicotine Degradation II	Down	20.9% (9/43)	3.26E-06
Leukocyte Extravasation Signaling	Up	11.7% (15/128)	4.54E-06
Nicotine Degradation III	Down	21.1% (8/38)	1.11E-05
Hepatic Stellate Cell Activation	Undet.	11.0% (13/118)	3.87E-05
Complement System	Undet.	23.1% (6/26)	8.41E-05

Figure 14. RNA-Seq reveals robust changes in inflammatory and metabolic gene signatures of aged livers. (A) Heatmap demonstrates 296 genes were differentially upregulated and 74 genes were differentially downregulated between the 3-month-old and 19-month-old WT NIA hepatocyte samples (fold change ±2, false discovery rate p-value <0.05, n=3). (B) Ingenuity Pathway Analysis identified 25 canonical signaling pathways with overlapping gene features. The top eight most significantly affected pathways are listed in order of most significantly different (p-value). Activation (upregulated, downregulated, or undetermined), and the overlap (percent genes differentially expressed in the pathway) are listed.

Ingenuity Pathway Analysis (IPA) identified several pathways influenced by aging in the liver using stringent filters for species (mouse), tissue (liver), and confidence (experimentally observed), including downregulation of the melatonin degradation I pathway, super-pathway of

melatonin degradation, and nicotine degradation II/III pathway; upregulation of the leukocyte extravasation pathway; and changes in the granulocyte adhesion and diapedesis, hepatic stellate cell activation, and complement system pathways (Figure 14B).

Interestingly, when the pathways are viewed as interconnecting nodes, the inflammatory and metabolic changes are linked by suppression of FXR/RXR signaling, suggesting this transcription factor family may be a master regulator of several age-related gene expression changes in the liver and warrants further study (Figure 15).

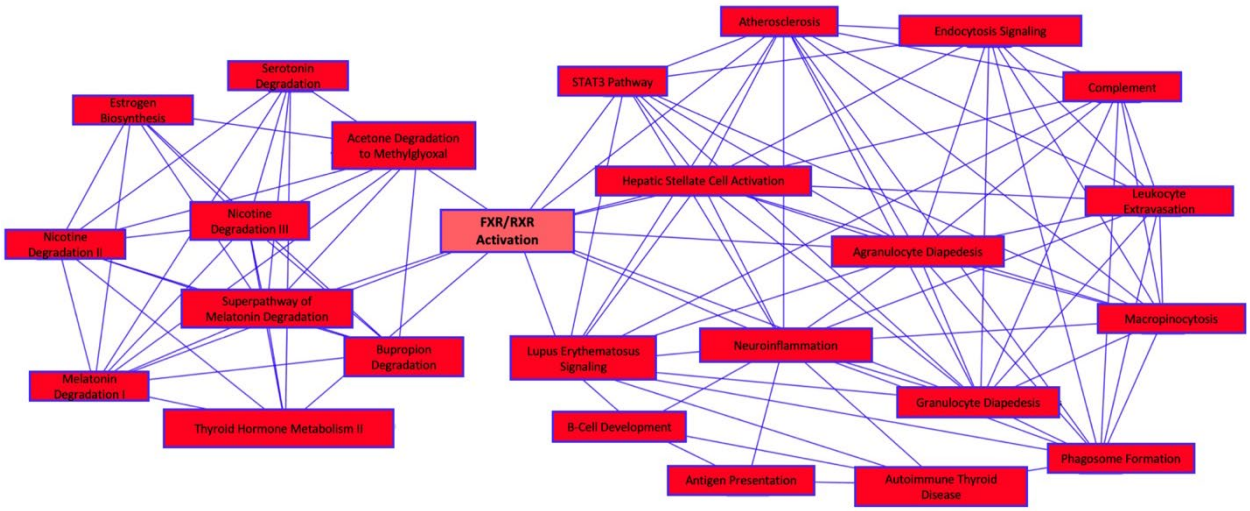

Figure 15. IPA Canonical Pathways Map.

Ingenuity Pathway Analysis (IPA) identified several pathways influenced by aging of the liver using stringent filters for species (mouse), tissue (liver), and confidence (experimentally observed), including melatonin degradation I, granulocyte adhesion and diapedesis, nicotine degradation II/III, leukocyte extravasation signaling, hepatic fibrosis / hepatic stellate cell activation, acetone degradation I, and complement system, which are connected by gene interactions. Inflammatory and metabolic pathways were linked by a decrease in FXR/RXR activation.

2.4 DISCUSSION

It is well established that body weight increases with age in mammals, as lipids move from subcutaneous to visceral and ectopic fat deposits in muscle, bone marrow, and the liver (Tchkonia et al., 2010). This accumulation of fat is thought to reduce muscle strength, lead to insulin resistance, decrease energy expenditure in brown adipose tissue, and impair the function of bone marrow stem cells (Palikaras et al., 2017). However, the molecular mechanisms coupling ectopic fat accumulation with aging remain obscure, and the influence of ectopic fat accumulation on liver function with aging has not been thoroughly studied.

In the present study, aged, 19-month-old female mice received from the National Institute of Aging (NIA) exhibited increased body weight, liver weight, serum alanine aminotransferase, hepatic triglycerides, inflammatory gene expression, and levels of $F4/80^+$ $CD11b^+$ macrophages when compared to their young, 3-month-old counterparts. The increase in hepatic lipids detected in the aged mice (186% increase in triglycerides) mimics what has been observed in elderly individuals in the absence of insulin resistance (K. F. Petersen et al., 2003). We also observed an increase in body weight, hepatic triglycerides, inflammatory gene expression, and levels of $F4/80^+$ $CD11b^+$ macrophages in a separate cohort of 19-month-old wild-type mice derived from Jackson Laboratories (JAX) compared to their young, 3-mont-old counterparts. Notably, the diet at Jackson Laboratories contains a higher percentage of calories provided fat (16% vs. 11%), which may account for some of the observed differences between the two cohorts (more robust steatosis, greater body weight in JAX mice).

Sublethal lipid overload in hepatocytes has very recently been shown to drive inflammation by the release of extracellular vesicles containing microRNAs, chemokines, and damage signals (Ibrahim, Hirsova, & Gores, 2018). Hepatocyte cell fractions from the aged

livers expressed a milieu of pro-inflammatory cytokines and chemokines, including TNFα, IL1β, IL6, and CCL2, as well as activation of canonical NFκB transcription factors p65 and p50. Work from other groups showed during high fat diet induced NASH, p65 was found to translocate to the nucleus of hepatocytes and drive production of TNFα and IL-6 downstream of high-mobility group box 1 (HMGB1) binding to toll-like receptor 4 (TLR4) (Li et al., 2011). Hepatocytes have also been shown to produce TNF, IL-6, and CCL2 in many additional contexts (LPS, bacterial hepatotoxin, hepatocyte growth factor, and infection with *P. gingivalis*) (Norris et al., 2014; Takano et al., 2012). Of note, the hepatocytes used in this study were purified by differential centrifugation and may contain 5-15% non-parenchymal cells, which could explain some of the observed changes in inflammatory gene expression. However, $F4/80^{+}CD11b^{+}$ hepatic macrophages purified by double magnetic selection showed an age-dependent reduction in transcript levels of IL1β and IL-6, and no change in TNFα levels (data not shown), suggesting these cells are not the source of inflammatory gene signatures. The influence of other non-parenchymal cells especially endothelial cells and stellate cells on the inflammatory gene expression in the aged liver remains an area of future study.

The accumulation of $F4/80^{+}CD11b^{+}$ macrophages in the aged liver presented here is a novel finding. To our knowledge, only one other study has systematically examined the effect of aging on liver-resident macrophages. Hilmer et al. determined that the number and basal activity of "Kupffer cells" was increased with old age in a rat model (Hilmer et al., 2007). However, this work was performed before the heterogeneity of liver macrophages was fully understood. Our work builds upon this study, demonstrating an increase in the total $F4/80^{+}$ macrophage pool, and specifically the cells that also express CD11b, thought to be derived from circulating monocyte progenitors. We found CD11b to be highly expressed on both small, motile

monocyte/macrophages organized in clusters as well as on spindle shaped cells throughout the aged hepatic parenchyma. CD11b functionally encodes integrin alpha M (ITGAM), one protein subunit of integrin alpha-M beta-2, also known as Mac-1 and complement receptor 3, which mediates leukocyte adhesion, migration, and phagocytosis (Solovjov, Pluskota, & Plow, 2005). The increase in CD11b expression may represent a phenotypical change in resident Kupffer cells, in addition to an influx in monocyte-derived macrophages. Fate tracing experiments using chimeric mice will be necessary to confirm the origin of the $F4/80^{+}CD11b^{+}$ hepatic macrophages.

As CCL2 was identified as a chemokine produced by aging hepatocytes that might influence macrophage dynamics, we sought to inhibit the CCL2-CCR2 signaling pathway in a natural aging mouse model. Inhibiting the CCL2-CCR2 axis by various means has been successful in ameliorating liver steatosis and inflammation in several models of NAFLD/NASH. Baeck et al. pharmacologically inhibited CCL2 with NOX-E36 in the methionine-choline deficient (MCD) diet induced NASH, and successfully diminished macrophage infiltration and steatohepatitis (Baeck et al., 2012). Another group found that CCL2 knockout mice on the MCD-diet had reduced fibrosis and inflammation in Balb/C strains (Galastri et al., 2012). Similarly, CCR2 knockout mice in the C57BL/6 background maintained on choline-deficient amino acid-defined (CDAA) diet showed reduced steatosis, inflammatory cell infiltration, and fibrosis compared to the controls (Miura, Yang, van Rooijen, Ohnishi, & Seki, 2012).

In the present study, aged CCR2 KO mice exhibited attenuated levels of liver triglycerides and significant decreases in the inflammatory gene signature of hepatocyte cell fractions compared to their young counterparts. Although hepatocytes produce CCL2, they are not known to express CCR2 (Seki, de Minicis, Inokuchi, et al., 2009), suggesting the changes in hepatocyte gene expression are secondary to other paracrine signaling pathways. This may be

related to inhibiting the binding of other CCR2 ligands such as CCL8, CCL7, and CCL12 in adipose tissue, stellate cells, or hepatic macrophage populations (Seki, de Minicis, Inokuchi, et al., 2009; Tsou et al., 2007). Global changes in adipose tissue organization, metabolism, and inflammatory secretion may have influenced the observed changes in the liver and will be an area of future exploration.

Surprisingly, there was no change in the hepatic macrophage profile of aged CCR2 KO mice compared to the aged WT mice. Both aged cohorts displayed an overall increase in $F4/80^{+}$ cells, specifically the $F4/80^{+}CD11b^{+}CD68^{-}$ subset, when compared to their young controls, which was also observed in the cohorts from the NIA. These results suggest that the accumulation of $F4/80^{+}CD11b^{+}$ macrophages in the aged liver is independent of CCL2-CCR2 signaling and was neither influenced by the reduction in lipids nor inflammatory gene expression in the aged liver. RNA-seq analysis of aged WT livers revealed several other chemokines that might be involved in the recruitment of $F4/80^{+}CD11b^{+}$ macrophages, including CXCL7, CXCL13, CCL22, CCL5 (RANTES), and CCL6. Of note, CCL2 was upregulated but was not flagged as a significantly differentially expressed gene in the RNA-seq screen due to the stringent filtering and false-discovery rates. Others have found that CCL2 promotes the recruitment of $CCR2^{+}CD11b^{+}$ myeloid cells from the bone marrow to metastatic cancer sites in the liver, but inhibition of CCL2 or CCR2 did not alter myeloid cell recruitment and had little effect on metastatic tumor burden. Deletion of the $CD11b^{+}$ cells by diphtheria toxin receptor (CD11b-DTR) markedly decreased metastatic growth and incidence (Lim, Yuzhalin, Gordon-Weeks, & Muschel, 2016; Zhao et al., 2013). Further studies will be necessary to determine which chemokines or signaling gradients are responsible for driving the increase in CD11b-expressing macrophages in the aged liver.

Our results suggest that inhibiting CCR2 signaling globally may be beneficial to reduce hepatic triglyceride levels and inflammatory gene expression in advanced age. Cenicriviroc, a dual CCR2/CCR5 antagonist, has now been studied in a Phase 2b, randomized, double-blind, placebo-controlled, multinational clinical trial to improve non-alcoholic fatty liver disease activity score, with no concurrent worsening of fibrosis stage (Friedman et al., 2016). The trial resulted in twice as many subjects achieving improvement in fibrosis and no worsening of steatohepatitis compared with placebo (Friedman SL, 2018). Subgroup analysis demonstrated that the therapy was similarly effective in patients above and below 56 years of age, suggesting this therapy may show promise in treating age-related NAFLD/NASH as well. Our study lends further support that targeting the CCL2-CCR2 pathway may be a promising strategy to reduce the onset and progression of hepatic fat accumulation and inflammation during the process of aging.

3.0 THE HOST RESPONSE TO ENGINEERED LUNG SCAFFOLDS

Chapter 3 is adapted from one published research manuscript:

Stahl EC[1,2], Bonvillain RW[3], Skillen CD[1,2], Burger BL[1,2], Hara H[4], Lee W[4], Trygg CB[5], Didier PJ[5], Grasperge BF[5], Pashos NC[5], Bunnell BA[5], Bianchi J[6], Ayares D[6], Guthrie KI[3], Brown BN[*,$,1,2], Petersen TH[$,3]. Evaluation of the host immune response to decellularized lung scaffolds derived from alpha-Gal knockout pigs in a non-human primate model. *Biomaterials.* 2018 Dec; 187:93-104. (Epub 2018 Sep 28.)

[1]McGowan Institute for Regenerative Medicine, University of Pittsburgh, Pittsburgh, PA; [2]Department of Bioengineering, University of Pittsburgh, Pittsburgh, PA; [3]Regenerative Medicine, United Therapeutics Corporation, Research Triangle Park, NC; [4]Thomas E. Starzl Transplantation Institute, University of Pittsburgh, Pittsburgh, PA; [5]Tulane National Primate Research Center, Tulane University, Covington, LA; [6]Revivicor Inc., Blacksburg, VA

3.1 INTRODUCTION

Chronic lower respiratory disease affects over 15 million people in the United States. A potential curative therapy does exist in the form of lung transplantation, however the short supply of human donor organs means that only 2,000 lung transplants are performed annually, while many more people die each year on the waiting list ("Facts and Myths," 2018). Bioengineering

approaches may offer an alternative solution to human organ shortages, by developing biocompatible tissues and organs derived from animal source material (Ott et al., 2010; T. H. Petersen et al., 2010).

Decellularization, the removal of cellular material from organs and tissues, has been utilized to engineer organ scaffolds for transplantation. Tissues can be decellularized by mechanical force and agitation as well as chemical detergent and enzyme washes to remove cellular proteins while keeping the extracellular matrix intact (Brown & Badylak, 2014; Gilbert et al., 2006). Once implanted, non-crosslinked acellular products are degraded and replaced with cells from the host, acting as a scaffold to direct site-appropriate tissue remodeling, or can be recellularized *ex vivo* with host derived cells to engineer functional tissues (Brown & Badylak, 2014).

Pigs have been investigated as sources of organs for xenotransplantation and as sources of tissues for decellularization as they breed and mature rapidly, produce large litters, and can be genetically modified and raised to be specific pathogen free (Ezzelarab et al., 2005). Whole human and pig lungs have been effectively decellularized and are currently being evaluated in allotransplantation and xenotransplantation applications (T. H. Petersen, Calle, Colehour, & Niklason, 2011; T. H. Petersen et al., 2010; Song et al., 2011). However, the host immune response to these materials has not yet been elucidated.

Carbohydrates play a major role in the rejection of porcine xenografts, and as a result are likely important in the immune response to decellularized porcine material (Cooper, Koren, & Oriol, 1994). α1,3Gal is a common carbohydrate structure found on the surface of mammalian cells, synthesized by the enzyme α1,3-galactosyltransferase (α1,3GT) (Macher & Galili, 2008). Importantly, humans, apes, and Old World monkeys (*e.g.* the rhesus macaque) exhibit a

frameshift mutation in the α1,3GT gene, and thus express alternative carbohydrate epitopes compared to those on porcine cells (Larsen, Rivera-Marrero, Ernst, Cummings, & Lowe, 1990). As such, these primates produce natural antibodies to the α1,3Gal epitope, including anti-Gal IgG, IgM, IgE, and IgA (Galili, 1993; Galili, Macher, Buehler, & Shohet, 1985; Galili, Rachmilewitz, Peleg, & Flechner, 1984). The deposition of Gal-specific antibodies onto xenografts following transplantation drives complement activation leading to hyperacute rejection and severe coagulation dysfunction within minutes (Lexer et al., 1986; Rose, Cooper, Human, Reichenspurner, & Reichart, 1991).

Although decellularization techniques aim to remove cellular antigens, the presence of the Gal epitope has been detected in decellularized porcine heart valves, anterior cruciate ligament, and small intestine submucosa (SIS) implants used clinically (Konakci et al., 2005; McPherson et al., 2000; Stone et al., 2007). The Gal epitope is associated with glycoproteins and glycolipids and has also been detected on ECM proteins including fibrinogen and laminin (Galili et al., 1988; Spiro & Bhoyroo, 1984; Thall & Galili, 1990; Towbin et al., 1987). The persistence of the Gal epitope in decellularized constructs may result in long-term degeneration and calcification of heart valves in patients (Badylak & Gilbert, 2008; Konakci et al., 2005). Therefore, combining decellularization strategies with the removal of the Gal epitope from porcine tissue might aid in the long-term goals of sustainable organ sources for transplantation (Michel, Madariaga, Villani, & Shanmugarajah, 2015; Nam et al., 2012).

Strategies to mask or remove the Gal epitope from animal tissues and organs have included crosslinking tissue matrices via glutaraldehyde, enzymatic treatment with α-galactosidase, and the development of genetically engineered pigs which lack the α1,3GT epitope (α-Gal KO) (Choi et al., 2012; Kolber-Simonds et al., 2004; Park, Kim, Choi, & Kim,

2009; Phelps et al., 2003). Xenotransplantation of α-Gal KO kidneys and hearts greatly reduced the occurrence of hyperacute reaction and prolonged the survival of the xenografts in non-human primates (Kuwaki et al., 2005; Yamada et al., 2005). However, the grafts eventually failed due to thrombotic microangiopathy, a form of acute vascular rejection, suggesting that further processing is needed to design a fully compatible organ (Kuwaki et al., 2005; Yamada et al., 2005).

In the present study, decellularized WT and α-Gal KO porcine lungs were implanted subcutaneously in a rhesus macaque model to assess the host response to the scaffolds *in vivo* for up to eight weeks. Sham injury, native porcine lung, and allogeneic decellularized macaque lung groups were included as controls. Following explant, fresh constructs were re-implanted into the previously exposed hosts to examine the outcome of chronic exposure and sensitization to Gal epitopes. The production of anti-Gal antibodies, circulating blood cells, and infiltrating immune cell subsets were evaluated to determine the biocompatibility of each implant type.

3.2 METHODS

Porcine Lung Tissue. All samples were collected by United Therapeutics and Revivicor and underwent quality control according to standard operating procedures. Lung tissues from wild type or α-Gal knockout pigs (α-Gal KO, GalSafe®) were received within 24 hours of sacrifice on wet ice. The lungs were flushed with sterile PBS and surgically reduced to the left superior and inferior cranial lobe, while maintaining intact vasculature and airways, to mimic the smaller size of macaque lungs and maintain similar tissue-to-fluid dynamics during decellularization. All genetically engineered (GE) pig derivatives, heart, lung, blood from a total of four animals

described herein were exclusively used for *in vitro* or *in vivo* studies in laboratory animals. No GE pig derivatives entered the food chain; all GE pig derivatives including all excess materials were disposed as regulated medical waste.

Macaque Lung Tissue. All samples were collected by Tulane National Primate Research Center (TNPRC). All donor animals were humanely euthanized due to chronic gastritis or as normal controls assigned to other studies. No experimental inoculations or treatments were performed on lung donor animals. Immediately upon animal sacrifice, the intact heart and lungs were removed from the thorax. The apex of the heart was removed midway through the ventricles, then the upper ventricles and atria were irrigated with sterile heparinized (500 U/L) PBS to wash out remnant blood. The trachea was removed, and the lungs were placed into a sterile container and transported to the lab for further washing.

Decellularization of Porcine and Macaque Lungs. Decellularization of porcine and macaque lungs was performed following recently published methods (Gilpin et al., 2014). Briefly, the left main pulmonary artery was cannulated as an inlet for decellularization fluids via the native vasculature, and the pulmonary veins and left main bronchus served as outlets for flow. Lungs were decellularized by vascular perfusion at 20 mmHg in a custom bioreactor system with 0.5% sodium dodecyl sulfate (5 days), 1% Triton X-100 (24 hours), water wash (24 hours), and PBS wash (5 days). Solutions were changed daily.

Implantation of Decellularized Lung Constructs or Sham Injury. The lung scaffolds were dissected to create implantable plugs of 2 x 2 x 0.5 centimeters. Prior to implantation, the lung scaffolds were rinsed in three consecutive washes of PBS. A pair of rhesus macaques (gender: male; age: 5-9 years) received either sham injury, native WT porcine lung, decellularized WT porcine lung, decellularized α-Gal KO porcine lung implants, or

decellularized macaque lung bilaterally on either side of the spine (n=10). Eight incisions (1-2 cm) were created along the midline of the back to form a subcutaneous pocket for insertion of the implant to be extracted in pairs at 1, 2, 4, and 8 weeks, and the medial and lateral margins were marked. For the re-implantation study, the same hosts received fresh implants just below the previous implantation site using the same methods (Figure 1A). All studies were performed in accordance with Tulane University's IACUC. Animals were monitored for general well-being and weight changes over the course of the study.

CBC and Chem12 Data. Blood was collected from animals at baseline and 1, 2, 4 and 8 weeks post-implantation. Complete blood count (CBC) was performed at the Tulane National Primate Research Center Veterinary Medicine Laboratory using the Sysmex XT2000iV hematology analyzer, in accordance with quality control from Insight at Sysmex. Chem12 data was collected with the Beckman AU400 chemistry analyzer, in accordance with quality control from Unity by BioRad.

Anti-Gal ELISA. Serum was collected at baseline and 8 weeks post-implantation, as well as pre-re-implantation, and 4 weeks and 8 weeks post-re-implantation. All serum samples were heat-inactivated at 57 degrees Celsius for 30 minutes. Anti-Gal ELISAs (Dextra Laboratories) were performed according to the manufacturer's protocol for binding by IgG and IgM (Yeh et al., 2010).

Harvest of Explanted Tissue. Implants were excised in duplicate pairs *en bloc* with the surrounding tissues at 1, 2, 4, and 8 weeks post-implant in naïve animals, and again at 1, 2, 4, and 8 weeks in the previously exposed hosts. Samples were immediately fixed in 10% neutral-buffered formalin, embedded in paraffin, and sent for histological analysis.

Histological Assessment. Samples embedded in paraffin blocks were sectioned at 7 μm thickness and affixed to glass slides. Histologic staining included hematoxylin and eosin (Thermo Fisher), Verhoff van Gieson (Sigma Aldrich), Masson's trichrome (Sigma Aldrich), Alcian blue (Sigma Aldrich), and Wright Giemsa (Polysciences, Inc.). stains were performed according to standard protocols per the manufacturer's instructions. Images were captured at 100x-magnification for histological assessment. Blinded qualitative analysis of the histologic appearance of the implanted test articles was documented. An independent qualitative analysis was performed by a pathologist, including the documentation of a semi-quantitative histological inflammation score for each explant.

Immunohistochemistry. Slides were stained with primary antibodies against immune cell markers including CD45 (Abcam ab10558, 1:900), CD3 (Invitrogen a0452, 1:150), CD4 (Abcam ab133616, 1:500), CD8 (Abcam ab4055, 1:500), CD20 (Abcam ab27093, 1:300), CD68 (Abcam ab955, 1:50), CD86 (Abcam ab53004, 1:150), and CD206 (Santa Cruz sc-34577, 1:150), as well as CD31 (Abcam ab9498, 1:20) and alpha smooth muscle actin (Abcam ab5694, 1:150). Briefly, slides were deparaffinized, underwent antigen retrieval, blocked, and stained overnight at 4 degrees Celsius. Secondary antibodies (biotinylated anti-rabbit IgG, biotinylated anti-mouse IgG, or biotinylated anti-goat IgG, Vector Laboratories) were applied for 30 minutes at room temperature. Vecta-Shield ABC Reagent (Vector Laboratories) was applied to sections for 30 minutes, followed by a 4% DAB solution (Vector Laboratories), and Hematoxylin QS (Vector Laboratories). Slides were dehydrated, cover slipped, and imaged at 200x-magnification.

Quantification of Immune Cell Subsets. Quantitative analysis of the stained sections was performed by blinded investigators using image analysis algorithms optimized for each immuno-stain. Five images were captured from a single slide at 200x-magnification per explant for each

IHC marker. Images were processed with a custom script using ImageJ software (NIH) to collect counts of nuclei, positively stained cells, and percent area of positive staining per field. The percentage of positively stained cells was calculated for a given marker. Figures were prepared in GraphPad Prism 7, where each data point represents the mean ± standard error.

Statistical Analysis. Differences in the percentage of positively stained cells or implant area was assessed for the implantation and re-implantation studies between groups at given time points using Kruskal-Wallis one-way ANOVA followed by Dunn's multiple comparisons test (n=4 explants per time point), after testing for Gaussian distribution with the Shapiro-Wilk normality test. To compare the implantation and re-implantation studies, a two-sample unequal variance t-test was performed. Statistical significance was determined by rejecting the null hypothesis at $\alpha = 0.05$.

3.3 RESULTS

Subcutaneous Implantation of Lung Scaffolds in Rhesus Macaque Model

Ten rhesus macaques received either sham control (SC), decellularized macaque lung (DC-M), native WT porcine lung (WT), decellularized WT porcine lung (DC-WT), or decellularized α-Gal KO porcine lung implants (DC-KO) subcutaneously implanted in duplicate down the mid-line of the spine to be harvested at 1, 2, 4, and 8 weeks post-implantation in naïve and previously exposed hosts (Figure 16A).

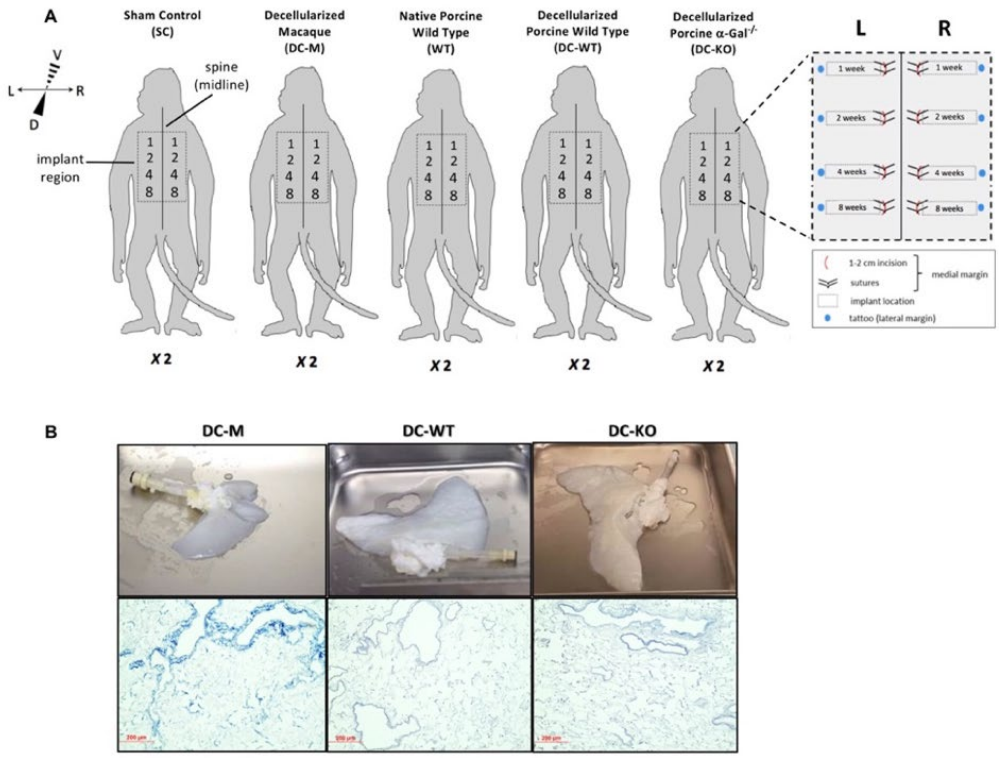

Figure 16. Lung construct implantation and harvest schematic.

A) Ten rhesus macaques received a sham injury control (SC), decellularized macaque lung (DC-M), native WT porcine lung (WT), decellularized WT porcine lung (DC-WT), or decellularized α-Gal KO porcine lungs (DC-KO). Implants were placed in duplicate down the midline of the spine and explanted at 1, 2, 4, and 8 weeks. B) Whole decellularized lung scaffolds prior to implantation, showing effective decellularization (top) and maintenance of native lung structures with Masson's Trichrome stain (bottom), scale bar = 200 μm.

The macaque, WT porcine, and α-Gal KO porcine lungs were effectively decellularized prior to implantation and maintained native bronchiolar structures as shown with Masson's Trichrome staining (Figure 16B). The body weight of each animal underwent minimal changes during the study as evidenced by less than 10% total decrease in body weight during both studies (Figure 17).

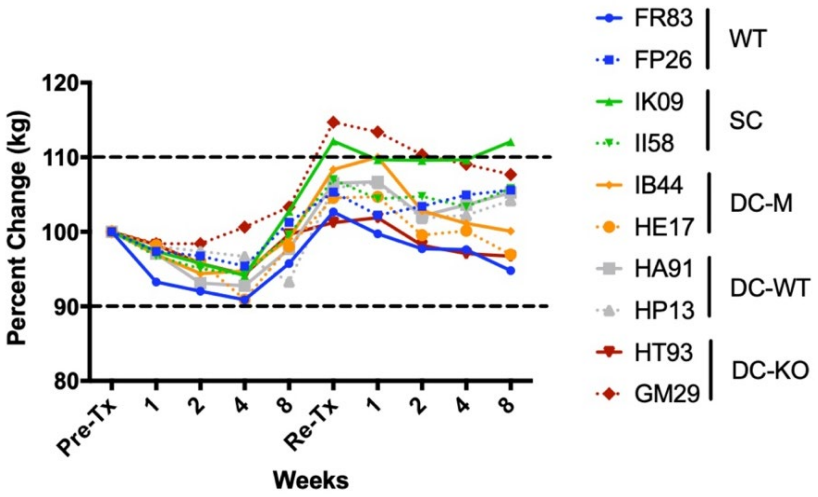

Figure 17. Relative body weight of rhesus macaques during study

Relative body weight of ten rhesus macaques (individual animal IDs listed) that received subcutaneous implantation of native wild type porcine (WT) lungs, sham injury control (SC), decellularized macaque (DC-M) lungs, decellularized wild type porcine (DC-WT) lungs, or decellularized α-Gal knockout (DC-KO) lungs before treatment or re-treatment, and 1, 2, 4, and 8 weeks following implantation. Body weight did not decrease below 10% of the starting value in any treated animal, while two animals recovered slightly more than 10% of the original body weight in the KO and SC groups.

Blood Biochemistry of Rhesus Macaques Implanted with Lung Scaffolds

Blood was collected for complete blood count (CBC) and comprehensive metabolic analysis (Chem12) three weeks prior to implantation and at 1, 2, 4, and 8 weeks post-implantation. Analyzing the change from baseline in circulating blood cell counts demonstrated an acute increase in white blood cells (WBCs) and neutrophils in the WT group at one and two weeks, suggesting rapid infiltration and encapsulation of the implants, while the decellularized porcine groups had sustained levels of WBCs and neutrophils out to eight weeks (Figure 18). One animal in the DC-KO group presented with above normal WBC counts (>15.5x10^3) at two and eight weeks, as well as elevated circulating neutrophils (>7.3x10^3) from weeks one to eight

(Figure 18A, B). Similarly, one animal in the DC-WT group had elevated circulating neutrophil levels (>7.3x10^3) from weeks two to eight (Figure 18B). Both animals in the WT group showed a spike in levels of circulating eosinophils (>0.8 x10^3) at two weeks, and one had above normal levels of circulating neutrophils at one-week post-implantation (>7.3x10^3) (Figure 18B,C).

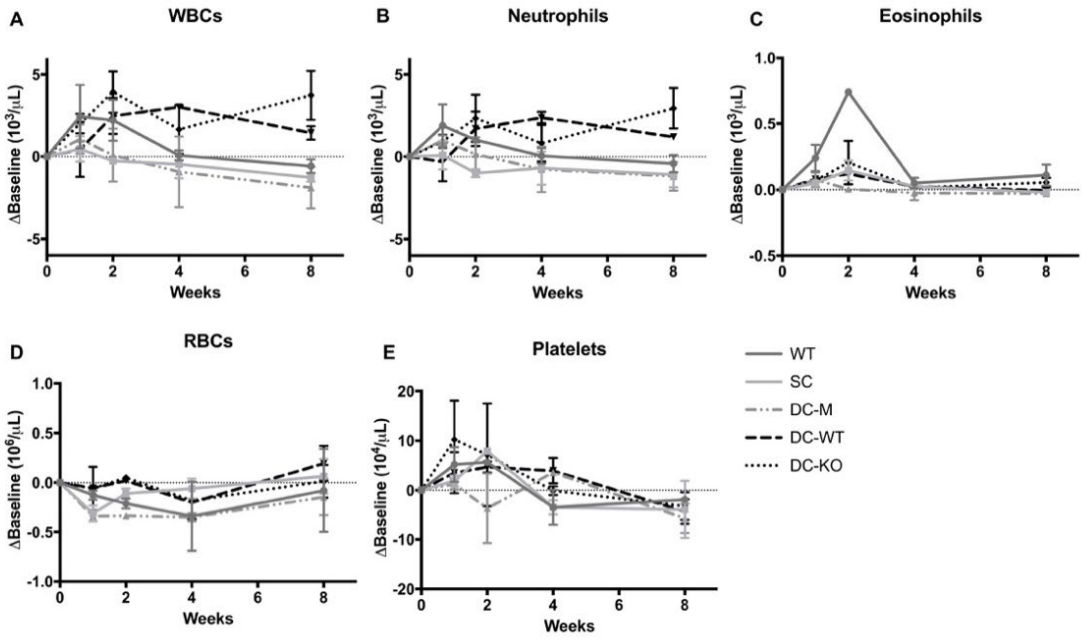

Figure 18. Change from baseline in complete blood counts post-implantation

Circulating levels of A) white blood cells (WBCs), B) neutrophils, C) eosinophils, D) red blood cells (RBCs), and E) platelets were measured pre-implantation and at 1, 2, 4, and 8 weeks post-implantation. Change from baseline was calculated at each time point to measure relative values of circulating cells (average ± standard deviation, n=2).

No changes in circulating immune subsets were observed in subjects that received sham injury or DC-M implants. In addition, no changes were observed in numbers of circulating lymphocytes, monocytes, or basophils over the course of the study in any group (data not shown). No differences in red blood cell number, hematocrit, hemoglobin, platelets, or platelet

volume were detected between the groups (Figure 18F, G), with the exception of one animal in the DC-KO group, which had elevated total platelets from weeks one to two (>$6.8x10^4$).

The Chem12 data indicated no changes in levels of sodium, potassium, chloride, total protein, albumin, globulin, blood urea nitrogen, glucose, creatinine, aspartate amino transferase, or alanine amino transferase in any implantation groups across the studies. All values were within empirically determined normal ranges for the rhesus macaque, listed in **Appendix C (page 128)**.

Sensitization of Treated Rhesus Macaques to the Gal Epitope

The presence of antibodies targeted against the Gal epitope was measured in recipient serum at baseline and after implantation or re-implantation of the lung constructs. Hosts were considered sensitized to the Gal epitope if antibody binding levels doubled upon exposure to the implants. Levels of anti-Gal IgM antibodies increased 2-fold only in the WT group from baseline to eight weeks of the initial implantation study and increased again to similar levels in the re-implantation study (Figure 19A).

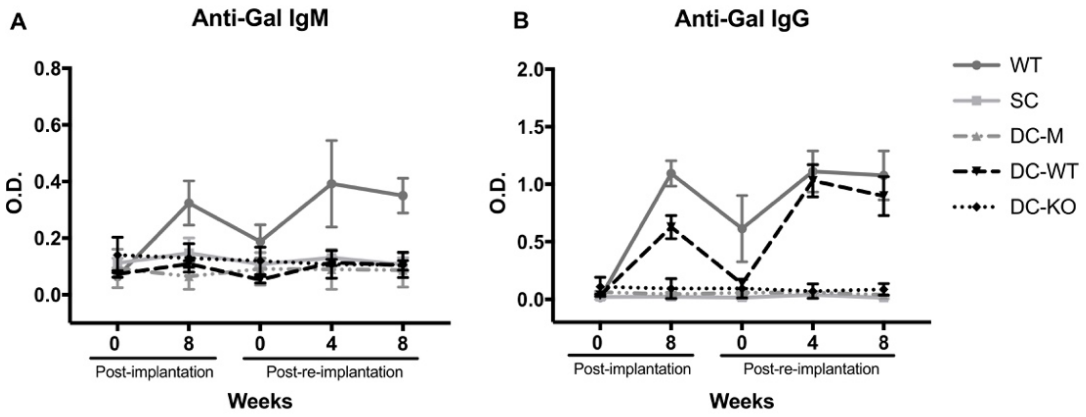

Figure 19. Production of Gal-specific antibodies in response to implanted lung constructs

Levels of A) IgM or B) IgG antibody were measured in rhesus macaque serum against the Gal epitope in naïve hosts from zero to eight weeks post-implantation, and zero to eight weeks post-re-implantation in the previously exposed hosts. Native wild type porcine (WT), sham control (SC), decellularized macaque (DC-M), decellularized WT porcine (DC-WT), and decellularized α-Gal KO porcine (DC-KO) lungs. Values are the average optical density (O.D. ± standard deviation, n=2) determined by ELISA.

Levels of anti-Gal IgG antibodies increased in both the WT and DC-WT groups from zero to eight weeks in the initial implantation study, where WT values increased by an average of 70-fold and DC-WT values increased by an average of 18-fold. Circulating levels of anti-Gal antibodies were reduced in both groups between the implantation and re-implantation studies but did not return to baseline. Levels of anti-Gal IgG increased again in the re-implantation study, returning to a 70-fold increase in the WT group and increasing further to a 25-fold increase in the DC-WT group (Figure 19B).

The SC and the DC-M groups showed no changes from baseline levels of anti-Gal IgM, and no detectable anti-Gal IgG over the course of the study, demonstrating the surgical procedure and allogeneic transplant did not affect the level of anti-Gal antibodies. Importantly, recipients of the DC-KO implants showed no increase in production of anti-Gal IgM or IgG

antibody throughout the study, confirming removal of the Gal epitope and absence of host sensitization.

Qualitative Biocompatibility of Implanted Lung Scaffolds

Qualitative analysis of the scaffolds post-implantation was performed on H&E, Masson's Trichrome, and Verhoff van Gieson stained tissue sections to identify scaffold degradation, infiltration by immune cells, and resolution of the foreign body host response.

The implantation surgery produced a linear defect extending from the epithelium to the deep dermis, filled with minimal fibrin, edema, and acute inflammatory cells across all implants and sham surgeries. The sutures induced minimal granulomatous reaction in the deep dermis on the medial margin of the implants. All implantation groups were infiltrated by immune cells migrating from the outer edges of the implants to the center over time. Migration was impeded by residual cartilage and thick elastin fibers surrounding large native vasculature as seen by Verhoff van Gieson stain (Figure 20).

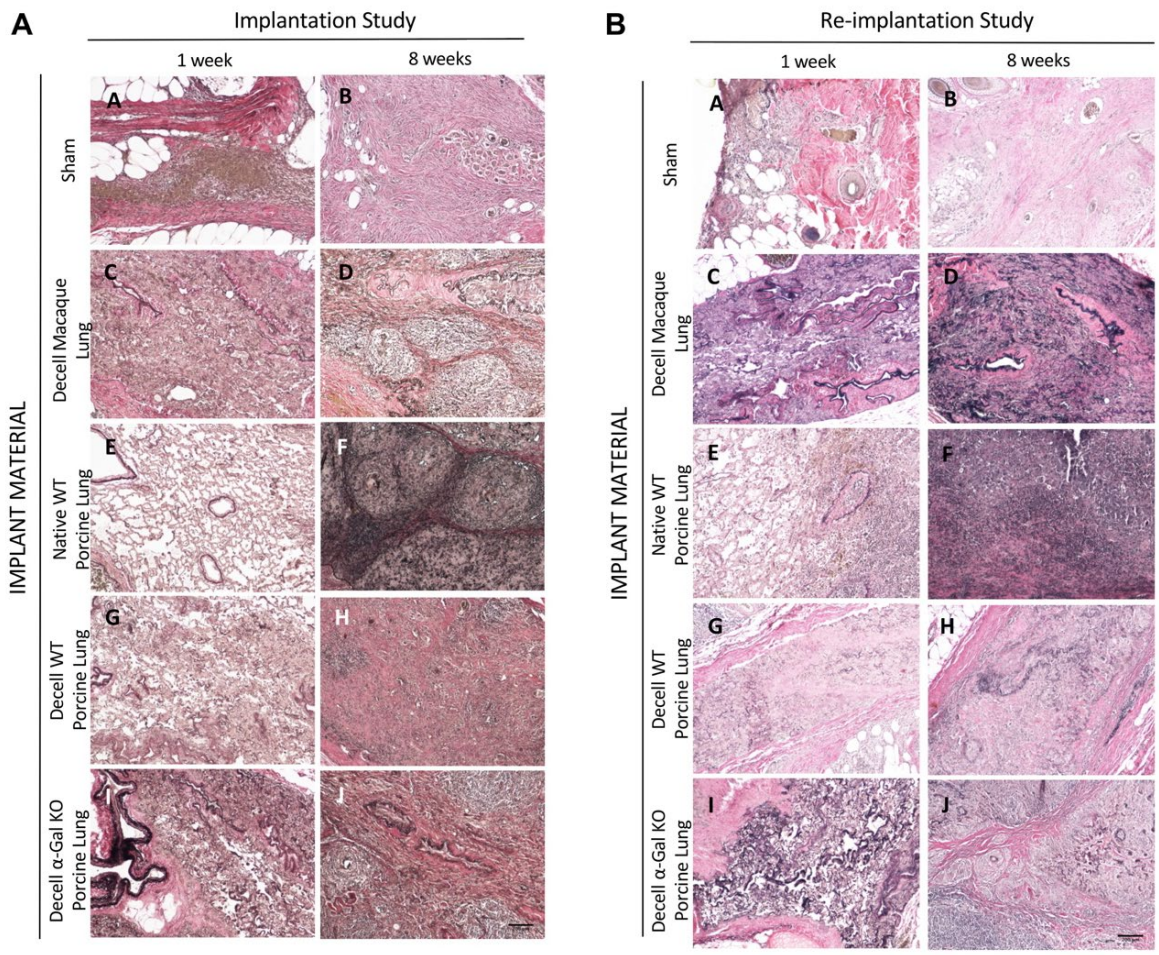

Figure 20. Degradation of elastin over time in lung implants

Verhoff van Gieson staining was used to assess scaffold degradation via lung elastin content (black) in the A) implantation and B) re-implantation study for the five implantation groups (magnification: 10x objective, scale bar: 200 μm). Thick elastin fibers were identified primarily around large vasculature, and thin fibers were present throughout the lung parenchyma. By eight weeks, elastin remained in several of the groups, demonstrating that the scaffolds were not completely degraded.

One week following injury, the SC group showed mild to moderate granulomatous inflammation with hyperplastic blood vessels in the dermis. At two and four weeks, moderate granulomatous inflammation with granulation tissue filled the defect. By eight weeks, there was complete regeneration of normal skin structures, with resolved inflammation and minimal fibrous scar remaining (Figure 21a,b).

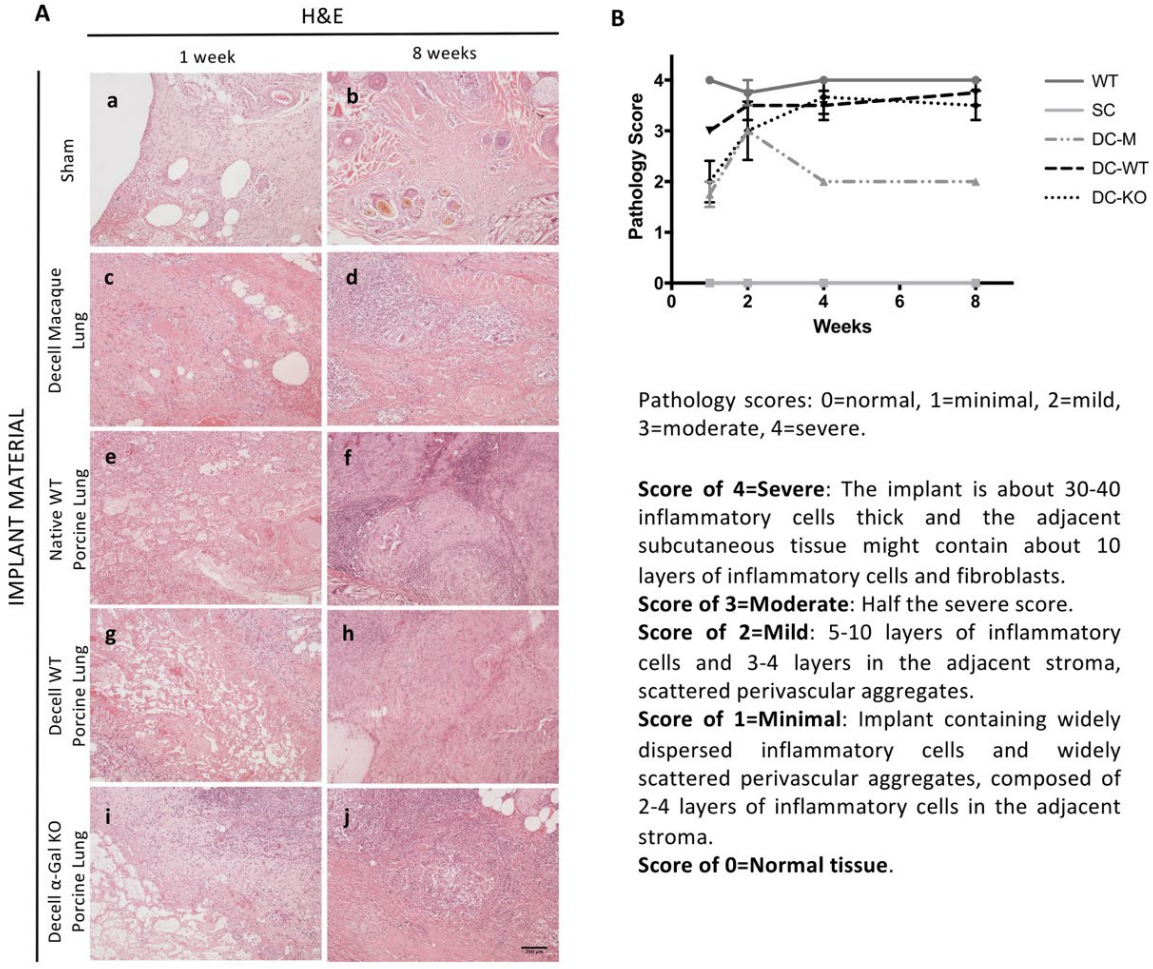

Figure 21. Qualitative assessment of tissue remodeling and biocompatibility in the implantation study

A) Representative H&E stained sections of the implantation sites at one and eight weeks post-implantation (scale bar = 200 μm). Sham control (SC, a,b), decellularized macaque lung (DC-M, c,d), native WT porcine lungs (WT, e,f), decellularized WT porcine group (DC-WT, g,h), decellularized α-Gal KO (DC-KO, i,j). B) The pathological score for each implant (scale 0-4, n=4) is semi-quantitatively displayed for each group at each time point.

The allogeneic DC-M lung implants were partially condensed and replaced with granulation tissue by one-week post-implantation, with minimal cell infiltrate, consisting primarily of histiocytes and small amounts of lymphocytes. At two weeks, inflammation persisted with few multinucleated giant cells (MNGCs), and granulation tissue. At four and eight weeks, the implant was mostly replaced with granulation tissue, contained residual cartilage, and a small lymphocytic infiltrate (Figure 21c,d).

The WT lung implants retained alveolar vascular structures at one-week post-implantation, with a large infiltration of PMNs, some histiocytes, and MNGCs. At two weeks, the implant was partially condensed with pyogranulomatous exudate consisting of large amounts of PMNs, some macrophages, and few MNGCs. Neovascularization and remnant cartilage were noted at two weeks. By four weeks, the infiltrating cells included large amounts of lymphocytes and numerous MNGCs; and implants showed signs of skin erosion. By eight weeks, extensive granulomas had formed including dense aggregates of macrophages, lymphocytes, and MNGCs with fibrous encapsulation (Figure 21e,f).

The DC-WT porcine lung implants were partially condensed at one-week post-implantation, with minimal granulation tissue, and mild infiltration of histiocytes and lymphocytes. At two weeks, the implant was partially replaced with granulation tissue, and showed moderate infiltration of histiocytes, macrophages, lymphocytes, and MNGCs. Residual cartilage was identified in the explants at two weeks. By four weeks, the implants were completely infiltrated and showed signs of granuloma, which persisted at eight weeks (Figure 21g,h).

The DC-KO porcine lung implants were partially condensed at one-week post-implantation, with mild infiltration of histiocytes, macrophages, and lymphocytes. At two weeks,

the implants were infiltrated by small amounts of PMNs, and moderate amounts of histiocytes, lymphocytes, and MNGCs. Neovascularization and remnant cartilage were noted at two weeks. By four weeks, the implants were replaced by moderate granulation tissue with dense lymphocytes. At eight weeks, cartilage was also noted in the explant, which was replaced with granulation tissue with scattered amounts of PMNs, histiocytes, MNGCs, and clusters of lymphocytes forming granulomas. All groups retained non-degraded scaffold structures by the final eight-week time point (Figure 21i,j).

A biocompatibility score was compiled to semi-quantitatively identify differences between the groups (Figure 21B). At one week, the SC group had no pathology detected (score =0); while the WT lung had a greater pathological score compared to all other groups (score =4). Of note, the DC-WT porcine lung had a greater pathological score (score =3) than the DC-KO porcine lung group (score =2) at one week. By four and eight weeks, both the SC and DC-M lung groups had significantly lower pathological scores than the porcine groups, which were indistinguishable based on this semi-quantitative metric.

Qualitative Biocompatibility of Re-Implanted Lung Scaffolds

In the re-implantation study, the SC was similar to the previously described reaction and regenerated into healthy skin (Figure 22a,b). The DC-M lungs showed some hyperplastic blood vessels and were minimally infiltrated with MNGCs at one-week post re-implantation. At two weeks, the scaffolds were partially condensed and moderately replaced with granulation tissue, along with more MNGCs, and some lymphocytes and macrophages. Finally, by eight weeks, some mature collagen was identified, and the residual scaffold remained moderately infiltrated by immune cells (Figure 22c,d).

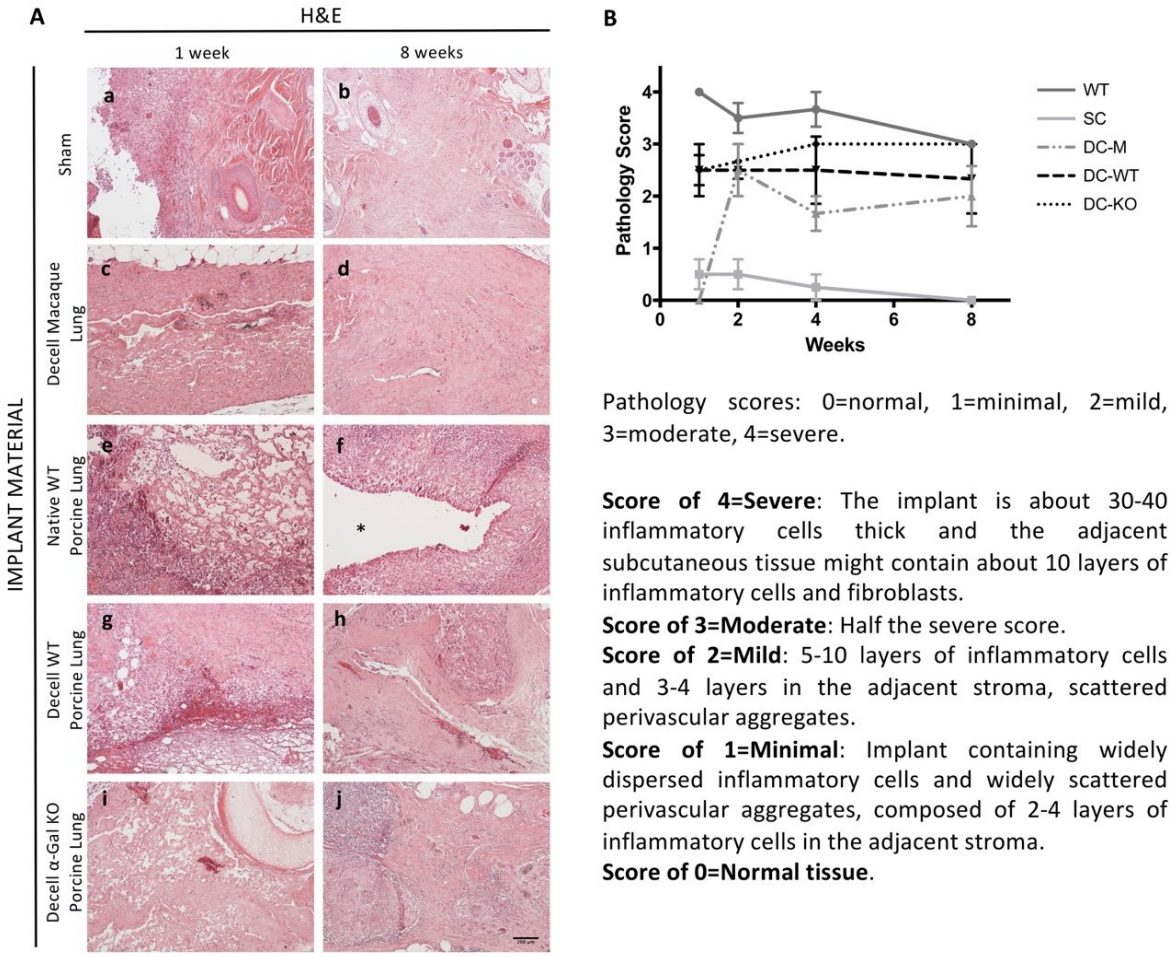

Figure 22. Qualitative assessment of tissue remodeling and biocompatibility in the re-implantation study

Representative H&E stained sections of the implantation sites at one and eight weeks post-re-implantation (scale bar = 200 μm). Sham control (SC, a,b), decellularized macaque lung (DC-M, c,d), native WT porcine lungs (WT, e,f *division/contortion), decellularized WT porcine group (DC-WT, g,h), decellularized α-Gal KO (DC-KO, i,j). B) The pathological score for each implant (scale 0-4, n=4) is semi-quantitatively displayed for each group at each time point.

The WT lung implants had thick layers of PMNCs, macrophages, MNGCs, and some lymphocytes as early as one week post re-implantation into the sensitized hosts. Residual alveolar structures were identified with some neovascularization. At two weeks, more MNGCs and lymphocytes appeared in the implant, which also retained PMNs, remnant cartilage, and

fibrotic outer zone. By four weeks, the implant was beginning to be replaced with granulation tissue. By eight weeks, residual granulation tissue, lymphocytes, and some signs of liquefaction and division of the implant was identified (Figure 22e,f).

The DC-WT implants showed peripheral infiltration of immune cells (PMNs, macrophages, and some MNGCs) as early as one week post re-implantation into the sensitized hosts. The implants were also partially condensed with some granulation tissue. At two weeks, large groups of MNGCs formed in the center of the implant surrounded by macrophages, PMNs, and outer regions of lymphocytes. By four weeks, the implants were severely infiltrated by inflammatory cells and by eight weeks, the scaffolds were completely replaced by ongoing inflammatory cells organized into granulomas (Figure 22g,h).

The DC-KO implants were also partially condensed and infiltrated with scattered MNGCs and lymphocytes at one week post re-implantation. By two weeks, granulation tissue began to form with discrete populations of macrophages, peripheral lymphocytes, and MNGCs, along with some remnant cartilage. At four weeks, large populations of macrophages and MNGCs replaced much of the scaffold with the formation of dense granulomas, which continued to eight weeks (Figure 22i,j).

Again, the biocompatibility scores were compiled to semi-quantitatively identify differences between the groups (Figure 22B). At one week, the SC and DC-M groups had similar scores (score < 1)., substantially lower than the porcine groups. In addition, both decellularized porcine lung constructs had similar pathological scores (score = 2.5); and the WT lung group had a significantly greater pathological score (score = 4). At two, four, and eight weeks, the SC group had a significantly lower pathological score than the others. No differences between the porcine

groups were identified from two to eight weeks post-re-implantation, similar to what was observed in the implantation study.

Quantitative Biocompatibility of Implanted Lung Scaffolds

In order to further characterize differences in the host response to the implanted lung scaffolds, immunostaining for specific cell markers was quantitatively analyzed at each time point including CD45, CD3, CD4, CD8, CD20, CD68, CD86, CD206, CD31, and alpha smooth muscle actin (α-SMA) and compared to total nuclei counts to determine the percentage of positive cells per field. Representative figures are included for one-week post-implantation (Figure 23) and eight weeks post-implantation (Figure 24).

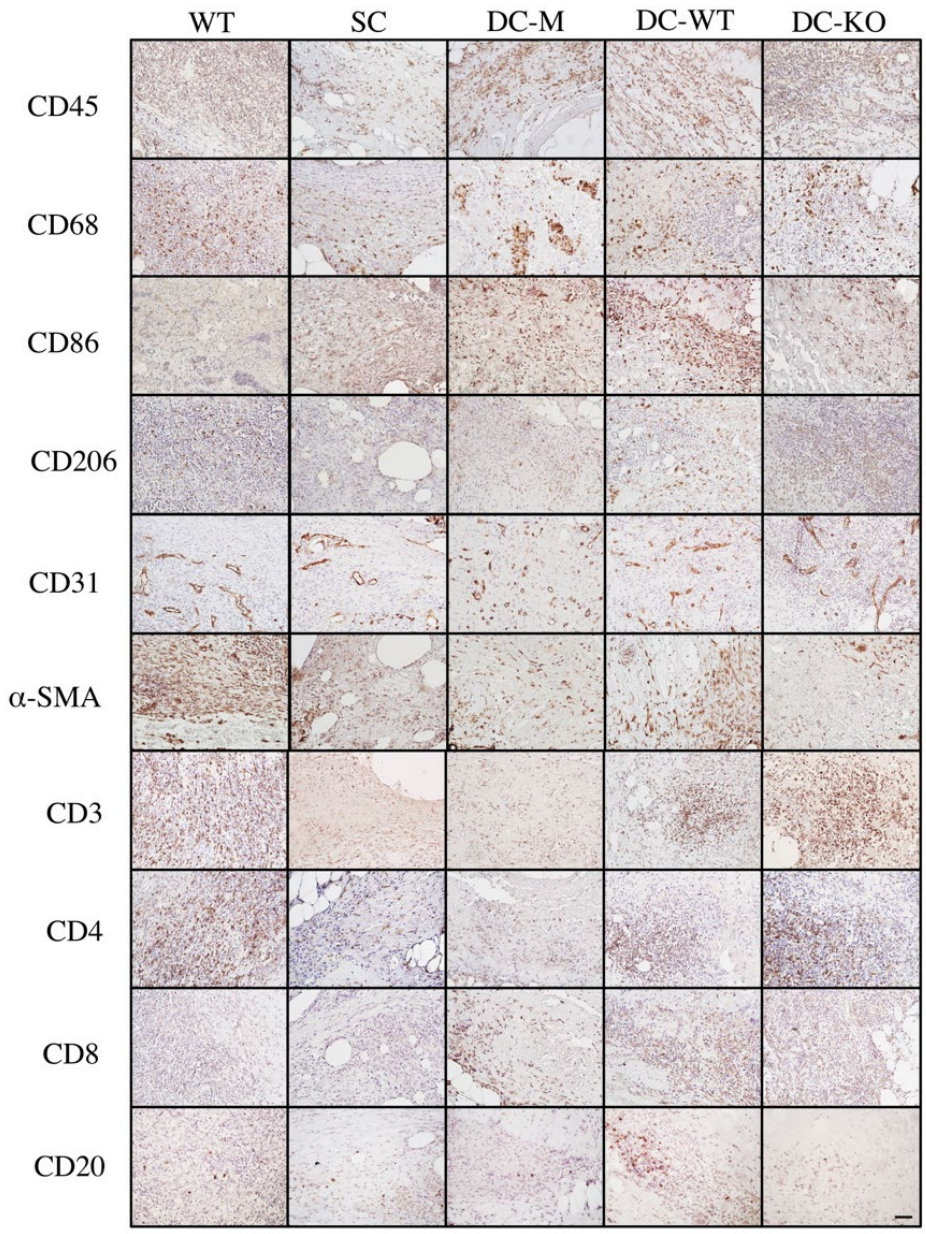

Figure 23. Representative IHC for implantation study, one-week post-implantation

Representative immunostaining for native porcine (WT) lungs, sham injury control (SC), decellularized macaque (DC-M) lungs, decellularized wild type porcine (DC-WT) lungs, or decellularized α-Gal knockout (DC-KO) at one-week post-implantation, scale bar = 50μm.

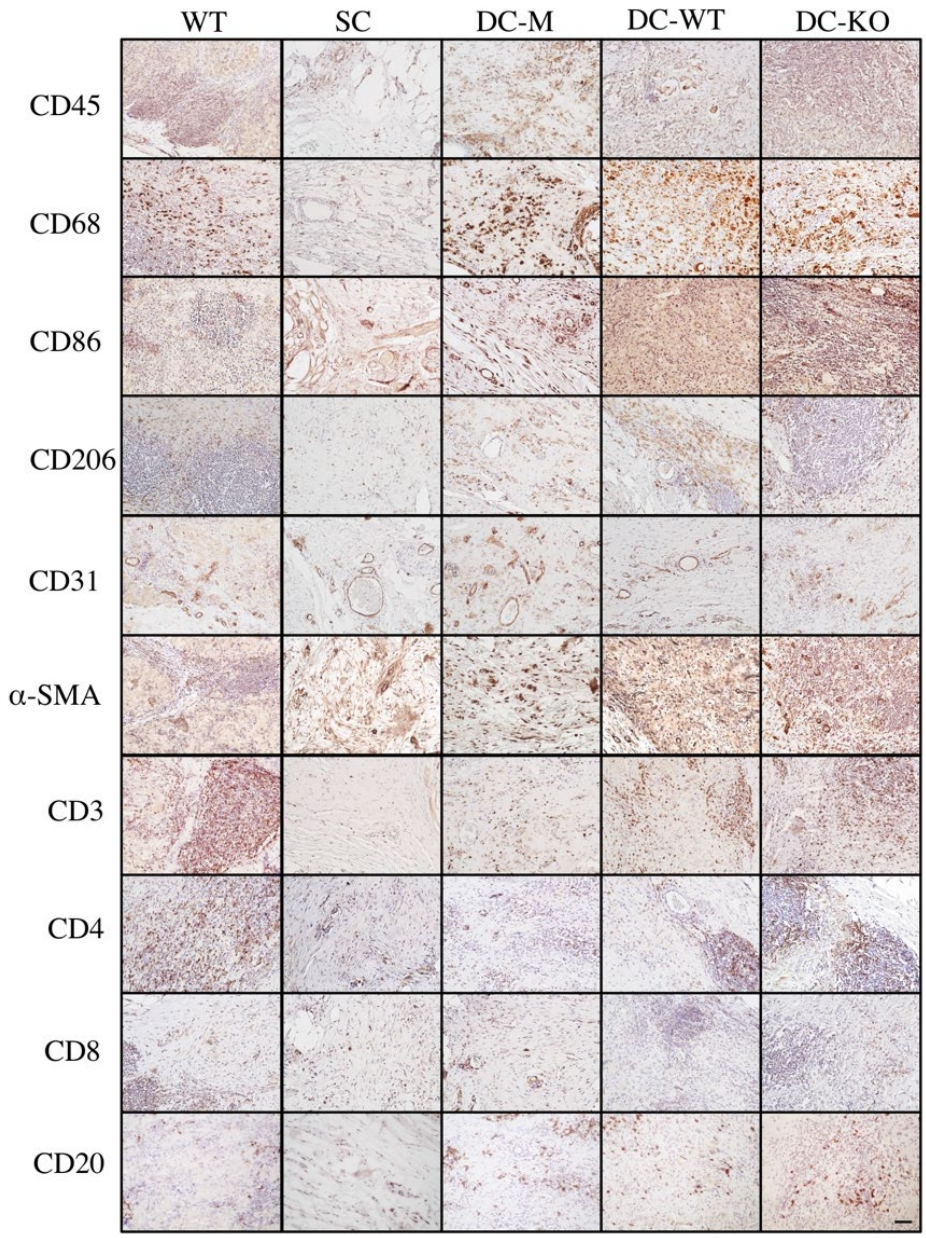

Figure 24. Representative IHC for implantation study, eight weeks post-implantation

Representative immunostaining for native porcine (WT) lungs, sham injury control (SC), decellularized macaque (DC-M) lungs, decellularized wild type porcine (DC-WT) lungs, or decellularized α-Gal knockout (DC-KO) at one-week post-implantation, scale bar = 50μm.

At one-week post-implantation, the WT group had a higher cellularity compared to the SC and DC-M groups. Cellularity peaked at four weeks in the WT and DC-WT groups but was delayed in the DC-KO group to eight weeks (Figure 25A).

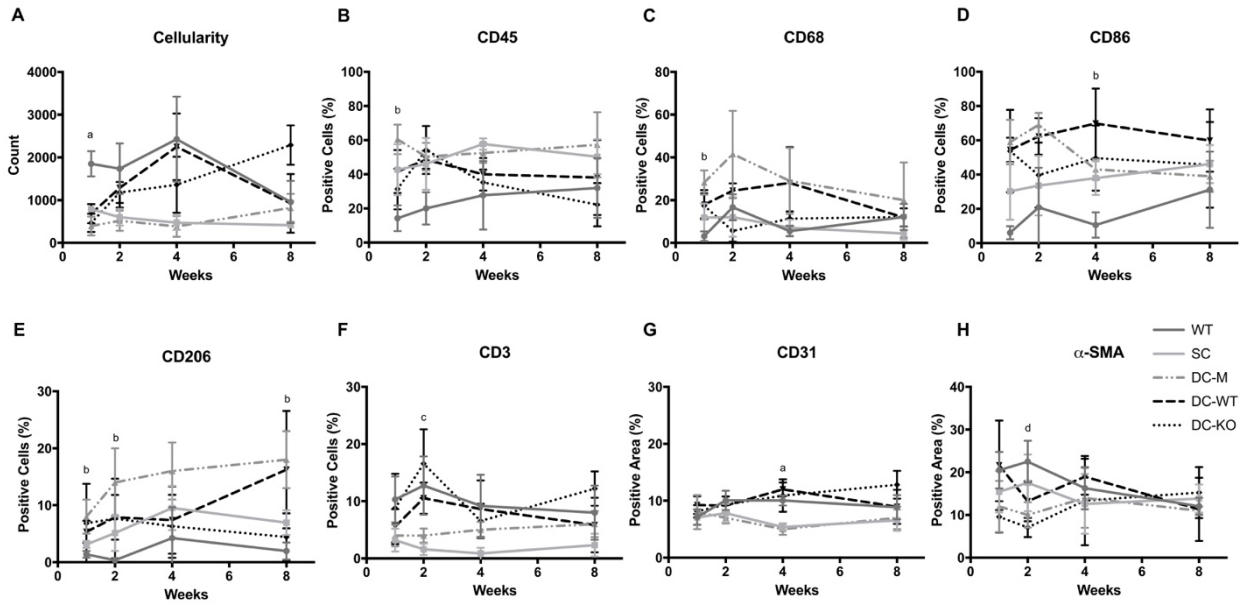

Figure 25. Quantitative assessment of specific cell subsets in the implantation study

A) Cellular infiltration was assessed by counting the number of hematoxylin-stained nuclei and averaged per five fields using ImageJ. B) The percentage of $CD45^+$ leukocytes, C) $CD68^+$ macrophages, and D) $CD86^+$ APCs, E) $CD206^+$ APCs, and F) $CD3^+$ T-cells were quantified by normalizing the number of positive cells to the number of nuclei and averaged per five fields. (G) The percent area of $CD31^+$ blood vessels and H) α-SMA^+ fibroblasts were quantified and averaged per five fields in the native porcine lung (WT), sham control (SC), decellularized macaque lung (DC-M), decellularized WT porcine lung (DC-WT), and decellularized a-Gal KO lung implants (DC-KO). Values are average ± standard error (n=4 implants per group). Significance (p<0.05) was measured by one-way Kruskal-Wallis ANOVA with Dunn's multiple comparisons at each time point designated by **a** (vs. SC/DC-M), **b** (vs. WT), **c** (vs. SC), **d** (vs. DC-KO) groups.

The percentage of $CD45^+$ cells, a pan-leukocyte marker, was significantly greater in the DC-M group compared to the WT group at one week. At all other time points, the percentage of

leukocytes was similar between groups (Figure 25B). Similarly, $CD68^+$ macrophages were increased in the DC-M group compared to the WT at one week (Figure 25C). The percentage of $CD86^+$ cells, a marker for pro-inflammatory macrophages and antigen presenting cells, was significantly increased in the DC-WT group compared to the WT group at 4 weeks (Figure 25D), while the percentage of $CD206^+$ cells, or anti-inflammatory macrophages, was significantly increased in the DC-M group compared to the WT group at one, two, and eight weeks post-implantation (Figure 25E).

In addition, the percentage of $CD3^+$ T-lymphocytes was elevated in the DC-KO group compared to the SC at two weeks post-implantation (Figure 25F). At four weeks, the porcine groups had elevated $CD31^+$ neovascularization, where the DC-WT group was significantly greater than the DC-M and SC groups (Figure 25G). Finally, the WT group had increased area of α-SMA positive cells, a marker of activated fibroblasts, compared to the DC-KO group at two weeks post-implantation (Figure 25H). No differences in the percentage of CD4, CD8, or CD20 expression was detected between the groups.

Quantitative Biocompatibility of Re-Implanted Lung Scaffolds

Immunohistochemical assessment was also performed on explants in the re-implantation study. Representative figures are included for one-week post re-implantation (Figure 26) and eight weeks post re-implantation (Figure 27).

One week following re-implantation of the scaffolds into previously exposed hosts, the WT group had greater cellularity than the SC and DC-M groups. However, by four weeks the DC-KO group had significantly more cellular infiltration than the SC and DC-M groups. Cell

numbers remained elevated in both the WT and DC-KO at eight weeks compared to the SC (Figure 28A).

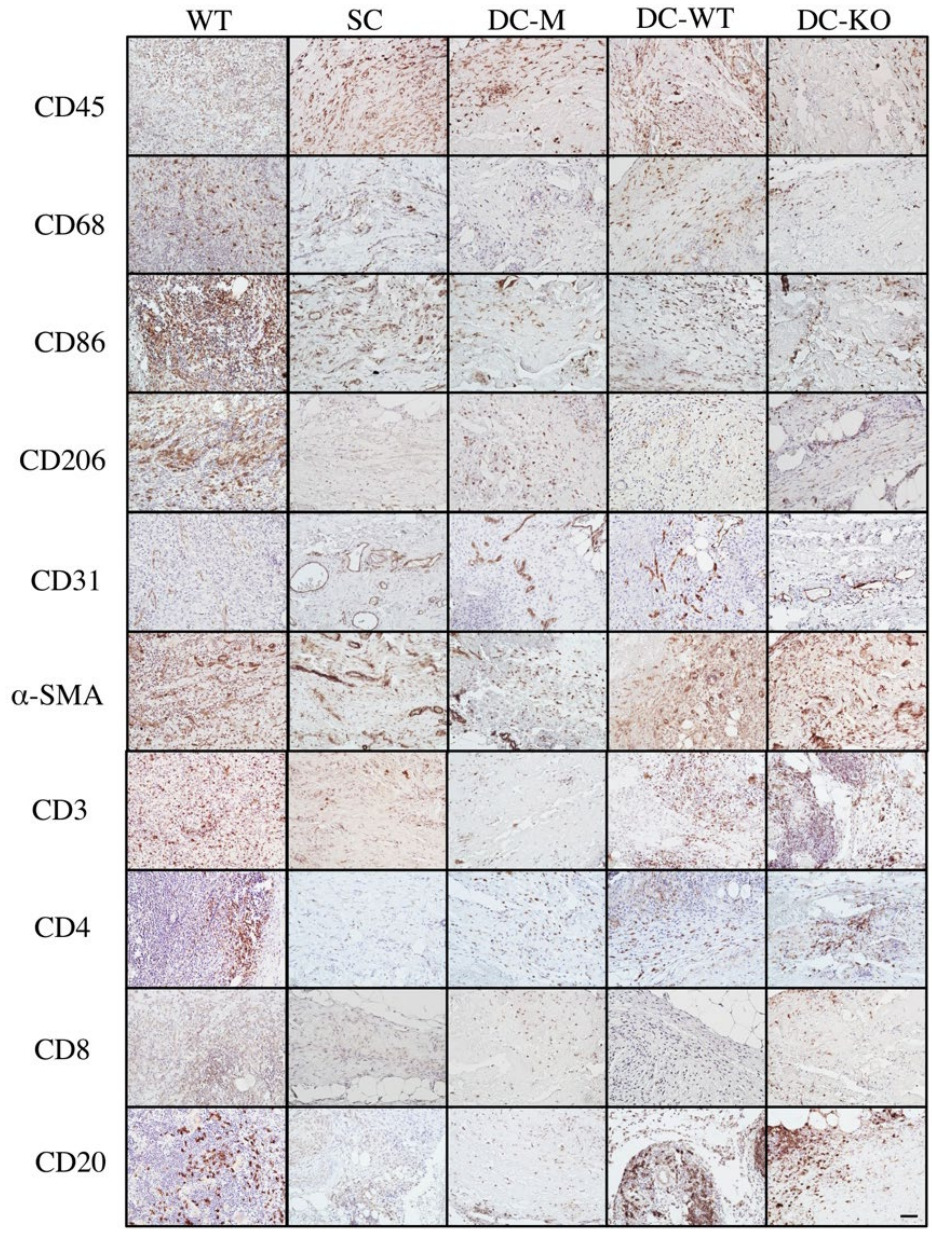

Figure 26. Representative IHC for re-implantation study, one-week post re-implantation

Representative immunostaining for native porcine (WT) lungs, sham injury control (SC), decellularized macaque (DC-M) lungs, decellularized wild type porcine (DC-WT) lungs, or decellularized α-Gal knockout (DC-KO) at one-week post-implantation, scale bar = 50μm.

The percentage of infiltrating $CD45^+$ leukocytes was lower in the WT group compared to DC-M at one, two, and four weeks although there were far fewer cells in the DC-M implants. By eight weeks, there were significantly fewer leukocytes in the DC-KO as compared to the DC-WT group (Figure 28B). In addition, the DC-KO group had increased neovascularization as compared to the SC and DC-M groups at two and four weeks post re-implantation (Figure 28C).

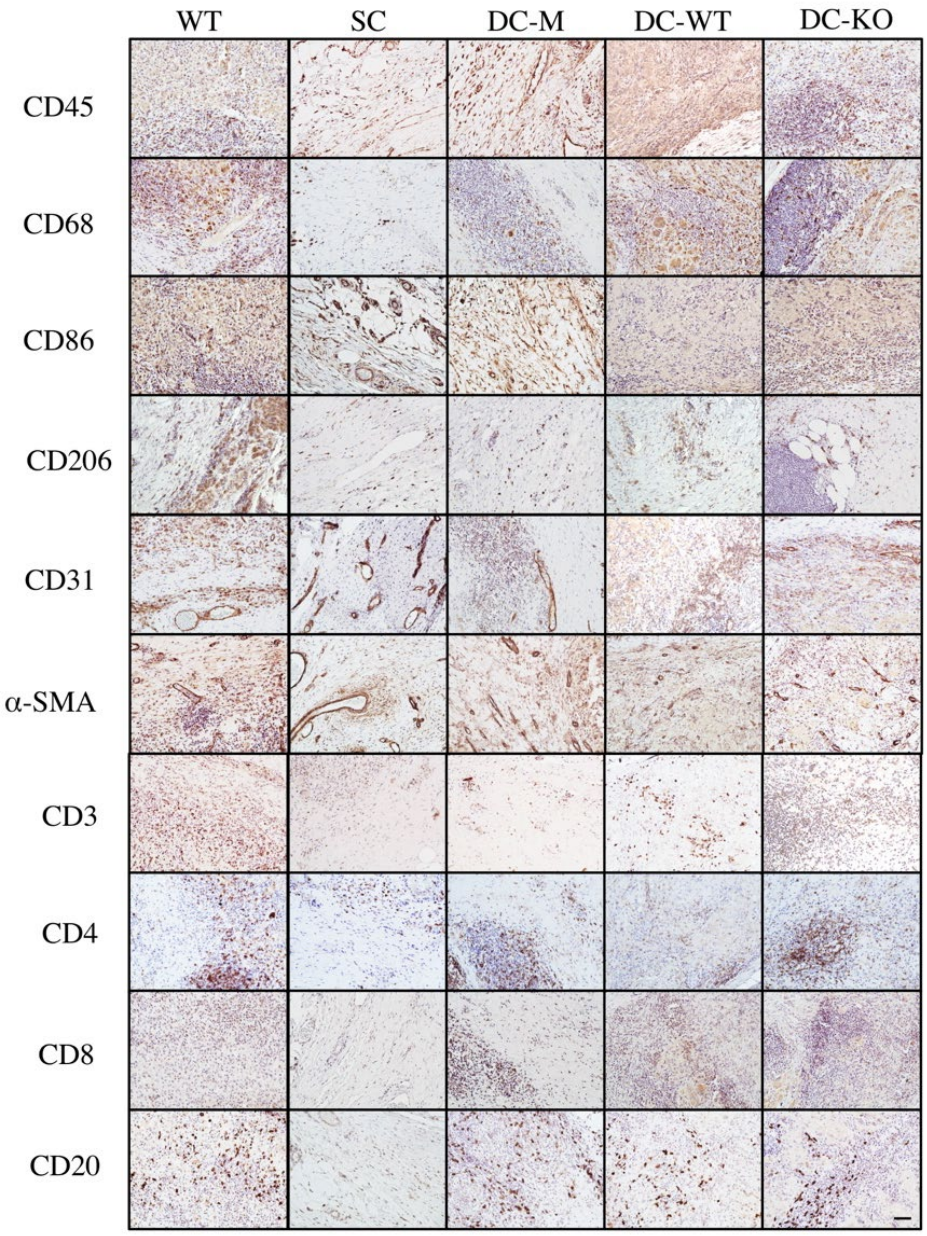

Figure 27. Representative IHC in re-implantation study, eight weeks post re-implantation

Representative immunostaining for native porcine (WT) lungs, sham injury control (SC), decellularized macaque (DC-M) lungs, decellularized wild type porcine (DC-WT) lungs, or decellularized α-Gal knockout (DC-KO) at one-week post-implantation, scale bar = 50μm.

The percentage of $CD3^+$ T-lymphocytes was increased in the DC-WT group compared to the SC at eight weeks (Figure 28D), while $CD8^+$ cytotoxic T-cells were elevated in the DC-M group relative to the WT group at one week post re-implantation (Figure 28E). No differences in CD4, CD20, CD68, CD86, CD206, or α-SMA expression were detected between the groups in the re-implantation study.

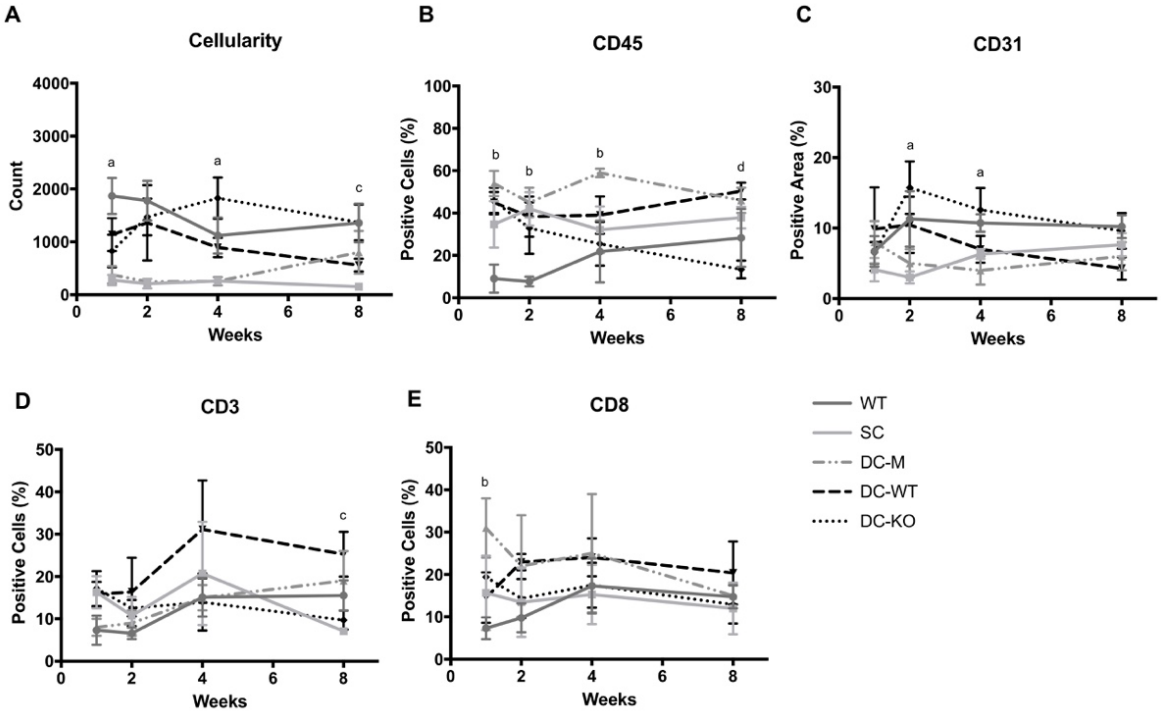

Figure 28. Quantitative assessment of specific cell subsets in the re-implantation study

A) Cellular infiltration was assessed by counting the number of hematoxylin-stained nuclei and averaged per five fields using ImageJ. B) The percentage of $CD45^+$ leukocytes, C) $CD31^+$ endothelial cells, and D) $CD3^+$ T-cells, and E) $CD8^+$ T-cells were quantified by normalizing the number of positive cells to the number of nuclei and averaged per five fields in the native porcine lung (WT), sham control (SC), decellularized macaque lung (DC-M), decellularized WT porcine lung (DC-WT), and decellularized a-Gal KO lung implants (DC-KO). Values are average ± standard error (n=4 implants per group). Significance ($p<0.05$) was measured by one-way Kruskal-Wallis ANOVA with Dunn's multiple comparisons at each time point designated by **a** (vs. SC / DC-M), **b** (vs. WT), **c** (vs. SC), **d** (vs. DC-KO) groups.

Adaptive Immune Response from Repeated Exposure

Chronic failure of xenotransplanted organs is most commonly attributed to the adaptive immune system, which retains immunological memory and exhibits potent cytotoxic abilities upon re-exposure events. Indeed, re-implantation of the DC-WT group induced a significant increase in $CD3^+$ T-cells at one and eight weeks compared to the initial implantation study, up to a 4-fold change increase (Figure 29A). The repeated sham injury also caused an increase in the presence of $CD3^+$ T-cells is the epidermis, and the DC-M had increased infiltration of $CD3^+$ T-cells in the re-implantation study at four weeks, up to a 3-fold increase. However, the percentage of $CD3^+$ T-cells levels were unchanged in the WT and DC-KO groups upon re-exposure.

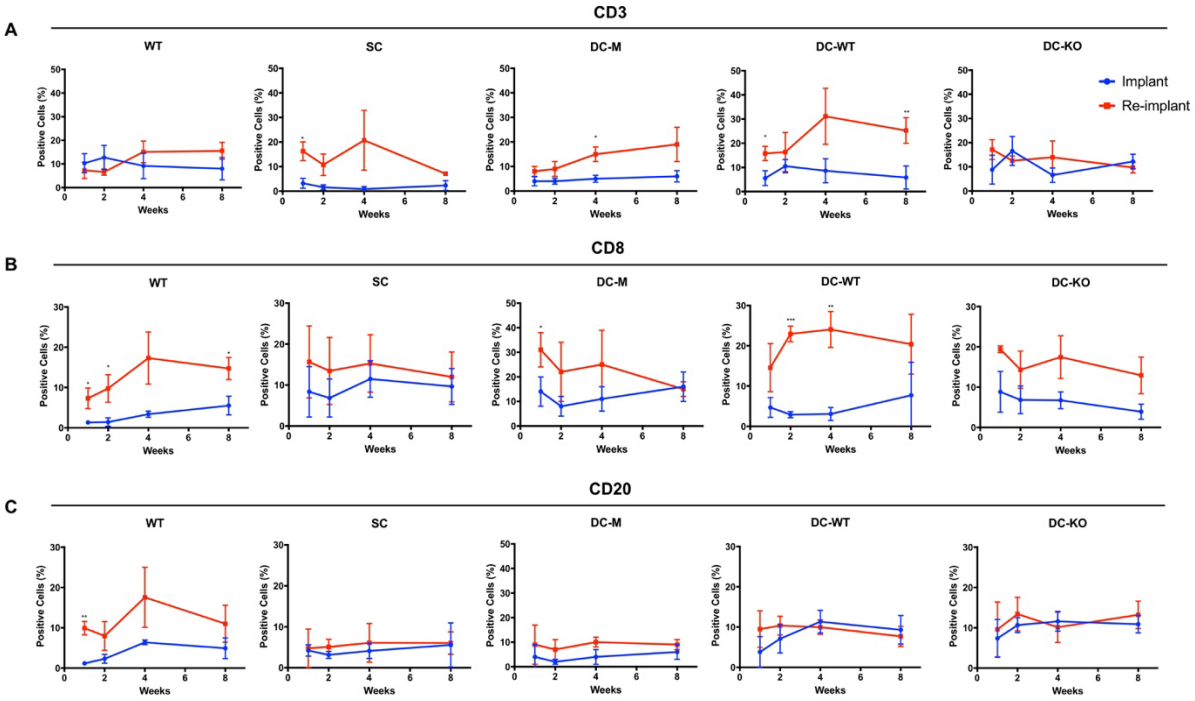

Figure 29. Comparison of the adaptive immune response between the implantation and re-implantation studies A) The percentage of $CD3^+$ T-cells, B) $CD8^+$ T-cells, and C) $CD20^+$ B-cells compared between the implantation and re-implantation studies over time for lung implant groups: native porcine lung (WT), sham control (SC), decellularized macaque lung (DC-M), decellularized WT porcine lung (DC-WT), and decellularized a-Gal KO lung implants (DC-KO). Differences were measured by a two-sample unequal variance t-test, (*p<0.05, **p<0.01, ***p<0.001). Values are average ± standard error (n=4 implants per group).

Furthermore, the levels of $CD8^+$ cytotoxic T-cells increased significantly in the WT, DC-WT, and DC-M groups from the implantation to the re-implantation study (Figure 29B). The WT group exhibited a significant 7-fold increase at two weeks, the DC-WT group showed up to an 8-fold increase at two and four weeks, and the DC-M group showed a 2-fold increase at one week. Neither the SC nor the DC-KO groups had significant increases in $CD8^+$ T-cells. Finally, the

level of $CD20^+$ B-cells was increased 8-fold in the WT group at one week after re-exposure, but no changes in B-cells were observed in the other groups (Figure 29C).

3.4 DISCUSSION

In this study, lungs from wild type or α-Gal knockout pigs were decellularized and subcutaneously implanted into a rhesus macaque model to comprehensively evaluate biocompatibility. The proportions of several immune cell subsets were compared between groups over time to assess the host response within the scaffolds and systemically in circulating blood. Measurements within the scaffolds are more sensitive at determining the host response as opposed to bulk blood work, given the subcutaneous implantation model, which results in a more moderate inflammatory response compared to whole organ transplant procedures. Furthermore, comparing percentages of immune cell subsets allows for a more accurate evaluation of the host response between groups, controlling for heterogenous cellularity across measurements and implant groups. The relative proportion of immune cells dictates the overall host response and signaling milieu more accurately than absolute cell numbers alone. Taken together, the results demonstrated differential profiles of circulating and infiltrating immune cell subsets and histological outcomes depending on the implanted tissue source and processing. The findings herein are limited by a small sample size of two animals per implant group but represent an important step towards the clinical development of biocompatible tissue engineered lungs.

Acellular scaffolds implanted *in vivo* elicit a well-defined host immune response, characterized by early recruitment of polymorphonuclear (PMN) and mononuclear innate immune cells, followed by adaptive immune cells (Badylak & Gilbert, 2008; Londono &

Badylak, 2015). The tissue source and processing of the scaffolds has been shown to direct the immune response and downstream outcomes (Keane, Swinehart, & Badylak, 2015). A positive outcome is associated with resolution of the immune response, vascularization, and site appropriate remodeling, while a negative outcome is characterized by chronic inflammation, formation of multi-nucleated giant cells, granulomas, and tissue necrosis (Brown & Badylak, 2014; Keane et al., 2015; Londono & Badylak, 2015). A greater proportion of "M2" anti-inflammatory macrophages, versus "M1" pro-inflammatory macrophages, has been linked to positive outcomes of implanted biomaterials as well as predominantly Th2 responses (Allman et al., 2001; Allman, McPherson, Merrill, Badylak, & Metzger, 2002; Brown, Londono, et al., 2012).

Subcutaneous transplantation of porcine tissue into the macaque without decellularization or Gal epitope removal is expected to result in rejection (Lexer et al., 1986; Rose et al., 1991). Indeed, the implanted native porcine lungs caused an acute increase in circulating levels of neutrophils and eosinophils in the rhesus macaques, as well as substantial production of anti-Gal IgM and IgG antibodies following exposure to the porcine tissue. The WT implants were consistently designated with a pathological score of 4 (severe inflammation). Quantitatively the WT tissue started with a higher cellularity than the other scaffolds, likely because these tissues were not decellularized. As such, the percentage of $CD45^+$ cells appeared lower than the other groups. However, qualitatively, polymorphonuclear cells, histiocytes, and multi-nucleated giant cells were identified as early as one week in the implants. By two weeks, the WT group had greater α-SMA staining than the DC-KO group, consistent with the resulting granulomas and fibrous encapsulation that was observed. During the re-implantation phase of the study, the fresh native porcine lung implants underwent liquefaction and distortion within the dermis, which

made quantifying distinct immune subsets more difficult and reflected in a slightly lower designated pathological score. The levels of anti-Gal antibodies continued to increase, suggesting host sensitization, and there were substantially more $CD8^+$ T-cells and $CD20^+$ B-cells present in the re-implanted tissues, which showed signs of rejection as anticipated.

A sham surgery was included to control for the effects of an immune response directed against the implantation procedure. As expected, no changes in circulating immune cells or antibodies were detected. The sham injury primarily affected the epidermis and resulted in minimal to no measurable influx of inflammatory cells. The cells that were present at the injury site were predominately $CD45^+$ leukocytes, with a large proportion of macrophages. Few lymphocytes were detected, however more $CD3^+$ T-cells appeared during the re-injury phase of the study. By the final time point, the injury to the epidermis was healed with granulation tissue and regenerated skin structures and no ongoing host response.

Similarly, the rhesus macaques implanted with decellularized allogeneic scaffolds underwent no changes in blood biochemistry, and no production of anti-Gal antibodies, as expected. The implants were designated with overall low pathological scores (2 = mild), associated with the expected immune response to implantation of decellularized scaffolds. In both the implantation and re-implantation study, there was an influx of immune cells from one to four weeks (primarily PMNs and macrophages), low $CD3^+$ lymphocyte counts, and low vascularization observed. In the implantation study, the DC-M implants were associated with a high $CD68^+$ and $CD206^+$ "M2" macrophage response. In the re-implantation study, the DC-M lung implants performed similarly with a mild pathological score. As with the implantation study, there were fewer total cells recruited to the DC-M implants, but the cells present were primarily leukocytes. At one week post re-implantation, the DC-M group had a greater

percentage of $CD8^+$ T-cells compared to the WT group. However, the absolute number of $CD8^+$ T-cells was similar between the groups (data not shown), likely representing residual memory T-cells from the primary implantation study and species-specific recognition in the DC-M group. By eight weeks, some elastin and other ECM components of the lung scaffolds remained but were being remodeled into granulation tissue and mature collagen.

Alternatively, the decellularized WT implants induced an increase in circulating neutrophils and substantial production of anti-Gal IgG antibodies by the hosts, especially following re-implantation. At early time points, the DC-WT porcine group had a significantly greater pathological score than the DC-KO group, but lower pathological score than the WT native porcine group (3 = moderate). By later time points, this metric was indistinguishable between the porcine groups. Quantitatively, the DC-WT scaffolds had similar levels of cellular infiltration as the WT group at four and eight weeks, but a higher proportion of $CD86^+$ "M1" macrophages, which appeared to be expressed on multi-nucleated giant cells. In the re-implantation study, the DC-WT implant induced greater levels of $CD45^+$ cells than the DC-KO group at eight weeks, along with an increase in the $CD3^+$ and $CD8^+$ T-cell response compared to the implantation study. Resolution of the immune response and scaffold degradation was incomplete by the final eight-week time point.

The decellularized α-Gal KO lung implants did not induce any change in the levels of anti-Gal IgM or IgG, as anticipated, demonstrating absence of the Gal epitope. However, one animal in the DC-KO group showed slightly higher levels of endogenous anti-Gal antibodies compared to other test subjects. The same animal had a significant increase in circulating white blood cells, particularly neutrophils, following exposure to the decellularized scaffolds. Qualitatively the DC-KO lung implant performed most similarly to the DC-WT group in the

implantation and re-implantation study. Quantitatively, the DC-KO implants were maximally infiltrated by cells at later time points than the other porcine groups and showed increased percentages of $CD3^+$ T-cells compared to the sham injury at two weeks, but not the WT or DC-WT implants. As there was no difference in percentages of CD4/CD8 T-cells, the physiological relevance of the observed increase in $CD3^+$ T-cells at 2 weeks is unclear. The DC-KO had fewer α-SMA^+ fibroblasts compared to the native WT group early in the implantation study. In the re-implantation study, the scaffolds were again infiltrated more slowly, contained fewer $CD45^+$ cells compared to the DC-WT group at eight weeks, and had increased neovascularization. By the final time points, scaffold materials were still present in the implant site and there was ongoing cellular reaction, including large granulomas, which were present in all the porcine groups.

At present, T-cell mediated chronic rejection of materials is a major remaining immunological barrier of xenotransplantation, which appears months to years after transplant, and is controlled with life-long immunosuppression. The animals in this study did not receive any immunosuppression, and thus experienced a robust T-cell response in the porcine groups, particularly post re-implantation. Interestingly, the percentage of $CD3^+/CD8^+$ T-cells was significantly increased in the DC-WT group following re-implantation, but not in the DC-KO group, suggesting that the absence of the Gal epitope may reduce some T-cell recognition upon re-exposure, which has also been demonstrated by others *in vitro* (Wilhite et al., 2012). Of note, there was no measured increase in $CD3^+$ T-cells in the re-implanted WT group despite showing signs of liquefaction and rejection, which might be explained by 1) higher levels of other immune or non-immune cells in the implants or 2) restriction of cellular migration through non-decellularized implants. The percentage of $CD20^+$ B-cells increased significantly in the WT

group post-re-implantation, further supporting sensitization to Gal and other porcine epitopes in the native implants.

This study is the first to examine the host response to decellularized lung constructs derived from WT and α-Gal KO pigs *in vivo* using an immunologically relevant model. Other groups have characterized extracellular matrices derived from wild type or α-Gal knockout small intestine submucosa and urinary bladder matrix and found no changes in the content of growth factors, mechanical properties, host response, or tissue remodeling, demonstrating that removal of the Gal-epitope does not significantly affect the function of the acellular scaffolds (Daly et al., 2009; Liang, Fisher, Yang, Hall, & Woo, 2011). In this study, the two groups behaved similarly overall, with a slight reduction in adaptive immunity observed in the re-implanted decellularized KO group.

In the context of lung tissue engineering, several challenges remain, including effective recellularization and surgical implantation of the decellularized lung constructs to recapitulate human organ function. Platz et al. successfully recellularized lung constructs derived from both wild type and α-Gal knockout porcine lungs, and determined that the scaffolds were capable of supporting the growth of human lung cells, including bronchial epithelial cells, fibroblasts, mesenchymal stromal cells, and pulmonary vascular endothelial cells in a cell culture system (Platz et al., 2016).

While α-Gal is a primary immunogen of porcine tissue, other antigens are capable of inducing an immune response following transplantation. In addition to α-Gal, other porcine antigens that contribute to preformed anti-pig antibody reactivity include N-glycolylneuraminic acid (Neu5Gc) and the glycan SD^a (a blood group antigen) (Byrne, Ahmad-Villiers, Du, & McGregor, 2018). Considering that both pig tissues and nonhuman primate donors express

Neu5Gc, the present study would not have distinguished this immunogenic reaction. Some but not all primates produce the glycan SD^a via beta-1,4-N-acetyl-galactosaminyltransferase 2 (B4GALNT2) while others have IgM anti-bodies directed to it (Byrne et al., 2018; Dall'Olio, Malagolini, Chiricolo, Trinchera, & Harduin-Lepers, 2014). Future studies may investigate the contribution of these antigens to the immunogenic response to porcine tissues. Combining the decellularized α-Gal knockout with additional tissue engineering approaches, such as recellularization with human cells, has the potential to further reduce the immune response over decellularization alone. Further studies will be necessary to assess the host immune response to recellularized lung scaffolds, particularly following implantation into the thorax, where direct blood contact might induce a more rapid immune response. Additional time points will be necessary to fully measure the degradation of the scaffolds and biocompatibility of both the decellularized and recellularized α-Gal KO versus WT porcine lungs in these contexts.

In conclusion, the decellularized α-Gal KO lung constructs performed similarly to the decellularized WT group after subcutaneous implantation in a non-human primate model from a histological and tissue remodeling standpoint. The genetic removal of the Gal epitope from porcine lung tissue appeared to delay immune cell infiltration and reduce the chronic T-cell mediated reaction against decellularized materials following re-implantation. Removal of the Gal epitope may be an effective strategy to extend the life-span of clinical grade decellularized constructs for use in heart valves, ligaments, and perhaps one day, tissue engineered whole organs. Further studies are needed to assess biocompatibility over longer time points in both decellularized and recellularized lung grafts.

4.0 GENERAL DISCUSSION

4.1 SIGNIFICANCE

By 2050, the number of individuals over the age of 65 is expected to increase by 71% to nearly 2 billion individuals worldwide, with the number of US citizens over the age of 65 surpassing 20% by 2030 (Ortman JM, 2014). These statistics mark an important turning point in US history where the population over the age of 65 will surpass those under the age of 18 for the first time (Census.gov, 2018). Furthermore, the number of working individuals to the number of retired individuals will decrease from 3.5:1 to 2.5:1, with major implications for health care and economics.

The primary explanation behind these shifting demographics is aging of the baby boomer generation with prolonged lifespans and decreased birth rates in the United States (Census.gov, 2018). Despite living longer, elderly populations are not necessarily living healthier lives. Over 75% of the elderly population will be diagnosed with at least one chronic condition, often presenting with systemic inflammation and in some cases requiring organ transplantation (NCOA, 2015). Currently over 114,000 people are enrolled on the organ transplant list and 20 people die each day waiting for a transplant (HHS.gov, 2018). The increased incidence of end-stage disease with aging necessitates a demand for viable organs and other regenerative medicine strategies to rejuvenate tissue function and reduce inflammation.

Macrophages are key cells that play important roles in the progression of chronic, inflammatory disease and regulate immune tolerance towards transplanted organs and materials by taking on classically activated or alternatively activated phenotypes.

Just within the past decade, the developmental heterogeneity of macrophage populations has been discovered (Hoeffel et al., 2012; Yona et al., 2013). In the liver, the embryonically derived population of macrophages, known as Kupffer cells, were found to be stable and maintained independently from infiltrating, monocyte-derived macrophages in the absence of infection or injury (Gomez Perdiguero et al., 2015; Jenkins et al., 2011; Schulz et al., 2012; Yona et al., 2013). However, very little is known about how these two hepatic macrophage populations are maintained during the natural process of aging, which may influence the onset and progression of chronic liver disease. Work presented in this dissertation identified a previously unknown accumulation of $CD11b^{+}$ "recruited" macrophages in aged livers, which may be driven in part by increased fat deposits leading to activation of inflammatory chemokine signatures from aged hepatocytes. A better understanding of the hallmarks of aging in the liver will be crucial in the development of preventative measures and treatments for end-stage liver disease in elderly patients.

While inhibiting the chemokine receptor CCR2 did not affect the aged liver macrophage profile, the results suggest that inhibiting CCR2 signaling may be beneficial to reduce hepatic triglyceride levels and inflammatory gene expression in advanced age; and further supports the use of CCR2 antagonists to treat age-related steatosis. Clinical studies have shown that treating patients with Cenicriviroc, a dual CCR2/CCR5 antagonist, resulted in twice as many subjects achieving improvement in fibrosis and no worsening of steatohepatitis compared with placebo (Friedman SL, 2018). Subgroup analysis demonstrated that the therapy was similarly effective in

patients above and below 56 years of age, suggesting this therapy may show promise in treating age-related NAFLD/NASH as well. Our study lends further support that targeting the CCL2-CCR2 pathway may be a promising strategy to reduce the onset and progression of hepatic fat accumulation and inflammation during the process of aging.

Another approach to treating end-stage disease is the generation of new organs and tissues for transplant. The work presented in this dissertation is the first to examine the host response to decellularized lung constructs derived from wild type and alpha-Gal knockout pigs *in vivo* using an immunologically relevant model. The results demonstrated differential profiles of circulating and infiltrating immune cell subsets and histological outcomes depending on the implanted tissue source and processing. Specifically, the genetic removal of the Gal epitope from porcine lung tissue delayed immune cell infiltration and reduced chronic T-cell mediated reaction following re-implantation. These studies suggest that removal of the Gal epitope may be an effective strategy to extend the life-span of clinically used decellularized constructs as heart valves and in other applications. Furthermore, this work supports the use of alpha-Gal knockout materials in future tissue engineering efforts to address the organ shortage crisis in the United States.

Taken together, these studies further our understanding of macrophage biology in the aging liver and in the host response to Gal-epitopes and aid in the design of novel strategies to reduce inflammation in chronic disease and tissue engineering contexts.

4.2 FUTURE DIRECTIONS AND CONCLUDING REMARKS

In "Chapter 2: A Study of Macrophages in the Aging Liver," there are several questions that remain to be addressed. Our studies demonstrated that the parenchymal fraction of the liver was more significantly associated with inflammatory gene expression than macrophages, which suggested that hepatocytes are the source of inflammatory signals. However, the influence of other non-parenchymal cells, such as endothelial cells and stellate cells, on the inflammatory gene expression in the aged liver remains an area of future study. While CD11b has been associated with monocyte-derived macrophages, fate tracing experiments will be necessary to confirm the origin of the $F4/80^{+}CD11b^{+}$ hepatic macrophages. Similarly, further studies will be necessary to determine the significance of this population as well as which chemokines or signaling gradients are responsible for driving the increase in CD11b-expressing macrophages in the aged liver, as inhibiting the receptor for MCP-1/CCL2 did not influence the proportions of hepatic macrophages. Results from RNA-Seq analysis suggest that *Cxcl7, Cxcl13, Ccl22, Ccl5*, and *Ccl6* may be important chemokines to target in the future. In addition, $CCR2^{-}$ $Ly6C^{lo}$ monocytes derived from the spleen may be one explanation for the increase in CD11b "M2-like" macrophages in the aged liver.

In "Chapter 3: The Host Response to Engineered Lung Scaffolds," there are several critical experiments and challenges that will be necessary to address in order to successfully translate the lung constructs from bench to bedside. In future studies, the lung scaffolds will be recellularized with host derived cells and implanted in a physiologically relevant way (*i.e.* connected to the trachea and pulmonary artery to mediate oxygenation of blood). Once porcine lung scaffolds are recellularized, Gal-epitopes may be further concealed, reducing the host response and perhaps negating the need for genetic deletion, however this hypothesis remains to be tested.

Alternatively, additional porcine antigens and porcine endogenous retrovirus (PERV) genes may need to be genetically removed. The advent of high-throughput genetic engineering technologies such as CRISPR allows for the targeted deletion of several porcine genes at once (Niu et al., 2017), but this remains to be studied in the context of biocompatibility. Presently the challenges in recellularizing constructs into functional tissues are the major hurdle to overcome in the generation of clinically relevant animal-derived whole organs for transplantation.

In general, the accumulation of infiltrating or M1-polarized monocytes/macrophages tends to exacerbate chronic disease and contribute to organ failure or rejection by promoting inflammation and recruiting adaptive immune cells. However, very few, if any, studies have systematically identified changes in the basal levels of macrophage populations in aging tissues and organs, or the dynamics of aged macrophages following injury, in either animal models or human patients, representing a hugely understudied area of research.

Therapies that suppress M1-polarization or infiltration of macrophages might reduce the progression of chronic disease from manageable early stages to chronic end-stages requiring organ transplantation. In the context of aging specifically, promoting M2-gene expression might delay the advancement of acute disease into chronic disease. Strategies to modulate the immune system and the host response are emerging across many disciplines of medical research and treatment.

Immunomodulatory drugs have been used for generations to either activate or suppress the immune system. In order to help manage organ transplantation and autoimmune disease, glucocorticoids, cytostatic drugs, and suppressive antibodies, such as anti-TNF biologics, have been widely used (Julier, Park, Briquez, & Martino, 2017). More recently, T-cells have been the

primary target of activating immunotherapies for treating cancer, using checkpoint inhibitors and chimeric antigen receptors with adoptive cell transfer (Hu, Ott, & Wu, 2018).

The local delivery of either activating or suppressing cytokines using engineered drug delivery systems has now been extensively studied preclinically. Our group has explored the use of an interleukin-4 drug-eluting coating on synthetic mesh to push responding macrophages towards M2 polarization, which has shown to improve tissue integration downstream (Hachim, LoPresti, et al., 2017). The local delivery of cytokines may be a future avenue of exploration for promoting M2 macrophage polarization in liver disease and in the host response to tissue engineered constructs. Importantly, M2 macrophages have been associated with tumor progression, including clinical hepatocellular carcinoma (HCC) specimens (Yeung et al., 2015). Thus, macrophage polarization must be closely monitored to balance the resolution of inflammation with promoting an environment permissive to tumorigenesis and fibrosis.

As our understanding of immune system continues to grow, particularly in the context of aging and other health disparities, coupled with the development of new technologies to modulate immune cells including macrophages, therapies may be able to improve the human health-span and contribute to the rejuvenation and replacement of tissues and organs.

APPENDIX A

ADDITIONAL METHODS FROM CHAPTER 2

***Serum quantification*.** Serum was collected from experimental animals and the levels of circulating proteins, including alanine transaminase (ALT), aspartate transaminase (AST), albumin, and total bilirubin, or serum cholesterol and triglycerides were determined by the University of Pittsburgh Medical Center Clinical Laboratory.

***Hepatic lipid quantification*.** Frozen liver pieces (~100 mg) were shipped overnight on dry ice to the Lipids and Lipoproteins Sub-core at the Vanderbilt Mouse Metabolic Phenotyping Center (MMPC) Analytical Resources Core. Lipids were extracted from liver tissue by thin layer chromatography, and total cholesterol, triglycerides, and fatty acids were quantified by gas chromatography.

***Hepatic bile acids quantification*.** Frozen liver pieces (~100 mg) were homogenized in 75% ethanol (DeconLabs, King of Prussia, PA) and incubated at 50 degrees Celsius for 2 hours. Digested lysates were centrifuged at 6000g for 10 minutes and the supernatant collected. Bile acids were quantified using the Mouse Total Bile Acids Kit (Crystal Chem, Elk Grove Village, IL).

Glucose tolerance test. Fasting glucose levels were measured from blood using EmbracePRO glucose monitor (Omnis Health, Nashville, TN). Mice received intra-peritoneal injection of 10% D-glucose solution (1g/kg, Fisher Scientific). Levels of glucose in the blood were measured at 15, 30, 60, and 120 minutes post-injection and recorded.

Liver histology and immunostaining. Paraffin blocks were sections at a thickness of 4 μm and affixed to glass slides. Sections were deparaffinized using xylene and graded ethanol (100-95%) washes then placed in tap water. Hematoxylin and eosin, Masson's trichrome, and Picrosirius red staining was performed in house according to standard protocols (Sigma-Aldrich). Staining was performed by the McGowan Institute for Regenerative Medicine histology core using ApopTag® Peroxidase In Situ Apoptosis Detection Kit (EMD Millipore, Burlington MA). OCT blocks were sectioned at a thickness of 7 μm and affixed to glass slides. Sections were brought to room temperature for 10 mins, then stained with Oil Red O (Sigma-Aldrich), or blocked with 5% donkey serum (Fisher Scientific), 1% bovine serum albumin (Sigma-Aldrich), 0.01% TritonX-Tween20 (Fisher Scientific) for one hour for immune-staining. Primary antibodies, rabbit anti-mouse CD68 (ab125212, 1:250, Abcam, Cambridge, MA) and rat anti-mouse CD11b (550282, 1:100, BD Biosciences, San Jose, CA) were applied to tissue sections overnight at 4 degrees Celsius. Slides were washed three times in PBS, then secondary antibodies were applied for one hour at 1:250 dilution (donkey anti-rabbit 647, donkey anti-rat 594, ThermoFisher Scientific). Slides were washed three times in PBS, then blocked in 5% rat serum (ThermoFisher Scientific) for 1 hour at room temperature. F4/80-FITC (ab105155, 1:50, Abcam) was applied for one hour at room temperature. Slides were washed three times in PBS, counterstained with DAPI (BioLegend, San Diego, CA), mounted, and coverslipped. Light microscopy was performed on Eclipse50i microscope, fluorescence microscopy was performed

on EclipseTiU (Nikon Instruments Inc., Melville, NY). Quantification of staining was performed in ImageJ (NIH) or Elements (Nikon) software.

Gene expression. RNA-later solution was removed from cell pellets. RNA was isolated using the RNeasy mini kit (Qiagen, Gaithersburg, MD). Briefly, cells were lysed with the RLT buffer and 70% ethanol, then applied to spin columns, washed, and eluted per the manufacturer's directions. RNA was quantified using a NanoDrop Lite Spectrophotometer (ThermoFisher). cDNA was generated using the RNA-to-cDNA kit (Applied Biosystems, Foster City, CA). Quantitative reverse-transcription polymerase chain reaction (qRT-PCR) was performed with 10ug of cDNA, TaqMan Gene Expression Master Mix (ThermoFisher), and TaqMan primers (ThermoFisher) on the Quant Studio 3 machine (Applied Biosystems). The primers used were Ccl2 (Mm00441242_m1), Tnfa (Mm00443258_m1), Il1b (Mm00434228_m1), Il6 (Mm00446190_m1), beta-actin (Mm00607939_s1). Fold change was calculated using the 2^(-delta(delta Ct)) method compared to young or young wild-type control samples unless otherwise stated.

Protein analysis. Hepatocyte protein lysates were quantified using a BCA Assay (ThermoFisher). CCL2 was measured with the murine JE/MCP-1 (CCL2) ELISA kit (Peprotech, Rocky Hill, NJ), according to the manufacturer's directions. Alternatively, 50 ug of protein was denatured with Bolt LDS Sample Buffer and Bolt Reducing Agent, then ran on a 4-12% Bolt-Tris Plus gel at 200 volts for 22 minutes in 1x SDS running buffer, according to the manufacturer's instructions (ThermoFisher). Protein was transferred to a nitrocellulose membrane using the iBlot Transfer Stack System (ThermoFisher). Blots were blocked in 5% bovine serum albumin prepared in wash buffer for one hour and cut. Primary antibodies were applied overnight: CCL2 (1:500, sc-52701), p-p50 (Ser 337, 1:500, sc-271908), and p-p65

(Ser536, 1:500, sc-136548) (Santa Cruz Biotechnology Inc., Dallas, TX). After washing, secondary antibodies were applied for 1 hour in 2.5% milk (goat anti-mouse IgG HRP, goat anti-rat HRP, and GAPDH-HRP (1:2000) (ThermoFisher). Blots were washed and developed with SuperSignal West Dura Extended Duration Substrate (ThermoFisher). Blots were imaged using ChemiDoc Imaging System (Bio-Rad, Hercules, CA).

Flow cytometry experiments. Non-parenchymal cells were washed in FACS buffer (5% fetal bovine serum and 1% bovine serum albumin in Hank's Buffered Saline Solution (Sigma-Aldrich) and stained with fixable near-infrared viability dye (1:1000, FisherScientific). Cells were blocked with Fc blocker (1:100, CD16/32, BD Biosciences), then surface stained with flow antibodies (1:20, F4/80-PE (BM8, eBioscience, ThermoFisher), CD11b-APC (1:20, M1/70, eBioscience, ThermoFisher), CD146-PerCypCy5.5 (1:20, ME-9F1, BD Biosciences), CD45-FITC (1:20, 30-F11, BD Biosciences)) for 20 mins at 4 degrees Celsius. Cells were fixed with Fixation Buffer (BioLegend) and stored overnight in FACS buffer. The following morning, cells were permeabilized with Intracellular Staining Permeabilization Wash Buffer (BioLegend) and stained with CD68-BV421 (1:20, FA-11, BioLegend). Cells were washed and analyzed on the MACSQuant Flow Cytometer (Miltenyi Biotec, Auburn, CA) and analyzed with FlowJo Software.

Hepatic macrophage cell culture experiments. Isolated F4/80+ hepatic macrophages were cultured at 100,000 cells in a tissue culture treated 96-well plate (Corning, Tewksburg, MA, 31.6 mm2 growth volume or 3165 cells/mm2) in RPMI-1640 media (Sigma-Aldrich) supplemented with 10% fetal bovine serum (Corning), 1% 1M HEPES (Sigma-Aldrich), and 1% Pen-Strep (Fisher Scientific). After allowing hepatic macrophages to adhere to the cell culture plates for 3 hours, media was replaced with fresh warmed media (M0 group), or fresh media

supplemented with recombinant murine interferon-gamma (20 ng/ml, Peprotech) and lipopolysaccharides from e. coli O55:B5 (100 ng/ml, Sigma-Aldrich) (M1 group), or supplemented with interleukin-4 (20ng/ml, Peprotech) (M2 group) for 12 hours. After 12 hours, the supernatants were collected for nitric oxide production assay using the Griess Reagent system. Briefly, supernatant was mixed with equal amounts of 1% sulfanilamide in 5% phosphoric acid and 0.1% N-(1-napthyl)ethylenediamine dihydrochloride (NED, Sigma-Aldrich) and absorbance was read at 540 nm on Synergy HTX plate reader (BioTek, Winooski VT), compared to a standard curve prepared from 0.1M sodium nitrite (Sigma-Aldrich). Cells were fixed with 2% paraformaldehyde, then blocked with 5% donkey serum (Fisher Scientific), 1% bovine serum albumin (Sigma-Aldrich), 0.01% TritonX-Tween20 (Fisher Scientific) for one hour for immune-staining. Primary antibodies, rabbit anti-mouse iNOS (1:200, ab3523, Abcam) and rabbit anti-mouse liver arginase (1:400, ab91279, Abcam) were applied to cells overnight at 4 degrees Celsius. Cells were washed three times in PBS, then secondary antibodies were applied for one hour at 1:250 dilution (donkey anti-rabbit 488, ThermoFisher), counterstained with DAPI (BioLegend), and imaged. Alternatively, cells were incubated with Vybrant Phagocytosis FITC-e.coli particles (ThermoFisher) at a 1:20 dilution in media for 2 hours at 37 degrees Celsius, then washed, and fixed with 2% paraformaldehyde, and counterstained with DAPI for analysis of phagocytosis. Urea production was measured by lysing cells in 0.001% Triton-X (Fisher Scientific) and combining with arginase activation solution (10mM MnCl2, 50mM Tris-HCl, Sigma-Aldrich) for 10 mins at 56 degrees Celsius, then incubating at 37 degrees Celsius for 22 hours with arginase substrate solution (0.5M L-arginine, Sigma-Aldrich). Urea was measured with detection solution (513 mg/L primaquine, 100 mg/L phthalaldehyde, 2.5 mol/L sulfuric

acid, 2.5 g/L boric acid, 0.03% Brij35, Sigma-Aldrich) against a urea standard curve and absorbance was read at 430nm on Synergy HTX plate reader (BioTek).

Endotoxin Assay and 16S rRNA from hepatic blood. Blood was collected from female 3-month-old and 19-month-old (NIA) mice fasted for six hours sterilely by inserting a catheter directly into the inferior vena cava. Blood was allowed to coagulate in a sterile tube for 15 minutes, centrifuged at 10,000xg for 10 mins, and the serum supernatant was collected and stored at -80C. Serum was diluted 1:10 and levels of endotoxin were quantified using the ToxinSensor LAL Chromogenic Endotoxin Quantitation Kit (VWR, Radnor, PA), according to the manufacturer's instructions. Alternatively, blood was collected in EDTA tubes (BD Biosciences), then DNA was isolated using the DNeasy Blood and Tissue Kit (Qiagen). qRT-PCR was performed on DNA for 16S rRNA (Taqman: Ba04930791_s1) according to methods described previously.

RNA-Seq and Pathway Analysis. RNA was processed by the University of Pittsburgh Health Sciences Sequencing Core for mRNA-Seq. Libraries were prepared with TruSeq Stranded mRNA kit (Illumina, San Diego, CA) according to manufacturer instructions. Sequencing was on a NextSeq 500 using a single mid-output flowcell and 150 base single read. Adapter sequences were trimmed during demultiplexing. Raw data was processed in CLC Genomics Workbench 11 (Qiagen). Reads were mapped to the mouse reference genome and differentially expressed genes were determined between young and aged hepatocyte samples using filters to select genes with reads per kilobase of transcript per million (RPKM $\geq$ 1), absolute fold change (FC > 1.5), and false discovery rate (FDR) $\leq$ 0.05. Differentially expressed genes were imported into Ingenuity Pathway Analysis (IPA) to determine signaling pathways and upstream regulators. Activation (positive z-score), inhibition (negative z-score), and interactions of canonical

pathways was examined based on experimentally determined gene expression changes reported in the literature.

APPENDIX B

RNA-SEQ DATA

Table 5. Differentially Expressed Genes in Aged Hepatocyte Fractions Compared to Young Identified by RNA-Seq

Name	Chromosome	Max group mean	Log_2 fold change	Fold change	P-value	FDR p-value
Dmbt1	7	0.59	-7.26	-152.90	9.58E-09	6.0E-06
Slco1a1	6	18.74	-7.25	-152.15	0	0.0E+00
Epdr1	13	0.36	-5.13	-35.05	2.04E-05	4.6E-03
Cib3	8	2.98	-4.65	-25.06	5.72E-09	3.7E-06
Clec2h	6	1.95	-4.52	-22.93	3.62E-14	6.1E-11
Serpina4-ps1	12	1.07	-3.67	-12.70	5.61E-08	3.2E-05
Cdh1	8	7.51	-3.60	-12.17	0	0.0E+00
4930452B06Rik	14	0.72	-3.55	-11.75	2.07E-08	1.2E-05
Arhgap44	11	0.07	-2.88	-7.38	3.07E-04	3.0E-02
Krt23	11	4.47	-2.81	-7.01	2.29E-12	3.0E-09
Smpd3	8	1.02	-2.78	-6.88	1.36E-05	3.3E-03
Hapln1	13	0.22	-2.48	-5.58	6.10E-05	1.0E-02
Adgrf1	17	1.20	-2.48	-5.56	1.09E-08	6.7E-06
Ugt2b38	5	0.90	-2.43	-5.38	1.61E-05	3.8E-03
Serpina1e	12	297.01	-2.38	-5.22	1.38E-11	1.5E-08
Cyp2d9	15	20.91	-2.31	-4.96	0	0.0E+00
Col4a3	1	1.38	-2.29	-4.89	4.73E-07	2.0E-04
Gm3839	14	7.08	-2.24	-4.72	1.94E-11	2.0E-08
Pls1	9	0.84	-2.21	-4.61	1.27E-04	2.0E-02
Cyp2b13	7	187.56	-2.20	-4.60	0	0.0E+00
Mup3	4	2822.47	-2.19	-4.56	0	0.0E+00
Cyp3a11	5	1496.76	-2.10	-4.29	0	0.0E+00

Table 5 continued

Aqp4	18	1.17	-2.09	-4.25	1.93E-05	4.5E-03
Reck	4	1.07	-2.08	-4.23	1.33E-07	6.6E-05
Acsm2	7	0.28	-2.04	-4.10	1.61E-05	3.8E-03
Mup20	4	95.94	-2.02	-4.05	0	0.0E+00
C8a	4	76.95	-1.97	-3.93	9.35E-14	1.4E-10
Susd4	1	0.42	-1.92	-3.80	4.68E-04	5.0E-02
Sort1	3	1.06	-1.85	-3.61	4.83E-12	5.8E-09
Lars2	9	409.73	-1.84	-3.57	5.59E-06	1.6E-03
Adamts7	9	0.85	-1.79	-3.46	1.18E-07	5.9E-05
Defb1	8	3.98	-1.73	-3.31	3.50E-05	6.7E-03
Etnppl	3	56.28	-1.68	-3.21	3.62E-07	1.6E-04
Ociad2	5	5.39	-1.67	-3.18	4.90E-12	5.8E-09
Hsd3b2	3	9.70	-1.60	-3.04	8.72E-13	1.2E-09
C8b	4	63.90	-1.58	-2.98	0	0.0E+00
Mup11	4	836.76	-1.55	-2.92	1.51E-07	7.3E-05
Col4a5	X	0.65	-1.54	-2.91	8.60E-05	1.0E-02
Itih5	2	3.41	-1.52	-2.87	1.32E-11	1.5E-08
Btc	5	0.80	-1.52	-2.87	2.77E-04	3.0E-02
Enpp2	15	25.92	-1.51	-2.84	5.00E-15	9.4E-12
Sel1l3	5	1.55	-1.48	-2.78	4.91E-10	3.8E-07
Abca8a	11	24.41	-1.47	-2.78	5.75E-06	1.6E-03
Fam81a	9	1.20	-1.47	-2.76	3.55E-05	6.7E-03
Inmt	6	465.76	-1.44	-2.72	1.63E-06	5.8E-04
Dpy19l3	7	0.30	-1.42	-2.67	1.54E-04	2.0E-02
Gm26822	16	1.10	-1.42	-2.67	2.65E-04	3.0E-02
Asap3	4	1.67	-1.38	-2.60	1.11E-06	4.2E-04
Dsg1c	18	3.41	-1.37	-2.59	1.01E-04	1.0E-02
Hsd3b3	3	23.65	-1.33	-2.51	7.26E-12	8.2E-09
Selenbp2	3	17.48	-1.32	-2.50	4.26E-09	2.8E-06
Mmd2	5	5.48	-1.28	-2.43	9.10E-08	4.8E-05
Ppp1r3g	13	8.82	-1.25	-2.38	1.94E-04	2.0E-02
Tceal8	X	5.84	-1.25	-2.38	2.56E-11	2.5E-08
Cldn1	16	13.46	-1.22	-2.33	1.37E-08	8.2E-06
Cyp2c55	19	2.43	-1.21	-2.32	1.74E-04	2.0E-02
Gm20547	17	6.89	-1.18	-2.27	1.44E-10	1.2E-07
Ces3b	8	133.49	-1.17	-2.25	1.53E-08	9.0E-06
Mug1	6	368.34	-1.16	-2.24	3.03E-06	9.7E-04

Table 5 continued

Fkbp11	15	5.59	-1.16	-2.23	1.47E-04	2.0E-02
Cyp2f2	7	758.89	-1.12	-2.18	1.60E-05	3.8E-03
Cyp2c54	19	209.59	-1.13	-2.18	1.27E-04	2.0E-02
1810011O10Rik	8	26.07	-1.12	-2.17	4.50E-04	4.0E-02
Ces3a	8	334.77	-1.11	-2.16	6.45E-06	1.8E-03
Egfr	11	18.05	-1.11	-2.15	1.12E-08	6.9E-06
Mup10	4	6681.44	-1.08	-2.12	1.36E-04	2.0E-02
Rnf125	18	54.07	-1.07	-2.10	5.99E-08	3.4E-05
Cyp4a31	4	5.17	-1.05	-2.08	2.01E-04	2.0E-02
Nudt7	8	26.28	-1.04	-2.06	4.05E-09	2.7E-06
Trib3	2	4.28	-1.04	-2.05	7.20E-05	1.0E-02
Arhgef16	4	1.45	-1.03	-2.05	3.37E-04	4.0E-02
Arl4d	11	55.90	-1.02	-2.02	2.29E-04	3.0E-02
Slc22a7	17	19.04	-1.00	-2.01	3.50E-06	1.1E-03
Adora1	1	4.38	-1.00	-2.00	6.82E-07	2.8E-04
Lgals1	15	13.15	1.02	2.03	4.03E-04	4.0E-02
Fcgr2b	1	5.06	1.04	2.06	3.09E-05	6.1E-03
Sult2a2	7	828.09	1.05	2.06	4.20E-06	1.3E-03
Grid1	14	1.22	1.06	2.08	4.41E-05	8.0E-03
Prex1	2	1.80	1.06	2.09	1.63E-06	5.8E-04
Npr2	4	11.91	1.08	2.12	3.50E-05	6.7E-03
Bag3	7	13.15	1.09	2.13	8.71E-10	6.5E-07
Plxnd1	6	1.25	1.10	2.14	1.12E-04	2.0E-02
Stab1	14	2.31	1.10	2.14	2.52E-05	5.2E-03
Glul	1	137.59	1.10	2.15	1.23E-06	4.6E-04
Rhbg	3	2.30	1.11	2.16	3.23E-04	3.0E-02
Kdr	5	3.39	1.12	2.17	9.81E-05	1.0E-02
Plekhb1	7	8.54	1.12	2.17	1.93E-11	2.0E-08
Rgs3	4	1.29	1.13	2.18	4.83E-05	8.5E-03
Pecam1	11	1.73	1.13	2.19	2.15E-04	3.0E-02
Myo7a	7	1.16	1.13	2.20	5.00E-06	1.5E-03
Clec14a	12	1.57	1.15	2.23	1.99E-04	2.0E-02
Gm14387	2	6.52	1.16	2.24	1.82E-06	6.3E-04
Gas6	8	17.23	1.18	2.26	1.15E-04	2.0E-02
Pag1	3	1.66	1.19	2.29	1.40E-09	1.0E-06
Iqgap1	7	1.02	1.21	2.31	1.50E-04	2.0E-02
S1pr5	9	3.30	1.21	2.31	9.85E-08	5.1E-05
Bmp2	2	2.51	1.21	2.32	2.01E-04	2.0E-02

Table 5 continued

Gdf15	8	14.53	1.22	2.32	2.46E-04	3.0E-02
Aqp1	6	17.12	1.22	2.33	2.26E-04	3.0E-02
Egfl7	2	1.71	1.25	2.38	4.60E-04	5.0E-02
Eng	2	6.38	1.25	2.38	2.86E-04	3.0E-02
Gm6484	9	28.43	1.25	2.38	6.28E-07	2.6E-04
Pltp	2	23.60	1.26	2.40	5.19E-10	3.9E-07
Flt4	11	1.60	1.26	2.40	3.87E-04	4.0E-02
Cyp2a22	7	67.49	1.27	2.42	7.97E-06	2.1E-03
Mrc1	2	4.95	1.28	2.43	5.30E-07	2.2E-04
Unc13b	4	0.42	1.29	2.44	3.66E-05	6.9E-03
Ltbp4	7	2.06	1.28	2.44	3.88E-05	7.2E-03
Csad	15	44.81	1.30	2.46	3.85E-04	4.0E-02
Ifi203	1	0.77	1.31	2.48	2.41E-04	3.0E-02
Alpk1	3	0.50	1.31	2.48	1.91E-04	2.0E-02
Dchs1	7	0.32	1.31	2.48	3.11E-04	3.0E-02
Ptprb	10	2.80	1.31	2.48	8.25E-06	2.2E-03
Ehd3	17	7.25	1.32	2.49	8.39E-06	2.2E-03
Sdc3	4	3.97	1.32	2.50	5.02E-04	5.0E-02
Sirpa	2	1.74	1.33	2.51	3.56E-05	6.7E-03
Tinagl1	4	1.46	1.33	2.51	2.92E-04	3.0E-02
Srgn	10	1.69	1.33	2.52	4.56E-04	5.0E-02
Ptgs1	2	1.63	1.34	2.54	1.80E-04	2.0E-02
Cd300lg	11	3.02	1.34	2.54	4.70E-05	8.3E-03
Setbp1_1	18	0.50	1.35	2.55	3.27E-05	6.4E-03
Abcc5	16	0.32	1.37	2.58	3.30E-04	4.0E-02
Nrp2	1	2.87	1.38	2.60	0	0.0E+00
Rgl1	1	1.01	1.38	2.60	3.48E-05	6.7E-03
Slc43a3	2	2.72	1.38	2.60	2.78E-05	5.7E-03
Slc13a3	2	2.01	1.38	2.60	2.17E-04	3.0E-02
Gimap4	6	2.20	1.39	2.61	3.41E-04	4.0E-02
Itga9	9	0.92	1.39	2.61	2.55E-04	3.0E-02
Ehbp1l1	19	1.64	1.38	2.61	8.88E-11	7.7E-08
Cdh5	8	2.82	1.39	2.62	1.68E-06	6.0E-04
Clec1b	6	1.03	1.39	2.63	7.65E-05	1.0E-02
C1qtnf1	11	1.99	1.41	2.65	1.19E-04	2.0E-02
Arrb1	7	0.49	1.42	2.67	3.78E-05	7.1E-03
Ly6a	15	6.43	1.42	2.68	3.54E-05	6.7E-03
Arhgap31	16	0.40	1.43	2.69	1.56E-04	2.0E-02

Table 5 continued

Pde2a	7	2.64	1.45	2.73	6.45E-05	1.0E-02
Slfn5	11	0.98	1.45	2.73	1.20E-04	2.0E-02
Adam23	1	0.69	1.47	2.76	2.47E-06	8.2E-04
Cyp4b1	4	4.23	1.46	2.76	1.94E-05	4.5E-03
Slc43a2	11	0.81	1.47	2.76	6.82E-09	4.3E-06
Mylip	13	1.91	1.47	2.77	2.91E-04	3.0E-02
Arap3	18	0.97	1.47	2.77	2.14E-04	3.0E-02
Robo4	9	1.43	1.47	2.78	1.56E-05	3.8E-03
Gpihbp1	15	2.36	1.49	2.80	1.21E-05	3.0E-03
Flna	X	1.01	1.49	2.80	3.14E-07	1.4E-04
Sp100	1	0.52	1.49	2.81	6.46E-05	1.0E-02
Slc1a2	2	7.64	1.49	2.81	1.84E-05	4.3E-03
Serpina7	X	8.26	1.49	2.81	1.16E-07	5.8E-05
Cd5l	3	23.30	1.49	2.82	3.30E-04	4.0E-02
Lpl	8	0.86	1.52	2.87	1.68E-04	2.0E-02
Itpripl2	7	0.51	1.53	2.89	2.96E-04	3.0E-02
Mndal	1	1.23	1.54	2.90	5.99E-05	1.0E-02
Id3	4	16.13	1.55	2.92	0	0.0E+00
Axl	7	2.30	1.55	2.93	1.83E-04	2.0E-02
Marcks	10	1.48	1.55	2.93	4.39E-05	8.0E-03
Vcam1	3	2.05	1.56	2.94	1.63E-04	2.0E-02
Fitm1	14	11.92	1.56	2.95	8.00E-08	4.3E-05
Msn	X	2.03	1.56	2.95	2.73E-06	8.9E-04
Dse	10	0.90	1.57	2.98	1.27E-04	2.0E-02
WI1-49P9.2	3	13.71	1.58	2.99	2.45E-10	2.0E-07
Kctd12	14	5.18	1.59	3.00	2.22E-16	4.6E-13
Cfp	X	6.66	1.59	3.02	1.66E-05	3.9E-03
Timp3	10	1.68	1.60	3.03	1.38E-07	6.7E-05
Adgrf5	17	2.56	1.61	3.06	9.84E-06	2.5E-03
Id1	2	8.50	1.64	3.13	2.62E-07	1.2E-04
Arhgdib	6	1.76	1.65	3.13	1.87E-04	2.0E-02
Vipr1	9	1.62	1.65	3.14	1.25E-04	2.0E-02
Itpkb	1	0.77	1.66	3.15	6.52E-05	1.0E-02
Clec4f	6	19.05	1.66	3.16	8.21E-05	1.0E-02
Sema6d	2	0.57	1.67	3.17	1.22E-04	2.0E-02
Adgre5	8	2.90	1.66	3.17	2.60E-06	8.6E-04
Sult2a1	7	838.56	1.67	3.18	2.98E-12	3.7E-09
Cd84	1	0.53	1.67	3.19	5.38E-05	9.2E-03

Table 5 continued

Colec10	15	1.42	1.67	3.19	2.97E-04	3.0E-02
Wdfy4	14	0.27	1.68	3.20	3.76E-04	4.0E-02
Cux2	5	8.86	1.69	3.22	5.14E-04	5.0E-02
Wfdc17	11	8.14	1.69	3.22	9.75E-05	1.0E-02
Arhgef2	3	0.26	1.69	3.23	3.78E-04	4.0E-02
Gm4070	7	0.70	1.69	3.23	1.29E-06	4.7E-04
Vim	2	2.39	1.70	3.25	5.68E-07	2.4E-04
Itgal	7	1.51	1.71	3.26	4.31E-06	1.3E-03
Zeb2	2	0.23	1.71	3.28	7.10E-06	1.9E-03
Csf1r	18	6.61	1.72	3.28	2.68E-05	5.5E-03
Hmha1	10	1.22	1.72	3.29	2.90E-07	1.3E-04
Wipf1	2	0.48	1.72	3.30	2.21E-04	3.0E-02
Tnfrsf19	14	0.59	1.74	3.34	1.60E-04	2.0E-02
Hecw2	1	0.19	1.75	3.36	2.59E-04	3.0E-02
Adgre1	17	3.47	1.76	3.38	4.39E-06	1.3E-03
Siglec1	2	0.92	1.76	3.39	2.42E-04	3.0E-02
Sh3tc1	5	0.55	1.77	3.40	9.63E-05	1.0E-02
Ar	X	3.18	1.78	3.42	0	0.0E+00
Tmsb4x	X	25.95	1.78	3.42	1.56E-13	2.3E-10
Nckap1l	15	1.03	1.78	3.44	3.94E-05	7.3E-03
Ntn4	10	1.10	1.79	3.45	2.24E-05	4.9E-03
Itga4	2	0.19	1.79	3.46	2.54E-04	3.0E-02
Slc11a1	1	1.07	1.80	3.49	1.19E-04	2.0E-02
Fgf21	7	2.42	1.81	3.51	4.03E-04	4.0E-02
C1qa	4	13.93	1.82	3.52	2.24E-05	4.9E-03
Lbh	17	0.78	1.82	3.52	1.13E-04	2.0E-02
Laptm5	4	3.10	1.82	3.54	4.25E-06	1.3E-03
Tyrobp	7	7.10	1.83	3.55	2.90E-04	3.0E-02
Cybb	X	2.16	1.83	3.56	1.53E-05	3.7E-03
Efnb2	8	0.73	1.84	3.58	2.08E-05	4.7E-03
Cerk	15	0.47	1.85	3.60	1.02E-04	1.0E-02
Neurl3	1	0.66	1.86	3.63	2.94E-04	3.0E-02
Srgap3	6	1.42	1.87	3.66	1.47E-11	1.6E-08
Serpine2	1	1.21	1.88	3.67	1.71E-06	6.0E-04
Itgb2	10	1.95	1.88	3.67	7.81E-05	1.0E-02
Hgf	5	0.36	1.88	3.69	9.85E-05	1.0E-02
C1qb	4	16.09	1.90	3.74	6.89E-06	1.9E-03
Notch4	17	0.23	1.91	3.75	8.64E-05	1.0E-02

Table 5 continued

Fermt3	19	1.08	1.91	3.75	9.86E-05	1.0E-02
Ppp1r18	17	0.44	1.91	3.76	2.66E-04	3.0E-02
Ctss	3	12.24	1.92	3.78	2.24E-05	4.9E-03
Cd53	3	2.25	1.92	3.78	8.75E-05	1.0E-02
Vav1	17	0.64	1.93	3.81	3.55E-04	4.0E-02
Rgs2	1	0.72	1.94	3.85	1.10E-04	2.0E-02
Pde1a	2	0.60	1.94	3.85	1.76E-07	8.3E-05
Vsig4	X	11.68	1.96	3.90	2.12E-05	4.7E-03
Lyz2	10	28.81	1.97	3.91	2.99E-09	2.1E-06
Adgre4	17	1.23	1.97	3.91	2.05E-04	2.0E-02
Prelp	1	1.82	1.97	3.93	4.81E-06	1.4E-03
AI607873	1	1.71	1.98	3.94	3.98E-07	1.7E-04
P2rx7	5	0.37	1.98	3.94	1.08E-04	2.0E-02
Sult2a5	7	31.58	1.98	3.95	3.89E-15	7.6E-12
Abi3	11	0.43	1.98	3.95	3.81E-04	4.0E-02
Entpd1	19	0.56	1.99	3.97	1.51E-04	2.0E-02
C1qc	4	8.17	1.99	3.98	7.64E-07	3.1E-04
Parvb	15	0.51	1.99	3.98	4.16E-05	7.6E-03
Gsn	2	0.63	2.02	4.07	1.60E-04	2.0E-02
Lrmp	6	0.36	2.03	4.08	4.65E-04	5.0E-02
Bgn	X	4.09	2.03	4.09	5.49E-06	1.6E-03
Bmp6	13	1.13	2.04	4.10	2.34E-05	5.0E-03
Lrrc32	7	1.15	2.04	4.11	7.42E-08	4.0E-05
1-Mar	8	0.30	2.04	4.11	4.33E-04	4.0E-02
Cd52	4	1.58	2.06	4.16	2.77E-04	3.0E-02
Fcgr3	1	2.28	2.08	4.21	2.16E-04	3.0E-02
Trpm2	10	0.43	2.08	4.22	2.06E-05	4.7E-03
Ccl6	11	3.10	2.08	4.22	4.66E-05	8.3E-03
Colec11	12	2.13	2.08	4.22	1.20E-04	2.0E-02
Slc15a3	19	0.61	2.08	4.23	2.35E-05	5.0E-03
Atp11a	8	1.42	2.09	4.25	1.75E-10	1.4E-07
Dock10	1	0.24	2.09	4.26	1.56E-04	2.0E-02
Nebl	2	0.19	2.09	4.27	4.77E-06	1.4E-03
Akna	4	0.33	2.09	4.27	1.60E-04	2.0E-02
Fxyd5	7	0.40	2.11	4.33	2.23E-04	3.0E-02
Selplg	5	0.73	2.12	4.35	3.81E-04	4.0E-02
Ptprc	1	0.60	2.12	4.36	8.74E-07	3.4E-04
Pirb	7	0.78	2.13	4.38	4.16E-04	4.0E-02

Table 5 continued

Ncf2	1	0.46	2.14	4.41	2.94E-04	3.0E-02
Syk	13	0.40	2.16	4.46	5.73E-05	9.8E-03
Ecm1	3	5.51	2.16	4.47	3.95E-06	1.2E-03
St3gal6	16	4.48	2.16	4.48	0	0.0E+00
Lilra5	7	0.91	2.17	4.51	2.99E-04	3.0E-02
Pla2r1_1	2	0.19	2.18	4.52	1.65E-04	2.0E-02
Fgl2	5	0.67	2.24	4.71	1.01E-04	1.0E-02
Coro1a	7	0.92	2.24	4.74	1.54E-04	2.0E-02
Ncf1	5	0.55	2.25	4.77	1.08E-04	2.0E-02
Cd300a	11	0.54	2.27	4.81	9.49E-05	1.0E-02
Abcc4	14	2.25	2.29	4.88	8.55E-15	1.5E-11
Rassf2	2	0.12	2.30	4.91	2.78E-04	3.0E-02
Pira2	7	0.89	2.31	4.95	6.82E-05	1.0E-02
Plek	11	0.81	2.31	4.95	1.81E-06	6.3E-04
Csf3r	4	0.41	2.31	4.96	2.97E-04	3.0E-02
Sla	15	0.28	2.31	4.97	6.11E-05	1.0E-02
Ctla2a	13	0.81	2.32	4.99	4.72E-04	5.0E-02
Hao2	3	21.36	2.32	5.00	3.08E-11	2.9E-08
Col14a1	15	0.67	2.34	5.05	3.44E-05	6.7E-03
Aatk	11	0.45	2.35	5.08	3.92E-06	1.2E-03
Rcan2	17	4.94	2.34	5.08	9.58E-14	1.4E-10
Serpinb1a	13	28.11	2.36	5.15	0	0.0E+00
Cd44	2	0.87	2.37	5.17	7.38E-08	4.0E-05
Cd74	18	30.21	2.37	5.17	3.07E-11	2.9E-08
Tlr8	X	0.50	2.37	5.17	2.27E-04	3.0E-02
Myo1f	17	0.41	2.37	5.18	4.86E-05	8.6E-03
Cyp26b1	6	1.27	2.39	5.23	1.38E-08	8.2E-06
Kif21b	1	0.16	2.39	5.25	1.44E-04	2.0E-02
Dcn	10	8.85	2.40	5.26	8.61E-07	3.4E-04
Ntrk2	13	1.57	2.40	5.27	3.65E-11	3.3E-08
Apbb1ip	2	0.20	2.44	5.42	1.57E-04	2.0E-02
Abcc9	6	0.57	2.44	5.44	5.70E-08	3.2E-05
Fcgr4	1	2.26	2.46	5.49	4.01E-05	7.4E-03
Clec9a	6	0.40	2.46	5.49	8.20E-05	1.0E-02
Bin2	15	0.85	2.46	5.50	3.03E-05	6.1E-03
Clec4n	6	1.00	2.46	5.51	2.29E-04	3.0E-02
H2-Eb1	17	10.91	2.46	5.52	1.37E-09	1.0E-06
Ampd3	7	0.15	2.48	5.59	4.34E-04	4.0E-02

Table 5 continued

H2-Aa	17	10.14	2.48	5.59	6.34E-11	5.6E-08
Siglece	7	0.89	2.51	5.69	8.61E-05	1.0E-02
Clec4a3	6	1.05	2.52	5.73	1.63E-04	2.0E-02
Fli1	9	0.37	2.52	5.73	4.44E-05	8.0E-03
Fmnl1	11	0.31	2.54	5.80	5.13E-05	8.9E-03
Ccrn4l	3	33.18	2.55	5.86	0	0.0E+00
Galnt15	14	0.37	2.61	6.09	2.57E-07	1.2E-04
Plcb2	2	0.18	2.61	6.12	1.54E-04	2.0E-02
Treml4	17	1.17	2.62	6.14	9.86E-06	2.5E-03
Cd207	6	2.43	2.65	6.29	2.34E-06	7.9E-04
Adcy7	8	0.48	2.66	6.33	1.11E-05	2.8E-03
Ccl5	11	0.91	2.66	6.34	4.03E-04	4.0E-02
Itgb7	15	0.50	2.68	6.42	5.84E-05	9.9E-03
H2-Ab1	17	8.32	2.68	6.43	1.22E-10	1.0E-07
Sod3	5	0.63	2.71	6.54	2.98E-05	6.0E-03
Il1b	2	0.63	2.72	6.60	2.16E-04	3.0E-02
D630033O11Rik	9	1.89	2.72	6.60	2.43E-05	5.1E-03
Bcl2	1	0.10	2.72	6.61	1.09E-04	2.0E-02
Rasgrp1	2	0.23	2.73	6.62	7.35E-05	1.0E-02
Atp2a3	11	0.27	2.74	6.70	5.08E-05	8.8E-03
Pla2g7	17	1.43	2.74	6.70	9.22E-08	4.8E-05
Efemp1	11	0.57	2.78	6.88	1.54E-04	2.0E-02
Dmrta1	4	1.44	2.79	6.93	5.44E-15	9.8E-12
Adgb	10	0.16	2.83	7.10	2.05E-04	2.0E-02
Gp49a	10	0.63	2.83	7.12	1.53E-04	2.0E-02
Cyp3a44	5	300.34	2.86	7.28	3.57E-11	3.3E-08
Hsf2bp	17	0.26	2.88	7.34	9.36E-05	1.0E-02
Dkk3	7	0.62	2.93	7.63	1.01E-06	3.9E-04
Fermt1	2	0.23	2.95	7.71	1.62E-05	3.8E-03
Grip2	6	0.09	2.99	7.95	4.91E-04	5.0E-02
Cd22	7	0.25	3.00	8.01	2.24E-05	4.9E-03
Cxcl13	5	1.86	3.01	8.05	1.81E-07	8.5E-05
Igha	12	0.81	3.02	8.10	1.57E-04	2.0E-02
Adcy1	11	0.10	3.04	8.25	2.51E-05	5.2E-03
Sult2a7	7	82.38	3.06	8.34	0	0.0E+00
Sult1e1	5	6.22	3.07	8.40	0	0.0E+00
Gm15401	6	1.91	3.08	8.45	3.89E-09	2.7E-06
Cytip	2	0.14	3.08	8.48	6.78E-05	1.0E-02

Table 5 continued

Cd48	1	0.99	3.09	8.54	1.59E-05	3.8E-03
Cygb	1	0.41	3.11	8.63	1.95E-04	2.0E-02
Cyp3a16	5	157.70	3.12	8.67	2.53E-05	5.2E-03
C130026I21Rik	1	0.25	3.16	8.95	4.98E-05	8.7E-03
Pla2g4f	2	0.31	3.19	9.14	3.13E-05	6.2E-03
Gm7609	1	0.85	3.24	9.45	1.16E-07	5.8E-05
E2f7	10	0.06	3.24	9.47	2.29E-04	3.0E-02
Nkd1	8	0.36	3.27	9.62	6.84E-07	2.8E-04
Chil3	3	0.38	3.31	9.89	4.83E-04	5.0E-02
Ctgf	10	1.66	3.43	10.77	0	0.0E+00
Nudt11	X	0.37	3.43	10.77	4.39E-06	1.3E-03
Napsa	7	0.26	3.47	11.11	3.51E-04	4.0E-02
S100a9	3	4.16	3.48	11.19	8.35E-07	3.3E-04
Adgrg2	X	0.32	3.51	11.36	1.70E-07	8.1E-05
Esm1	13	0.43	3.55	11.72	2.17E-05	4.8E-03
Pou2af1	9	0.26	3.75	13.42	2.87E-04	3.0E-02
Itgb3	11	0.44	3.83	14.22	1.05E-10	8.9E-08
Id4	13	2.24	3.90	14.96	6.30E-13	8.9E-10
S100a8	3	2.32	3.92	15.10	2.11E-06	7.2E-04
Cyp4f18	8	0.29	3.95	15.44	4.38E-04	4.0E-02
Tmem28	X	0.30	4.19	18.21	2.41E-06	8.1E-04
Cdh19	1	1.56	4.21	18.50	0	0.0E+00
Igkv4-55	6	3.85	4.21	18.53	9.22E-05	1.0E-02
Cyp3a41b	5	271.54	4.26	19.13	4.39E-14	7.1E-11
Iglv1	16	2.48	4.32	19.91	8.00E-05	1.0E-02
Bnc2	4	0.09	4.35	20.34	5.10E-05	8.8E-03
Igj	5	3.79	4.38	20.81	8.63E-13	1.2E-09
Iglc1	16	1.90	4.64	24.99	1.19E-04	2.0E-02
Pcdh11x	X	0.04	4.78	27.50	4.10E-04	4.0E-02
Sult2a3	7	95.27	4.89	29.60	0	0.0E+00
Adamtsl2	2	0.08	5.03	32.63	3.09E-04	3.0E-02
Igkv14-126	6	1.83	5.05	33.18	2.74E-04	3.0E-02
Ppbp/CXCL7	5	1.53	5.11	34.50	8.16E-07	3.3E-04
Ighv1-26	12	6.33	6.00	64.18	2.84E-06	9.2E-04
Ighg2b	12	1.24	6.09	68.33	3.31E-10	2.6E-07
Ighv1-53	12	21.82	6.35	81.40	5.80E-12	6.7E-09
Ighm	12	58.20	6.66	101.16	0	0.0E+00
Igkv1-110	6	5.60	6.80	111.48	1.23E-06	4.6E-04

Table 5 continued

Igkc	6	103.70	7.12	138.75	0	0.0E+00
Ighv1-55	12	10.45	7.76	217.46	3.12E-07	1.4E-04
Ighg1	12	1.09	9.02	519.44	2.53E-04	3.0E-02
Ighv3-6	12	9.17	9.26	614.19	1.36E-04	2.0E-02
Igkv5-39	6	20.38	10.41	1362.79	1.98E-05	4.5E-03
Igkv3-2	6	44.53	11.62	3149.68	2.62E-06	8.6E-04

APPENDIX C

COMPREHENSIVE METABOLIC PANEL (CHEM12)

Table 6. Chem12 Data from Rhesus Macaques Implanted with Lung Scaffolds

Group	Animal	Weeks	Na[a] (144-160 mEq/L)	K[b] (3.3-6.4 mEq/L)	Cl[c] (106-117 mEq/L)	Pro[d] (5.9-7.8 g/dL)	Alb[e] (3.0-5.9 g/dL)	Glob[f] (1.9-3.9 g/dL)	A/G ratio[g] (0.5-3.5)
WT	FR83	0	143*	3.6	106	7.2	4.2	3.0	1.4
		1	146	3.6	108	7.3	3.7	3.6	1.0
		2	146	3.9	108	7.4	3.8	3.6	1.1
		4	144	3.8	107	6.7	3.8	2.9	1.3
		8	145	3.9	108	6.9	3.8	3.1	1.2
	FP26	0	145	3.2*	110	6.7	4.1	2.6	1.6
		1	147	3.6	108	7.4	3.9	3.5	1.1
		2	146	3.2*	109	7.7	4.1	3.6	1.1
		4	147	3.4	109	7.4	4.2	3.2	1.3
		8	148	3.4	109	7.4	4.3	3.1	1.4
SC	IK09	0	144	3.5	107	6.9	4.2	2.7	1.6
		1	146	3.8	107	7.3	4.0	3.3	1.2
		2	145	3.9	105*	7.1	4.0	3.1	1.3
		4	144	3.7	106	6.8	4.1	2.7	1.5
		8	146	4.0	108	6.9	4.3	2.6	1.7
	II58	0	143*	3.5	106	6.5	3.7	2.8	1.3
		1	144	3.9	108	6.7	3.5	3.2	1.1
		2	145	4.1	107	6.8	3.5	3.3	1.1
		4	144	4.1	108	6.6	3.8	2.8	1.4
		8	146	4.4	109	6.8	3.9	2.9	1.3

Table 6 continued

DC-M	IB44	0	146	3.9	107	7.6	4.3	3.3	1.3
		1	146	4.0	107	7.6	4.0	3.6	1.1
		2	146	3.7	106	7.1	3.9	3.2	1.2
		4	146	3.7	107	7.0	4.1	2.9	1.4
		8	146	4.3	107	7.1	4.2	2.9	1.4
	HE17	0	144	3.5	109	7.4	3.8	3.6	1.1
		1	144	3.8	108	7.1	3.5	3.6	1.0
		2	145	3.6	107	7.0	3.6	3.4	1.1
		4	144	4.1	108	7.6	4.0	3.6	1.1
		8	147	4.1	108	7.3	4.1	3.2	1.3
DC-WT	HA91	0	146	3.4	108	7.2	4.1	3.1	1.3
		1	146	3.8	107	6.9	3.8	3.1	1.2
		2	146	3.6	107	7.0	4.2	2.8	1.5
		4	144	4.2	104*	6.9	4.1	2.8	1.5
		8	147	3.7	105*	7.0	4.3	2.7	1.6
	HP13	0	143*	3.7	107	6.6	3.6	3.0	1.2
		1	145	4.1	106	6.7	3.6	3.1	1.2
		2	145	4.3	105*	6.7	3.8	2.9	1.3
		4	144	4.5	107	6.3	3.5	2.8	1.3
		8	147	3.9	107	6.2	3.8	2.4	1.6
DC-KO	HT93	0	147	3.2*	111	7.6	3.9	3.7	1.1
		1	147	3.9	108	7.5	3.7	3.8	1.0
		2	146	3.6	108	7.4	3.8	3.6	1.1
		4	145	3.6	107	7.1	3.7	3.4	1.1
		8	148	3.6	110	7.2	4.0	3.2	1.3
	GM29	0	145	3.4	106	6.6	2.8*	3.8	0.7
		1	145	4.1	107	6.5	2.6*	3.9	0.7
		2	145	3.9	105*	6.3	2.8*	3.5	0.8
		4	144	4.1	106	6.7	3.1	3.6	0.9
		8	145	4.2	106	6.2	2.8*	3.4	0.8

*Indicates a value below the anticipated threshold
[a] Sodium (Na^+)
[b] Potassium (K^+)
[c] Chloride (Cl^-)
[d] Total protein (pro)
[e] Albumin (alb)
[f] Globulin (glob)
[g] Ratio of albumin to globulin (alb/glob)

Table 7. Chem12 Data (cont.) from Rhesus Macaques Implanted with Lung Scaffolds

Group	Animal	Weeks	Bun[h] (13-27 mg/dL)	Glu[i] (48-119 mg/dL)	Crt[j] (0.4-1.4 mg/dL)	Ast[k] (25-120 IU/L)	Alt[l] (20-126 IU/L)	Bn/Crt ratio[m] (11-60)
WT	FR83	0	21.0	67	1.10	41	43	19.1
		1	19.0	71	0.94	35	48	20.2
		2	22.0	62	0.99	34	44	22.2
		4	24.0	57	1.04	27	32	23.1
		8	22.0	63	1.04	33	40	21.2
	FP26	0	16.0	83	0.97	25	45	16.5
		1	13.0	66	0.99	22*	37	13.1
		2	16.0	68	0.91	22*	36	17.6
		4	15.0	84	0.95	21*	34	15.8
		8	16.0	88	1.02	23*	34	15.7
SC	IK09	0	16.0	73	0.91	30	19*	17.6
		1	16.0	76	0.91	26	28	17.6
		2	18.0	68	0.83	25	17*	21.7
		4	17.0	71	0.83	28	17*	20.5
		8	18.0	67	0.84	27	18*	21.4
	II58	0	15.0	75	0.72	37	39	20.8
		1	15.0	70	0.75	26	24	20.0
		2	13.0	63	0.66	31	25	19.7
		4	15.0	57	0.77	30	28	19.5
		8	17.0	55	0.71	28	34	23.9
DC-M	IB44	0	14.0	69	0.96	24*	22	14.6
		1	15.0	68	0.85	26	26	17.6
		2	15.0	72	0.88	22*	42	17.0
		4	13.0	73	0.97	35	28	13.4
		8	15.0	72	0.86	30	26	17.4
	HE17	0	16.0	105	1.20	42	19*	13.3
		1	17.0	71	1.07	36	27	15.9
		2	18.0	89	1.18	29	18*	15.3
		4	17.0	79	1.19	72	40	14.3
		8	17.0	58	1.12	29	20	15.2

Table 7 continued

DC-WT	HA91	0	16.0	98	1.08	33	22	14.8
		1	19.0	61	0.97	28	25	19.6
		2	18.0	81	0.93	26	23	19.4
		4	19.0	86	0.97	59	34	19.6
		8	16.0	80	0.95	24*	21	16.8
	HP13	0	15.0	74	0.97	35	38	15.5
		1	19.0	71	0.89	25	37	21.3
		2	15.0	75	0.92	21*	31	16.3
		4	16.0	66	0.91	43	40	17.6
		8	17.0	68	0.74	18*	35	23.0
DC-KO	HT93	0	12.0*	128+	0.94	27	43	12.8
		1	16.0	58	0.67	24*	22	23.9
		2	12.0*	66	0.64	24*	33	18.8
		4	11.0*	68	0.73	37	35	15.1
		8	13.0	73	0.64	25	37	20.3
	GM29	0	18.0	79	0.87	22*	16*	20.7
		1	21.0	55	0.75	22*	16*	28.0
		2	17.0	61	0.78	19*	16*	21.8
		4	18.0	68	0.80	32	21	22.5
		8	19.0	62	0.68	22*	12*	27.9

*Indicates a value below the anticipated threshold
+Indicates a value above the anticipated threshold
[h] Blood urea nitrogen (bun)
[i] Glucose (glu)
[j] Creatinine (crt)
[k] Aspartate amino transferase (ast)
[l] Alanine amino transferase (alt)
[m] Ratio of blood urea nitrogen to creatinine (bn/crt)

BIBLIOGRAPHY

Abais, J. M., Xia, M., Zhang, Y., Boini, K. M., & Li, P. L. (2015). Redox regulation of NLRP3 inflammasomes: ROS as trigger or effector? *Antioxid Redox Signal, 22*(13), 1111-1129. doi:10.1089/ars.2014.5994

Allman, A. J., McPherson, T. B., Badylak, S. F., Merrill, L. C., Kallakury, B., Sheehan, C., . . . Metzger, D. W. (2001). Xenogeneic extracellular matrix grafts elicit a TH2-restricted immune response. *Transplantation, 71*(11), 1631-1640.

Allman, A. J., McPherson, T. B., Merrill, L. C., Badylak, S. F., & Metzger, D. W. (2002). The Th2-restricted immune response to xenogeneic small intestinal submucosa does not influence systemic protective immunity to viral and bacterial pathogens. *Tissue Eng, 8*(1), 53-62. doi:10.1089/107632702753503054

American Geriatrics Society Beers Criteria Update Expert, P. (2012). American Geriatrics Society updated Beers Criteria for potentially inappropriate medication use in older adults. *J Am Geriatr Soc, 60*(4), 616-631. doi:10.1111/j.1532-5415.2012.03923.x

Amit, I., Winter, D. R., & Jung, S. (2016). The role of the local environment and epigenetics in shaping macrophage identity and their effect on tissue homeostasis. *Nat Immunol, 17*(1), 18-25. doi:10.1038/ni.3325

Anderson, J. M. (1988). Inflammatory response to implants. *ASAIO Trans, 34*(2), 101-107.

Anderson, J. M., Rodriguez, A., & Chang, D. T. (2008). Foreign body reaction to biomaterials. *Semin Immunol, 20*(2), 86-100. doi:10.1016/j.smim.2007.11.004

Aravinthan, A., Challis, B., Shannon, N., Hoare, M., Heaney, J., & Alexander, G. J. (2015). Selective insulin resistance in hepatocyte senescence. *Exp Cell Res, 331*(1), 38-45. doi:10.1016/j.yexcr.2014.09.025

Aravinthan, A. D., & Alexander, G. J. M. (2016). Senescence in chronic liver disease: Is the future in aging? *J Hepatol, 65*(4), 825-834. doi:10.1016/j.jhep.2016.05.030

Aschoff, L. (1924). Das reticuloendotheliale System. *Erg. Inn. Med. Kinderheilk, 26*, 1-118.

Ashcroft, G. S., Horan, M. A., & Ferguson, M. W. (1998). Aging alters the inflammatory and endothelial cell adhesion molecule profiles during human cutaneous wound healing. *Lab Invest, 78*(1), 47-58.

Aw, D., Silva, A. B., & Palmer, D. B. (2007). Immunosenescence: emerging challenges for an ageing population. *Immunology, 120*(4), 435-446. doi:10.1111/j.1365-2567.2007.02555.x

Badylak, S. F., & Gilbert, T. W. (2008). Immune response to biologic scaffold materials. *Semin Immunol, 20*(2), 109-116. doi:10.1016/j.smim.2007.11.003

Baeck, C., Wehr, A., Karlmark, K. R., Heymann, F., Vucur, M., Gassler, N., . . . Tacke, F. (2012). Pharmacological inhibition of the chemokine CCL2 (MCP-1) diminishes liver macrophage infiltration and steatohepatitis in chronic hepatic injury. *Gut, 61*(3), 416-426. doi:10.1136/gutjnl-2011-300304

Bain, C. C., Hawley, C. A., Garner, H., Scott, C. L., Schridde, A., Steers, N. J., . . . Jenkins, S. J. (2016). Long-lived self-renewing bone marrow-derived macrophages displace embryo-derived cells to inhabit adult serous cavities. *Nat Commun, 7*, ncomms11852. doi:10.1038/ncomms11852

Ballestri, S., Nascimbeni, F., Baldelli, E., Marrazzo, A., Romagnoli, D., & Lonardo, A. (2017). NAFLD as a Sexual Dimorphic Disease: Role of Gender and Reproductive Status in the Development and Progression of Nonalcoholic Fatty Liver Disease and Inherent Cardiovascular Risk. *Adv Ther, 34*(6), 1291-1326. doi:10.1007/s12325-017-0556-1

Barzilai, N., Huffman, D. M., Muzumdar, R. H., & Bartke, A. (2012). The critical role of metabolic pathways in aging. *Diabetes, 61*(6), 1315-1322. doi:10.2337/db11-1300

Ben-Porath, I., & Weinberg, R. A. (2005). The signals and pathways activating cellular senescence. *Int J Biochem Cell Biol, 37*(5), 961-976. doi:10.1016/j.biocel.2004.10.013

Benoit, M., Desnues, B., & Mege, J. L. (2008). Macrophage polarization in bacterial infections. *J Immunol, 181*(6), 3733-3739.

Bieghs, V., Rensen, P. C., Hofker, M. H., & Shiri-Sverdlov, R. (2012). NASH and atherosclerosis are two aspects of a shared disease: central role for macrophages. *Atherosclerosis, 220*(2), 287-293. doi:10.1016/j.atherosclerosis.2011.08.041

Bilzer, M., Roggel, F., & Gerbes, A. L. (2006). Role of Kupffer cells in host defense and liver disease. *Liver Int, 26*(10), 1175-1186. doi:10.1111/j.1478-3231.2006.01342.x

Blackman, M. A., & Woodland, D. L. (2011). The narrowing of the CD8 T cell repertoire in old age. *Curr Opin Immunol, 23*(4), 537-542. doi:10.1016/j.coi.2011.05.005

Boehmer, E. D., Meehan, M. J., Cutro, B. T., & Kovacs, E. J. (2005). Aging negatively skews macrophage TLR2- and TLR4-mediated pro-inflammatory responses without affecting the IL-2-stimulated pathway. *Mech Ageing Dev, 126*(12), 1305-1313. doi:10.1016/j.mad.2005.07.009

Bonvillain, R. W., Danchuk, S., Sullivan, D. E., Betancourt, A. M., Semon, J. A., Eagle, M. E., . . . Bunnell, B. A. (2012). A nonhuman primate model of lung regeneration: detergent-mediated decellularization and initial in vitro recellularization with mesenchymal stem cells. *Tissue Eng Part A, 18*(23-24), 2437-2452. doi:10.1089/ten.TEA.2011.0594

Brouwer, A., & Knook, D. L. (1983). The reticuloendothelial system and aging: a review. *Mech Ageing Dev, 21*(3-4), 205-228.

Brown, B. N., & Badylak, S. F. (2014). Extracellular matrix as an inductive scaffold for functional tissue reconstruction. *Transl Res, 163*(4), 268-285. doi:10.1016/j.trsl.2013.11.003

Brown, B. N., Londono, R., Tottey, S., Zhang, L., Kukla, K. A., Wolf, M. T., . . . Badylak, S. F. (2012). Macrophage phenotype as a predictor of constructive remodeling following the implantation of biologically derived surgical mesh materials. *Acta Biomater, 8*(3), 978-987. doi:10.1016/j.actbio.2011.11.031

Brown, B. N., Ratner, B. D., Goodman, S. B., Amar, S., & Badylak, S. F. (2012). Macrophage polarization: an opportunity for improved outcomes in biomaterials and regenerative medicine. *Biomaterials, 33*(15), 3792-3802. doi:10.1016/j.biomaterials.2012.02.034

Brown, B. N., Sicari, B. M., & Badylak, S. F. (2014). Rethinking regenerative medicine: a macrophage-centered approach. *Front Immunol, 5*, 510. doi:10.3389/fimmu.2014.00510

Brown, B. N., Valentin, J. E., Stewart-Akers, A. M., McCabe, G. P., & Badylak, S. F. (2009). Macrophage phenotype and remodeling outcomes in response to biologic scaffolds with and without a cellular component. *Biomaterials, 30*(8), 1482-1491. doi:10.1016/j.biomaterials.2008.11.040

Byrne, G., Ahmad-Villiers, S., Du, Z., & McGregor, C. (2018). B4GALNT2 and xenotransplantation: A newly appreciated xenogeneic antigen. *Xenotransplantation*, e12394. doi:10.1111/xen.12394

Campisi, J. (1996). Replicative senescence: an old lives' tale? *Cell, 84*(4), 497-500.

Campoccia, D., Montanaro, L., & Arciola, C. R. (2013). A review of the biomaterials technologies for infection-resistant surfaces. *Biomaterials, 34*(34), 8533-8554. doi:10.1016/j.biomaterials.2013.07.089

Cecilio, C. A., Costa, E. H., Simioni, P. U., Gabriel, D. L., & Tamashiro, W. M. (2011). Aging alters the production of iNOS, arginase and cytokines in murine macrophages. *Braz J Med Biol Res, 44*(7), 671-681.

Census.gov. (2018). Older People Projected to Outnumber Children for First Time in U.S. History [Press release]. Retrieved from https://www.census.gov/newsroom/press-releases/2018/cb18-41-population-projections.html

Chen, C. J., Shi, Y., Hearn, A., Fitzgerald, K., Golenbock, D., Reed, G., . . . Rock, K. L. (2006). MyD88-dependent IL-1 receptor signaling is essential for gouty inflammation stimulated by monosodium urate crystals. *J Clin Invest, 116*(8), 2262-2271. doi:10.1172/JCI28075

Chinenov, Y., Gupte, R., & Rogatsky, I. (2013). Nuclear receptors in inflammation control: repression by GR and beyond. *Mol Cell Endocrinol, 380*(1-2), 55-64. doi:10.1016/j.mce.2013.04.006

Cho, S. H., Chen, J. A., Sayed, F., Ward, M. E., Gao, F., Nguyen, T. A., . . . Gan, L. (2015). SIRT1 deficiency in microglia contributes to cognitive decline in aging and neurodegeneration via epigenetic regulation of IL-1beta. *J Neurosci, 35*(2), 807-818. doi:10.1523/JNEUROSCI.2939-14.2015

Choi, S. Y., Jeong, H. J., Lim, H. G., Park, S. S., Kim, S. H., & Kim, Y. J. (2012). Elimination of alpha-gal xenoreactive epitope: alpha-galactosidase treatment of porcine heart valves. *J Heart Valve Dis, 21*(3), 387-397.

Cichoz-Lach, H., & Michalak, A. (2014). Oxidative stress as a crucial factor in liver diseases. *World J Gastroenterol, 20*(25), 8082-8091. doi:10.3748/wjg.v20.i25.8082

Cicin-Sain, L., Brien, J. D., Uhrlaub, J. L., Drabig, A., Marandu, T. F., & Nikolich-Zugich, J. (2012). Cytomegalovirus infection impairs immune responses and accentuates T-cell pool changes observed in mice with aging. *PLoS Pathog, 8*(8), e1002849. doi:10.1371/journal.ppat.1002849

Cohen-Naftaly, M., & Friedman, S. L. (2011). Current status of novel antifibrotic therapies in patients with chronic liver disease. *Therap Adv Gastroenterol, 4*(6), 391-417. doi:10.1177/1756283X11413002

Cooper, D. K., Koren, E., & Oriol, R. (1994). Oligosaccharides and discordant xenotransplantation. *Immunol Rev, 141*, 31-58.

Coppe, J. P., Patil, C. K., Rodier, F., Sun, Y., Munoz, D. P., Goldstein, J., . . . Campisi, J. (2008). Senescence-associated secretory phenotypes reveal cell-nonautonomous functions of oncogenic RAS and the p53 tumor suppressor. *PLoS Biol, 6*(12), 2853-2868. doi:10.1371/journal.pbio.0060301

Crispe, I. N. (2009). The liver as a lymphoid organ. *Annu Rev Immunol, 27*, 147-163. doi:10.1146/annurev.immunol.021908.132629

Dal-Secco, D., Wang, J., Zeng, Z., Kolaczkowska, E., Wong, C. H., Petri, B., . . . Kubes, P. (2015). A dynamic spectrum of monocytes arising from the in situ reprogramming of CCR2+ monocytes at a site of sterile injury. *J Exp Med, 212*(4), 447-456. doi:10.1084/jem.20141539

Dall'Olio, F., Malagolini, N., Chiricolo, M., Trinchera, M., & Harduin-Lepers, A. (2014). The expanding roles of the Sd(a)/Cad carbohydrate antigen and its cognate glycosyltransferase B4GALNT2. *Biochim Biophys Acta, 1840*(1), 443-453. doi:10.1016/j.bbagen.2013.09.036

Daly, K. A., Stewart-Akers, A. M., Hara, H., Ezzelarab, M., Long, C., Cordero, K., . . . Badylak, S. F. (2009). Effect of the alphaGal epitope on the response to small intestinal submucosa extracellular matrix in a nonhuman primate model. *Tissue Eng Part A, 15*(12), 3877-3888. doi:10.1089/ten.TEA.2009.0089

Dey, A., Allen, J., & Hankey-Giblin, P. A. (2014). Ontogeny and polarization of macrophages in inflammation: blood monocytes versus tissue macrophages. *Front Immunol, 5*, 683. doi:10.3389/fimmu.2014.00683

Dimitrijevic, M., Stanojevic, S., Kustrimovic, N., Mitic, K., Vujic, V., Aleksic, I., . . . Leposavic, G. (2013). The influence of aging and estradiol to progesterone ratio on rat macrophage phenotypic profile and NO and TNF-alpha production. *Exp Gerontol, 48*(11), 1243-1254. doi:10.1016/j.exger.2013.07.001

Doherty, D. G., Norris, S., Madrigal-Estebas, L., McEntee, G., Traynor, O., Hegarty, J. E., & O'Farrelly, C. (1999). The human liver contains multiple populations of NK cells, T cells, and CD3+CD56+ natural T cells with distinct cytotoxic activities and Th1, Th2, and Th0 cytokine secretion patterns. *J Immunol, 163*(4), 2314-2321.

Duewell, P., Kono, H., Rayner, K. J., Sirois, C. M., Vladimer, G., Bauernfeind, F. G., . . . Latz, E. (2010). NLRP3 inflammasomes are required for atherogenesis and activated by cholesterol crystals. *Nature, 464*(7293), 1357-1361. doi:10.1038/nature08938

Dusseaux, M., Martin, E., Serriari, N., Peguillet, I., Premel, V., Louis, D., . . . Lantz, O. (2011). Human MAIT cells are xenobiotic-resistant, tissue-targeted, CD161hi IL-17-secreting T cells. *Blood, 117*(4), 1250-1259. doi:10.1182/blood-2010-08-303339

Duval, C., Thissen, U., Keshtkar, S., Accart, B., Stienstra, R., Boekschoten, M. V., . . . Muller, M. (2010). Adipose tissue dysfunction signals progression of hepatic steatosis towards nonalcoholic steatohepatitis in C57BL/6 mice. *Diabetes, 59*(12), 3181-3191. doi:10.2337/db10-0224

Ebert, R. F., HW. (1939). The extravascular development of the monocyte observed in vivo. *Br. J. Exp. Pathol., 20*, 342-356.

Epelman, S., Lavine, K. J., Beaudin, A. E., Sojka, D. K., Carrero, J. A., Calderon, B., . . . Mann, D. L. (2014). Embryonic and adult-derived resident cardiac macrophages are maintained through distinct mechanisms at steady state and during inflammation. *Immunity, 40*(1), 91-104. doi:10.1016/j.immuni.2013.11.019

Epelman, S., Lavine, K. J., & Randolph, G. J. (2014). Origin and functions of tissue macrophages. *Immunity, 41*(1), 21-35. doi:10.1016/j.immuni.2014.06.013

Ezzelarab, M., Ayares, D., & Cooper, D. K. (2005). Carbohydrates in xenotransplantation. *Immunol Cell Biol, 83*(4), 396-404. doi:10.1111/j.1440-1711.2005.01344.x

Facts and Myths. (2018). *American Transplant Foundation.* Retrieved from https://www.americantransplantfoundation.org/about-transplant/facts-and-myths/

Faulk, D. M., Johnson, S. A., Zhang, L., & Badylak, S. F. (2014). Role of the extracellular matrix in whole organ engineering. *J Cell Physiol, 229*(8), 984-989. doi:10.1002/jcp.24532

Fishman JM, W. K., Wood KJ. (2015). Chapter 8: The Acquired Immune System Response to Biomaterials, Including Both Naturally Occurring and Synthetic Biomaterials. In *Host Response to Biomaterials*.

Fontana, L., Zhao, E., Amir, M., Dong, H., Tanaka, K., & Czaja, M. J. (2013). Aging promotes the development of diet-induced murine steatohepatitis but not steatosis. *Hepatology, 57*(3), 995-1004. doi:10.1002/hep.26099

Frantz, C., Stewart, K. M., & Weaver, V. M. (2010). The extracellular matrix at a glance. *Journal of Cell Science, 123*(24), 4195-4200. doi:10.1242/jcs.023820

Frasca, D., Landin, A. M., Lechner, S. C., Ryan, J. G., Schwartz, R., Riley, R. L., & Blomberg, B. B. (2008). Aging down-regulates the transcription factor E2A, activation-induced cytidine deaminase, and Ig class switch in human B cells. *J Immunol, 180*(8), 5283-5290.

Friedman, S., Sanyal, A., Goodman, Z., Lefebvre, E., Gottwald, M., Fischer, L., & Ratziu, V. (2016). Efficacy and safety study of cenicriviroc for the treatment of non-alcoholic steatohepatitis in adult subjects with liver fibrosis: CENTAUR Phase 2b study design. *Contemp Clin Trials, 47*, 356-365. doi:10.1016/j.cct.2016.02.012

Friedman SL, R. V., Harrison SA, Abdelmalek MF, Aithal GP, Caballeria J, Francque S, Farrell G, Kowdley KV, Craxi A, Simon K, Fischer L, Melchor-Khan L, Vest J, Wiens BL, Vig P, Seyedkazemi S, Goodman Z, Wong VW, Loomba R, Tacke F, Sanyal A, Lefebvre E. (2018). A randomized, placebo-controlled trial of cenicriviroc for treatment of nonalcoholic steatohepatitis with fibrosis. *Hepatology, 67*(5), 1754-1767. doi:10.1002/hep.29477

Frith, J., Day, C. P., Henderson, E., Burt, A. D., & Newton, J. L. (2009). Non-alcoholic fatty liver disease in older people. *Gerontology, 55*(6), 607-613. doi:10.1159/000235677

Fulop, T., Larbi, A., Douziech, N., Fortin, C., Guerard, K. P., Lesur, O., . . . Dupuis, G. (2004). Signal transduction and functional changes in neutrophils with aging. *Aging Cell, 3*(4), 217-226. doi:10.1111/j.1474-9728.2004.00110.x

Galastri, S., Zamara, E., Milani, S., Novo, E., Provenzano, A., Delogu, W., . . . Marra, F. (2012). Lack of CC chemokine ligand 2 differentially affects inflammation and fibrosis according to the genetic background in a murine model of steatohepatitis. *Clin Sci (Lond), 123*(7), 459-471. doi:10.1042/CS20110515

Galili, U. (1993). Evolution and pathophysiology of the human natural anti-alpha-galactosyl IgG (anti-Gal) antibody. *Springer Semin Immunopathol, 15*(2-3), 155-171.

Galili, U., Macher, B. A., Buehler, J., & Shohet, S. B. (1985). Human natural anti-alpha-galactosyl IgG. II. The specific recognition of alpha (1----3)-linked galactose residues. *J Exp Med, 162*(2), 573-582.

Galili, U., Rachmilewitz, E. A., Peleg, A., & Flechner, I. (1984). A unique natural human IgG antibody with anti-alpha-galactosyl specificity. *J Exp Med, 160*(5), 1519-1531.

Galili, U., Shohet, S. B., Kobrin, E., Stults, C. L., & Macher, B. A. (1988). Man, apes, and Old World monkeys differ from other mammals in the expression of alpha-galactosyl epitopes on nucleated cells. *J Biol Chem, 263*(33), 17755-17762.

Gao, B., Jeong, W. I., & Tian, Z. (2008). Liver: An organ with predominant innate immunity. *Hepatology, 47*(2), 729-736. doi:10.1002/hep.22034

Garg, S. K., Delaney, C., Shi, H., & Yung, R. (2014). Changes in adipose tissue macrophages and T cells during aging. *Crit Rev Immunol, 34*(1), 1-14.

Gilbert, T. W., Sellaro, T. L., & Badylak, S. F. (2006). Decellularization of tissues and organs. *Biomaterials, 27*(19), 3675-3683. doi:10.1016/j.biomaterials.2006.02.014

Gilpin, S. E., Guyette, J. P., Gonzalez, G., Ren, X., Asara, J. M., Mathisen, D. J., . . . Ott, H. C. (2014). Perfusion decellularization of human and porcine lungs: bringing the matrix to clinical scale. *J Heart Lung Transplant, 33*(3), 298-308. doi:10.1016/j.healun.2013.10.030

Ginhoux, F., Greter, M., Leboeuf, M., Nandi, S., See, P., Gokhan, S., . . . Merad, M. (2010). Fate mapping analysis reveals that adult microglia derive from primitive macrophages. *Science, 330*(6005), 841-845. doi:10.1126/science.1194637

Gomez Perdiguero, E., Klapproth, K., Schulz, C., Busch, K., Azzoni, E., Crozet, L., . . . Rodewald, H. R. (2015). Tissue-resident macrophages originate from yolk-sac-derived erythro-myeloid progenitors. *Nature, 518*(7540), 547-551. doi:10.1038/nature13989

Gonzalez-Rodriguez, A., Mayoral, R., Agra, N., Valdecantos, M. P., Pardo, V., Miquilena-Colina, M. E., . . . Valverde, A. M. (2014). Impaired autophagic flux is associated with increased endoplasmic reticulum stress during the development of NAFLD. *Cell Death Dis, 5*, e1179. doi:10.1038/cddis.2014.162

Guilliams, M., Ginhoux, F., Jakubzick, C., Naik, S. H., Onai, N., Schraml, B. U., . . . Yona, S. (2014). Dendritic cells, monocytes and macrophages: a unified nomenclature based on ontogeny. *Nat Rev Immunol, 14*(8), 571-578. doi:10.1038/nri3712

Guo, R., Merkel, A. R., Sterling, J. A., Davidson, J. M., & Guelcher, S. A. (2015). Substrate modulus of 3D-printed scaffolds regulates the regenerative response in subcutaneous implants through the macrophage phenotype and Wnt signaling. *Biomaterials, 73*, 85-95. doi:10.1016/j.biomaterials.2015.09.005

Hachim, D., LoPresti, S. T., Yates, C. C., & Brown, B. N. (2017). Shifts in macrophage phenotype at the biomaterial interface via IL-4 eluting coatings are associated with improved implant integration. *Biomaterials, 112*, 95-107. doi:10.1016/j.biomaterials.2016.10.019

Hachim, D., Wang, N., LoPresti, S. T., Stahl, E. C., Rege, R., Umeda, Y., . . . Brown, B. N. (2017). Effects of Aging upon the Host Response to Implants. *J Biomed Mater Res A, In Press.*

Hayflick, L. (1965). The Limited in Vitro Lifetime of Human Diploid Cell Strains. *Exp Cell Res, 37*, 614-636.

Haynes, L., & Lefebvre, J. S. (2011). Age-related Deficiencies in Antigen-Specific CD4 T cell Responses: Lessons from Mouse Models. *Aging Dis, 2*(5), 374-381.

Haynes, L., Linton, P. J., Eaton, S. M., Tonkonogy, S. L., & Swain, S. L. (1999). Interleukin 2, but not other common gamma chain-binding cytokines, can reverse the defect in generation of CD4 effector T cells from naive T cells of aged mice. *J Exp Med, 190*(7), 1013-1024.

Hearps, A. C., Martin, G. E., Angelovich, T. A., Cheng, W. J., Maisa, A., Landay, A. L., . . . Crowe, S. M. (2012). Aging is associated with chronic innate immune activation and dysregulation of monocyte phenotype and function. *Aging Cell, 11*(5), 867-875. doi:10.1111/j.1474-9726.2012.00851.x

Hefendehl, J. K., Neher, J. J., Suhs, R. B., Kohsaka, S., Skodras, A., & Jucker, M. (2014). Homeostatic and injury-induced microglia behavior in the aging brain. *Aging Cell, 13*(1), 60-69. doi:10.1111/acel.12149

Helder, M. R. K., Stoyles, N. J., Tefft, B. J., Hennessy, R. S., Hennessy, R. R. C., Dyer, R., . . . Lerman, A. (2017). Xenoantigenicity of porcine decellularized valves. *J Cardiothorac Surg, 12*(1), 56. doi:10.1186/s13019-017-0621-5

Helmy, K. Y., Katschke, K. J., Jr., Gorgani, N. N., Kljavin, N. M., Elliott, J. M., Diehl, L., . . . van Lookeren Campagne, M. (2006). CRIg: a macrophage complement receptor required for phagocytosis of circulating pathogens. *Cell, 124*(5), 915-927. doi:10.1016/j.cell.2005.12.039

Herrero, C., Sebastian, C., Marques, L., Comalada, M., Xaus, J., Valledor, A. F., . . . Celada, A. (2002). Immunosenescence of macrophages: reduced MHC class II gene expression. *Exp Gerontol, 37*(2-3), 389-394.

Heymann, F., Hammerich, L., Storch, D., Bartneck, M., Huss, S., Russeler, V., . . . Tacke, F. (2012). Hepatic macrophage migration and differentiation critical for liver fibrosis is mediated by the chemokine receptor C-C motif chemokine receptor 8 in mice. *Hepatology, 55*(3), 898-909. doi:10.1002/hep.24764

HHS.gov. (2018). Organ Donation Statistics.

Hilmer, S. N., Cogger, V. C., & Le Couteur, D. G. (2007). Basal activity of Kupffer cells increases with old age. *J Gerontol A Biol Sci Med Sci, 62*(9), 973-978.

Hoeffel, G., Chen, J., Lavin, Y., Low, D., Almeida, F. F., See, P., . . . Ginhoux, F. (2015). C-Myb(+) erythro-myeloid progenitor-derived fetal monocytes give rise to adult tissue-resident macrophages. *Immunity, 42*(4), 665-678. doi:10.1016/j.immuni.2015.03.011

Hoeffel, G., Wang, Y., Greter, M., See, P., Teo, P., Malleret, B., . . . Ginhoux, F. (2012). Adult Langerhans cells derive predominantly from embryonic fetal liver monocytes with a minor contribution of yolk sac-derived macrophages. *J Exp Med, 209*(6), 1167-1181. doi:10.1084/jem.20120340

Hohn, A., & Grune, T. (2013). Lipofuscin: formation, effects and role of macroautophagy. *Redox Biol, 1*, 140-144. doi:10.1016/j.redox.2013.01.006

Holt, M. P., Cheng, L., & Ju, C. (2008). Identification and characterization of infiltrating macrophages in acetaminophen-induced liver injury. *J Leukoc Biol, 84*(6), 1410-1421. doi:10.1189/jlb.0308173

Hu, Z., Ott, P. A., & Wu, C. J. (2018). Towards personalized, tumour-specific, therapeutic vaccines for cancer. *Nat Rev Immunol, 18*(3), 168-182. doi:10.1038/nri.2017.131

Ibrahim, S. H., Hirsova, P., & Gores, G. J. (2018). Non-alcoholic steatohepatitis pathogenesis: sublethal hepatocyte injury as a driver of liver inflammation. *Gut, 67*(5), 963-972. doi:10.1136/gutjnl-2017-315691

Ingersoll, M. A., Spanbroek, R., Lottaz, C., Gautier, E. L., Frankenberger, M., Hoffmann, R., . . . Randolph, G. J. (2010). Comparison of gene expression profiles between human and mouse monocyte subsets. *Blood, 115*(3), e10-19. doi:10.1182/blood-2009-07-235028

Janeway, C. A., Jr. (1992). The immune system evolved to discriminate infectious nonself from noninfectious self. *Immunol Today, 13*(1), 11-16. doi:10.1016/0167-5699(92)90198-G

Jenkins, S. J., Ruckerl, D., Cook, P. C., Jones, L. H., Finkelman, F. D., van Rooijen, N., . . . Allen, J. E. (2011). Local macrophage proliferation, rather than recruitment from the blood, is a signature of TH2 inflammation. *Science, 332*(6035), 1284-1288. doi:10.1126/science.1204351

Jin, C., Frayssinet, P., Pelker, R., Cwirka, D., Hu, B., Vignery, A., . . . Flavell, R. A. (2011). NLRP3 inflammasome plays a critical role in the pathogenesis of hydroxyapatite-associated arthropathy. *Proc Natl Acad Sci U S A, 108*(36), 14867-14872. doi:10.1073/pnas.1111101108

Johnson, K. M., Owen, K., & Witte, P. L. (2002). Aging and developmental transitions in the B cell lineage. *Int Immunol, 14*(11), 1313-1323.

Ju, C., & Tacke, F. (2016). Hepatic macrophages in homeostasis and liver diseases: from pathogenesis to novel therapeutic strategies. *Cell Mol Immunol, 13*(3), 316-327. doi:10.1038/cmi.2015.104

Julier, Z., Park, A. J., Briquez, P. S., & Martino, M. M. (2017). Promoting tissue regeneration by modulating the immune system. *Acta Biomater, 53*, 13-28. doi:10.1016/j.actbio.2017.01.056

Kakinuma, Y., Kimura, T., & Watanabe, Y. (2017). Possible Involvement of Liver Resident Macrophages (Kupffer Cells) in the Pathogenesis of Both Intrahepatic and Extrahepatic Inflammation. *Can J Gastroenterol Hepatol, 2017*, 2896809. doi:10.1155/2017/2896809

Kapetanovic, R., Bokil, N. J., & Sweet, M. J. (2015). Innate immune perturbations, accumulating DAMPs and inflammasome dysregulation: A ticking time bomb in ageing. *Ageing Res Rev, 24*(Pt A), 40-53. doi:10.1016/j.arr.2015.02.005

Kazankov, K., Moller, H. J., Lange, A., Birkebaek, N. H., Holland-Fischer, P., Solvig, J., . . . Gronbaek, H. (2015). The macrophage activation marker sCD163 is associated with changes in NAFLD and metabolic profile during lifestyle intervention in obese children. *Pediatr Obes, 10*(3), 226-233. doi:10.1111/ijpo.252

Keane, T. J., & Badylak, S. F. (2015). The host response to allogeneic and xenogeneic biological scaffold materials. *J Tissue Eng Regen Med, 9*(5), 504-511. doi:10.1002/term.1874

Keane, T. J., Swinehart, I. T., & Badylak, S. F. (2015). Methods of tissue decellularization used for preparation of biologic scaffolds and in vivo relevance. *Methods, 84*, 25-34. doi:10.1016/j.ymeth.2015.03.005

Keeney, M., Waters, H., Barcay, K., Jiang, X., Yao, Z., Pajarinen, J., . . . Yang, F. (2013). Mutant MCP-1 protein delivery from layer-by-layer coatings on orthopedic implants to modulate inflammatory response. *Biomaterials, 34*(38), 10287-10295. doi:10.1016/j.biomaterials.2013.09.028

Kenna, T., Golden-Mason, L., Norris, S., Hegarty, J. E., O'Farrelly, C., & Doherty, D. G. (2004). Distinct subpopulations of gamma delta T cells are present in normal and tumor-bearing human liver. *Clin Immunol, 113*(1), 56-63. doi:10.1016/j.clim.2004.05.003

Kenna, T., Golden-Mason, L., Porcelli, S. A., Koezuka, Y., Hegarty, J. E., O'Farrelly, C., & Doherty, D. G. (2003). NKT cells from normal and tumor-bearing human livers are phenotypically and functionally distinct from murine NKT cells. *J Immunol, 171*(4), 1775-1779.

Khalil, H., Tazi, M., Caution, K., Ahmed, A., Kanneganti, A., Assani, K., . . . Amer, A. O. (2016). Aging is associated with hypermethylation of autophagy genes in macrophages. *Epigenetics, 11*(5), 381-388. doi:10.1080/15592294.2016.1144007

Kim, I. H., Kisseleva, T., & Brenner, D. A. (2015). Aging and liver disease. *Curr Opin Gastroenterol, 31*(3), 184-191. doi:10.1097/MOG.0000000000000176

Kim, M. S., Lim, H. G., & Kim, Y. J. (2016). Calcification of decellularized and alpha-galactosidase-treated bovine pericardial tissue in an alpha-Gal knock-out mouse implantation model: comparison with primate pericardial tissue. *Eur J Cardiothorac Surg, 49*(3), 894-900. doi:10.1093/ejcts/ezv189

Kingham, T. P., Chaudhry, U. I., Plitas, G., Katz, S. C., Raab, J., & DeMatteo, R. P. (2007). Murine liver plasmacytoid dendritic cells become potent immunostimulatory cells after Flt-3 ligand expansion. *Hepatology, 45*(2), 445-454. doi:10.1002/hep.21457

Kinoshita, M., Miyazaki, H., Nakashima, H., Nakashima, M., Nishikawa, M., Ishikiriyama, T., . . . Seki, S. (2017). In vivo Lipopolysaccharide Tolerance Recruits CD11b+ Macrophages to the Liver with Enhanced Bactericidal Activity and Low Tumor Necrosis Factor-Releasing Capability, Resulting in Drastic Resistance to Lethal Septicemia. *J Innate Immun, 9*(5), 493-510. doi:10.1159/000475931

Kinoshita, M., Uchida, T., Sato, A., Nakashima, M., Nakashima, H., Shono, S., . . . Seki, S. (2010). Characterization of two F4/80-positive Kupffer cell subsets by their function and phenotype in mice. *J Hepatol, 53*(5), 903-910. doi:10.1016/j.jhep.2010.04.037

Klein, I., Cornejo, J. C., Polakos, N. K., John, B., Wuensch, S. A., Topham, D. J., . . . Crispe, I. N. (2007). Kupffer cell heterogeneity: functional properties of bone marrow derived and sessile hepatic macrophages. *Blood, 110*(12), 4077-4085. doi:10.1182/blood-2007-02-073841

Klopfleisch, R., & Jung, F. (2016). The pathology of the foreign body reaction against biomaterials. *J Biomed Mater Res A*. doi:10.1002/jbm.a.35958

Klose, C. S., & Artis, D. (2016). Innate lymphoid cells as regulators of immunity, inflammation and tissue homeostasis. *Nat Immunol, 17*(7), 765-774. doi:10.1038/ni.3489

Knolle, P., Schlaak, J., Uhrig, A., Kempf, P., Meyer zum Buschenfelde, K. H., & Gerken, G. (1995). Human Kupffer cells secrete IL-10 in response to lipopolysaccharide (LPS) challenge. *J Hepatol, 22*(2), 226-229.

Knolle, P. A., & Wohlleber, D. (2016). Immunological functions of liver sinusoidal endothelial cells. *Cell Mol Immunol, 13*(3), 347-353. doi:10.1038/cmi.2016.5

Koehler, E. M., Schouten, J. N., Hansen, B. E., van Rooij, F. J., Hofman, A., Stricker, B. H., & Janssen, H. L. (2012). Prevalence and risk factors of non-alcoholic fatty liver disease in the elderly: results from the Rotterdam study. *J Hepatol, 57*(6), 1305-1311. doi:10.1016/j.jhep.2012.07.028

Koh, T. J., & DiPietro, L. A. (2011). Inflammation and wound healing: the role of the macrophage. *Expert Rev Mol Med, 13*, e23. doi:10.1017/S1462399411001943

Kolber-Simonds, D., Lai, L., Watt, S. R., Denaro, M., Arn, S., Augenstein, M. L., . . . Hawley, R. J. (2004). Production of alpha-1,3-galactosyltransferase null pigs by means of nuclear transfer with fibroblasts bearing loss of heterozygosity mutations. *Proc Natl Acad Sci U S A, 101*(19), 7335-7340. doi:10.1073/pnas.0307819101

Konakci, K. Z., Bohle, B., Blumer, R., Hoetzenecker, W., Roth, G., Moser, B., . . . Ankersmit, H. J. (2005). Alpha-Gal on bioprostheses: xenograft immune response in cardiac surgery. *Eur J Clin Invest, 35*(1), 17-23. doi:10.1111/j.1365-2362.2005.01441.x

Kubes, P., & Mehal, W. Z. (2012). Sterile inflammation in the liver. *Gastroenterology, 143*(5), 1158-1172. doi:10.1053/j.gastro.2012.09.008

Kumar, A., Sharma, A., Duseja, A., Das, A., Dhiman, R. K., Chawla, Y. K., . . . Bhansali, A. (2013). Patients with Nonalcoholic Fatty Liver Disease (NAFLD) have Higher Oxidative Stress in Comparison to Chronic Viral Hepatitis. *J Clin Exp Hepatol, 3*(1), 12-18. doi:10.1016/j.jceh.2012.10.009

Kuwaki, K., Tseng, Y. L., Dor, F. J., Shimizu, A., Houser, S. L., Sanderson, T. M., . . . Cooper, D. K. (2005). Heart transplantation in baboons using alpha1,3-galactosyltransferase gene-knockout pigs as donors: initial experience. *Nat Med, 11*(1), 29-31. doi:10.1038/nm1171

Labrie, J. E., 3rd, Sah, A. P., Allman, D. M., Cancro, M. P., & Gerstein, R. M. (2004). Bone marrow microenvironmental changes underlie reduced RAG-mediated recombination and B cell generation in aged mice. *J Exp Med, 200*(4), 411-423. doi:10.1084/jem.20040845

Lanthier, N. (2015). Targeting Kupffer cells in non-alcoholic fatty liver disease/non-alcoholic steatohepatitis: Why and how? *World J Hepatol, 7*(19), 2184-2188. doi:10.4254/wjh.v7.i19.2184

Laria, A., Lurati, A., Marrazza, M., Mazzocchi, D., Re, K. A., & Scarpellini, M. (2016). The macrophages in rheumatic diseases. *J Inflamm Res, 9*, 1-11. doi:10.2147/JIR.S82320

Larsen, R. D., Rivera-Marrero, C. A., Ernst, L. K., Cummings, R. D., & Lowe, J. B. (1990). Frameshift and nonsense mutations in a human genomic sequence homologous to a murine UDP-Gal:beta-D-Gal(1,4)-D-GlcNAc alpha(1,3)-galactosyltransferase cDNA. *J Biol Chem, 265*(12), 7055-7061.

Lavin, Y., Mortha, A., Rahman, A., & Merad, M. (2015). Regulation of macrophage development and function in peripheral tissues. *Nat Rev Immunol, 15*(12), 731-744. doi:10.1038/nri3920

Lavine, K. J., Epelman, S., Uchida, K., Weber, K. J., Nichols, C. G., Schilling, J. D., . . . Mann, D. L. (2014). Distinct macrophage lineages contribute to disparate patterns of cardiac recovery and remodeling in the neonatal and adult heart. *Proc Natl Acad Sci U S A, 111*(45), 16029-16034. doi:10.1073/pnas.1406508111

Leibovich SJ, R. R. (1975). The role of the macrophage in wound repair. A study with hydrocortisone and antimacrophage serum. *Am J Pathol, 78*(1), 71-100.

Lexer, G., Cooper, D. K., Rose, A. G., Wicomb, W. N., Rees, J., Keraan, M., & Du Toit, E. (1986). Hyperacute rejection in a discordant (pig to baboon) cardiac xenograft model. *J Heart Transplant, 5*(6), 411-418.

Li, L., Chen, L., Hu, L., Liu, Y., Sun, H. Y., Tang, J., . . . Wang, H. Y. (2011). Nuclear factor high-mobility group box1 mediating the activation of Toll-like receptor 4 signaling in hepatocytes in the early stage of nonalcoholic fatty liver disease in mice. *Hepatology, 54*(5), 1620-1630. doi:10.1002/hep.24552

Liang, R., Fisher, M., Yang, G., Hall, C., & Woo, S. L. (2011). Alpha1,3-galactosyltransferase knockout does not alter the properties of porcine extracellular matrix bioscaffolds. *Acta Biomater, 7*(4), 1719-1727. doi:10.1016/j.actbio.2011.01.001

Lim, S. Y., Yuzhalin, A. E., Gordon-Weeks, A. N., & Muschel, R. J. (2016). Targeting the CCL2-CCR2 signaling axis in cancer metastasis. *Oncotarget, 7*(19), 28697-28710. doi:10.18632/oncotarget.7376

Linehan, E., Dombrowski, Y., Snoddy, R., Fallon, P. G., Kissenpfennig, A., & Fitzgerald, D. C. (2014). Aging impairs peritoneal but not bone marrow-derived macrophage phagocytosis. *Aging Cell, 13*(4), 699-708. doi:10.1111/acel.12223

Linton, P. J., & Dorshkind, K. (2004). Age-related changes in lymphocyte development and function. *Nat Immunol, 5*(2), 133-139. doi:10.1038/ni1033

Liu, Y., & Cao, X. (2015). The origin and function of tumor-associated macrophages. *Cell Mol Immunol, 12*(1), 1-4. doi:10.1038/cmi.2014.83

Londono, R., & Badylak, S. F. (2015). Biologic scaffolds for regenerative medicine: mechanisms of in vivo remodeling. *Ann Biomed Eng, 43*(3), 577-592. doi:10.1007/s10439-014-1103-8

LoPresti, S. T., & Brown, B. N. (2018). Effect of Source Animal Age upon Macrophage Response to Extracellular Matrix Biomaterials. *J Immunol Regen Med, 1*, 57-66. doi:10.1016/j.regen.2018.03.004

Lynch, H. E., Goldberg, G. L., Chidgey, A., Van den Brink, M. R., Boyd, R., & Sempowski, G. D. (2009). Thymic involution and immune reconstitution. *Trends Immunol, 30*(7), 366-373. doi:10.1016/j.it.2009.04.003

Macher, B. A., & Galili, U. (2008). The Galalpha1,3Galbeta1,4GlcNAc-R (alpha-Gal) epitope: a carbohydrate of unique evolution and clinical relevance. *Biochim Biophys Acta, 1780*(2), 75-88. doi:10.1016/j.bbagen.2007.11.003

Maeso-Diaz, R., Ortega-Ribera, M., Fernandez-Iglesias, A., Hide, D., Munoz, L., Hessheimer, A. J., . . . Gracia-Sancho, J. (2018). Effects of aging on liver microcirculatory function and sinusoidal phenotype. *Aging Cell*, e12829. doi:10.1111/acel.12829

Mahbub, S., Deburghgraeve, C. R., & Kovacs, E. J. (2012). Advanced age impairs macrophage polarization. *J Interferon Cytokine Res, 32*(1), 18-26. doi:10.1089/jir.2011.0058

Malm, T., Koistinaho, M., Muona, A., Magga, J., & Koistinaho, J. (2010). The role and therapeutic potential of monocytic cells in Alzheimer's disease. *Glia, 58*(8), 889-900. doi:10.1002/glia.20973

Mariathasan, S., Weiss, D. S., Newton, K., McBride, J., O'Rourke, K., Roose-Girma, M., . . . Dixit, V. M. (2006). Cryopyrin activates the inflammasome in response to toxins and ATP. *Nature, 440*(7081), 228-232. doi:10.1038/nature04515

Martinez, F. O., & Gordon, S. (2014). The M1 and M2 paradigm of macrophage activation: time for reassessment. *F1000Prime Rep, 6*, 13. doi:10.12703/P6-13

Mass, E., Ballesteros, I., Farlik, M., Halbritter, F., Gunther, P., Crozet, L., . . . Geissmann, F. (2016). Specification of tissue-resident macrophages during organogenesis. *Science, 353*(6304). doi:10.1126/science.aaf4238

McLean, A. J., Cogger, V. C., Chong, G. C., Warren, A., Markus, A. M., Dahlstrom, J. E., & Le Couteur, D. G. (2003). Age-related pseudocapillarization of the human liver. *J Pathol, 200*(1), 112-117. doi:10.1002/path.1328

McPherson, T. B., Liang, H., Record, R. D., & Badylak, S. F. (2000). Galalpha(1,3)Gal epitope in porcine small intestinal submucosa. *Tissue Eng, 6*(3), 233-239. doi:10.1089/10763270050044416

Medzhitov, R., & Janeway, C. A., Jr. (1997). Innate immunity: the virtues of a nonclonal system of recognition. *Cell, 91*(3), 295-298.

Metchnikoff, E. (1891). *Leçons sur la Pathologie Comparée de l'Inflammation Faites*, l'Institut Pasteur.

Michel, S. G., Madariaga, M. L., Villani, V., & Shanmugarajah, K. (2015). Current progress in xenotransplantation and organ bioengineering. *Int J Surg, 13*, 239-244. doi:10.1016/j.ijsu.2014.12.011

Mikolasevic, I., Filipec-Kanizaj, T., Mijic, M., Jakopcic, I., Milic, S., Hrstic, I., . . . Burra, P. (2018). Nonalcoholic fatty liver disease and liver transplantation - Where do we stand? *World J Gastroenterol, 24*(14), 1491-1506. doi:10.3748/wjg.v24.i14.1491

Miller, J. P., & Allman, D. (2003). The decline in B lymphopoiesis in aged mice reflects loss of very early B-lineage precursors. *J Immunol, 171*(5), 2326-2330.

Mills, C. D. (2012). M1 and M2 Macrophages: Oracles of Health and Disease. *Crit Rev Immunol, 32*(6), 463-488.

Mills, C. D., Kincaid, K., Alt, J. M., Heilman, M. J., & Hill, A. M. (2000). M-1/M-2 macrophages and the Th1/Th2 paradigm. *J Immunol, 164*(12), 6166-6173.

Min, H., Montecino-Rodriguez, E., & Dorshkind, K. (2004). Reduction in the developmental potential of intrathymic T cell progenitors with age. *J Immunol, 173*(1), 245-250.

Min, H., Montecino-Rodriguez, E., & Dorshkind, K. (2006). Effects of aging on the common lymphoid progenitor to pro-B cell transition. *J Immunol, 176*(2), 1007-1012.

Miura, K., Yang, L., van Rooijen, N., Ohnishi, H., & Seki, E. (2012). Hepatic recruitment of macrophages promotes nonalcoholic steatohepatitis through CCR2. *Am J Physiol Gastrointest Liver Physiol, 302*(11), G1310-1321. doi:10.1152/ajpgi.00365.2011

Mohamad, M., Mitchell, S. J., Wu, L. E., White, M. Y., Cordwell, S. J., Mach, J., . . . Cogger, V. C. (2016). Ultrastructure of the liver microcirculation influences hepatic and systemic insulin activity and provides a mechanism for age-related insulin resistance. *Aging Cell, 15*(4), 706-715. doi:10.1111/acel.12481

Mokarram, N., Merchant, A., Mukhatyar, V., Patel, G., & Bellamkonda, R. V. (2012). Effect of modulating macrophage phenotype on peripheral nerve repair. *Biomaterials, 33*(34), 8793-8801. doi:10.1016/j.biomaterials.2012.08.050

Montecino-Rodriguez, E., Berent-Maoz, B., & Dorshkind, K. (2013). Causes, consequences, and reversal of immune system aging. *J Clin Invest, 123*(3), 958-965. doi:10.1172/JCI64096

Mossanen, J. C., Krenkel, O., Ergen, C., Govaere, O., Liepelt, A., Puengel, T., . . . Tacke, F. (2016). Chemokine (C-C motif) receptor 2-positive monocytes aggravate the early phase of acetaminophen-induced acute liver injury. *Hepatology, 64*(5), 1667-1682. doi:10.1002/hep.28682

Movita, D., Kreefft, K., Biesta, P., van Oudenaren, A., Leenen, P. J., Janssen, H. L., & Boonstra, A. (2012). Kupffer cells express a unique combination of phenotypic and functional characteristics compared with splenic and peritoneal macrophages. *J Leukoc Biol, 92*(4), 723-733. doi:10.1189/jlb.1111566

Murphy, N., Grehan, B., & Lynch, M. A. (2014). Glial uptake of amyloid beta induces NLRP3 inflammasome formation via cathepsin-dependent degradation of NLRP10. *Neuromolecular Med, 16*(1), 205-215. doi:10.1007/s12017-013-8274-6

Murray, P. J., Allen, J. E., Biswas, S. K., Fisher, E. A., Gilroy, D. W., Goerdt, S., . . . Wynn, T. A. (2014). Macrophage activation and polarization: nomenclature and experimental guidelines. *Immunity, 41*(1), 14-20. doi:10.1016/j.immuni.2014.06.008

Murray, P. J., & Wynn, T. A. (2011). Protective and pathogenic functions of macrophage subsets. *Nat Rev Immunol, 11*(11), 723-737. doi:10.1038/nri3073

Nakashima, H., Nakashima, M., Kinoshita, M., Ikarashi, M., Miyazaki, H., Hanaka, H., . . . Seki, S. (2016). Activation and increase of radio-sensitive CD11b+ recruited Kupffer cells/macrophages in diet-induced steatohepatitis in FGF5 deficient mice. *Sci Rep, 6*, 34466. doi:10.1038/srep34466

Nakashima, H., Ogawa, Y., Shono, S., Kinoshita, M., Nakashima, M., Sato, A., . . . Seki, S. (2013). Activation of CD11b+ Kupffer cells/macrophages as a common cause for exacerbation of TNF/Fas-ligand-dependent hepatitis in hypercholesterolemic mice. *PLoS One, 8*(1), e49339. doi:10.1371/journal.pone.0049339

Nam, J., Choi, S. Y., Sung, S. C., Lim, H. G., Park, S. S., Kim, S. H., & Kim, Y. J. (2012). Changes of the Structural and Biomechanical Properties of the Bovine Pericardium after the Removal of alpha-Gal Epitopes by Decellularization and alpha-Galactosidase Treatment. *Korean J Thorac Cardiovasc Surg, 45*(6), 380-389. doi:10.5090/kjtcs.2012.45.6.380

NCOA. (2015). *Chronic Disease Management*. Retrieved from https://www.ncoa.org/healthy-aging/chronic-disease/.

Nguyen, D. H., Espinoza, J. C., & Taub, D. D. (2004). Cellular cholesterol enrichment impairs T cell activation and chemotaxis. *Mech Ageing Dev, 125*(9), 641-650. doi:10.1016/j.mad.2004.08.002

Nishiyama, K., Nakashima, H., Ikarashi, M., Kinoshita, M., Nakashima, M., Aosasa, S., . . . Yamamoto, J. (2015). Mouse CD11b+Kupffer Cells Recruited from Bone Marrow Accelerate Liver Regeneration after Partial Hepatectomy. *PLoS One, 10*(9), e0136774. doi:10.1371/journal.pone.0136774

Niu, D., Wei, H. J., Lin, L., George, H., Wang, T., Lee, I. H., . . . Yang, L. (2017). Inactivation of porcine endogenous retrovirus in pigs using CRISPR-Cas9. *Science, 357*(6357), 1303-1307. doi:10.1126/science.aan4187

Norris, C. A., He, M., Kang, L. I., Ding, M. Q., Radder, J. E., Haynes, M. M., . . . Mars, W. M. (2014). Synthesis of IL-6 by hepatocytes is a normal response to common hepatic stimuli. *PLoS One, 9*(4), e96053. doi:10.1371/journal.pone.0096053

Noureddin, M., Yates, K. P., Vaughn, I. A., Neuschwander-Tetri, B. A., Sanyal, A. J., McCullough, A., . . . Nash, C. R. N. (2013). Clinical and histological determinants of nonalcoholic steatohepatitis and advanced fibrosis in elderly patients. *Hepatology, 58*(5), 1644-1654. doi:10.1002/hep.26465

Novak, M. L., & Koh, T. J. (2013). Macrophage phenotypes during tissue repair. *J Leukoc Biol, 93*(6), 875-881. doi:10.1189/jlb.1012512

Ogrodnik, M., Miwa, S., Tchkonia, T., Tiniakos, D., Wilson, C. L., Lahat, A., . . . Jurk, D. (2017). Cellular senescence drives age-dependent hepatic steatosis. *Nat Commun, 8*, 15691. doi:10.1038/ncomms15691

Olsson, J., Wikby, A., Johansson, B., Lofgren, S., Nilsson, B. O., & Ferguson, F. G. (2000). Age-related change in peripheral blood T-lymphocyte subpopulations and cytomegalovirus infection in the very old: the Swedish longitudinal OCTO immune study. *Mech Ageing Dev, 121*(1-3), 187-201.

Onyema, O. O., Njemini, R., Forti, L. N., Bautmans, I., Aerts, J. L., De Waele, M., & Mets, T. (2015). Aging-associated subpopulations of human CD8+T-lymphocytes identified by their CD28 and CD57 phenotypes. *Archives of Gerontology and Geriatrics, 61*(3), 494-502. doi:10.1016/j.archger.2015.08.007

Ortman JM, V. V., Hogan H. (2014). An Aging Nation: The Older Population in the United States. *US Census Bureau*.

Ott, H. C., Clippinger, B., Conrad, C., Schuetz, C., Pomerantseva, I., Ikonomou, L., . . . Vacanti, J. P. (2010). Regeneration and orthotopic transplantation of a bioartificial lung. *Nat Med, 16*(8), 927-933. doi:10.1038/nm.2193

Overturf, K., Al-Dhalimy, M., Tanguay, R., Brantly, M., Ou, C. N., Finegold, M., & Grompe, M. (1996). Hepatocytes corrected by gene therapy are selected in vivo in a murine model of hereditary tyrosinaemia type I. *Nat Genet, 12*(3), 266-273. doi:10.1038/ng0396-266

Palikaras, K., Mari, M., Petanidou, B., Pasparaki, A., Filippidis, G., & Tavernarakis, N. (2017). Ectopic fat deposition contributes to age-associated pathology in Caenorhabditis elegans. *J Lipid Res, 58*(1), 72-80. doi:10.1194/jlr.M069385

Park, S., Kim, W. H., Choi, S. Y., & Kim, Y. J. (2009). Removal of alpha-Gal epitopes from porcine aortic valve and pericardium using recombinant human alpha galactosidase A. *J Korean Med Sci, 24*(6), 1126-1131. doi:10.3346/jkms.2009.24.6.1126

Petersen, K. F., Befroy, D., Dufour, S., Dziura, J., Ariyan, C., Rothman, D. L., . . . Shulman, G. I. (2003). Mitochondrial dysfunction in the elderly: possible role in insulin resistance. *Science, 300*(5622), 1140-1142. doi:10.1126/science.1082889

Petersen, T. H., Calle, E. A., Colehour, M. B., & Niklason, L. E. (2011). Bioreactor for the long-term culture of lung tissue. *Cell Transplant, 20*(7), 1117-1126. doi:10.3727/096368910X544933

Petersen, T. H., Calle, E. A., Zhao, L., Lee, E. J., Gui, L., Raredon, M. B., . . . Niklason, L. E. (2010). Tissue-engineered lungs for in vivo implantation. *Science, 329*(5991), 538-541. doi:10.1126/science.1189345

Phelps, C. J., Koike, C., Vaught, T. D., Boone, J., Wells, K. D., Chen, S. H., . . . Ayares, D. L. (2003). Production of alpha 1,3-galactosyltransferase-deficient pigs. *Science, 299*(5605), 411-414. doi:10.1126/science.1078942

Pinto, A. R., Godwin, J. W., Chandran, A., Hersey, L., Ilinykh, A., Debuque, R., . . . Rosenthal, N. A. (2014). Age-related changes in tissue macrophages precede cardiac functional impairment. *Aging (Albany NY), 6*(5), 399-413. doi:10.18632/aging.100669

Platz, J., Bonenfant, N. R., Uhl, F. E., Coffey, A. L., McKnight, T., Parsons, C., . . . Weiss, D. J. (2016). Comparative Decellularization and Recellularization of Wild-Type and Alpha 1,3 Galactosyltransferase Knockout Pig Lungs: A Model for Ex Vivo Xenogeneic Lung Bioengineering and Transplantation. *Tissue Eng Part C Methods, 22*(8), 725-739. doi:10.1089/ten.TEC.2016.0109

Poulose, N., & Raju, R. (2014). Aging and injury: alterations in cellular energetics and organ function. *Aging Dis, 5*(2), 101-108. doi:10.14336/AD.2014.0500101

Puzianowska-Kuznicka, M., Owczarz, M., Wieczorowska-Tobis, K., Nadrowski, P., Chudek, J., Slusarczyk, P., . . . Mossakowska, M. (2016). Interleukin-6 and C-reactive protein, successful aging, and mortality: the PolSenior study. *Immun Ageing, 13*, 21. doi:10.1186/s12979-016-0076-x

Reid, D. T., Reyes, J. L., McDonald, B. A., Vo, T., Reimer, R. A., & Eksteen, B. (2016). Kupffer Cells Undergo Fundamental Changes during the Development of Experimental NASH and Are Critical in Initiating Liver Damage and Inflammation. *PLoS One, 11*(7), e0159524. doi:10.1371/journal.pone.0159524

Rhee, I., Zhong, M. C., Reizis, B., Cheong, C., & Veillette, A. (2014). Control of dendritic cell migration, T cell-dependent immunity, and autoimmunity by protein tyrosine phosphatase PTPN12 expressed in dendritic cells. *Mol Cell Biol, 34*(5), 888-899. doi:10.1128/MCB.01369-13

Robinson, M. W., Harmon, C., & O'Farrelly, C. (2016). Liver immunology and its role in inflammation and homeostasis. *Cell Mol Immunol, 13*(3), 267-276. doi:10.1038/cmi.2016.3

Rose, A. G., Cooper, D. K., Human, P. A., Reichenspurner, H., & Reichart, B. (1991). Histopathology of hyperacute rejection of the heart: experimental and clinical observations in allografts and xenografts. *J Heart Lung Transplant, 10*(2), 223-234.

Rossi, D. J., Bryder, D., Zahn, J. M., Ahlenius, H., Sonu, R., Wagers, A. J., & Weissman, I. L. (2005). Cell intrinsic alterations underlie hematopoietic stem cell aging. *Proc Natl Acad Sci U S A, 102*(26), 9194-9199. doi:10.1073/pnas.0503280102

Rubinsztein, D. C., Marino, G., & Kroemer, G. (2011). Autophagy and Aging. *Cell, 146*(5), 682-695. doi:10.1016/j.cell.2011.07.030

Sadtler, K., Estrellas, K., Allen, B. W., Wolf, M. T., Fan, H., Tam, A. J., . . . Elisseeff, J. H. (2016). Developing a pro-regenerative biomaterial scaffold microenvironment requires T helper 2 cells. *Science, 352*(6283), 366-370. doi:10.1126/science.aad9272

Salminen, A., Kaarniranta, K., & Kauppinen, A. (2012). Inflammaging: disturbed interplay between autophagy and inflammasomes. *Aging (Albany NY), 4*(3), 166-175. doi:10.18632/aging.100444

Sastre, J., Pallardo, F. V., Pla, R., Pellin, A., Juan, G., O'Connor, J. E., . . . Vina, J. (1996). Aging of the liver: age-associated mitochondrial damage in intact hepatocytes. *Hepatology, 24*(5), 1199-1205. doi:10.1002/hep.510240536

Sato, A., Nakashima, H., Nakashima, M., Ikarashi, M., Nishiyama, K., Kinoshita, M., & Seki, S. (2014). Involvement of the TNF and FasL produced by CD11b Kupffer cells/macrophages in CCl4-induced acute hepatic injury. *PLoS One, 9*(3), e92515. doi:10.1371/journal.pone.0092515

Schroder, K., & Tschopp, J. (2010). The inflammasomes. *Cell, 140*(6), 821-832. doi:10.1016/j.cell.2010.01.040

Schulz, C., Gomez Perdiguero, E., Chorro, L., Szabo-Rogers, H., Cagnard, N., Kierdorf, K., . . . Geissmann, F. (2012). A lineage of myeloid cells independent of Myb and hematopoietic stem cells. *Science, 336*(6077), 86-90. doi:10.1126/science.1219179

Scott, C. L., Zheng, F., De Baetselier, P., Martens, L., Saeys, Y., De Prijck, S., . . . Guilliams, M. (2016). Bone marrow-derived monocytes give rise to self-renewing and fully differentiated Kupffer cells. *Nat Commun, 7*, 10321. doi:10.1038/ncomms10321

Sebastián, C., Lloberas, J., & Celada, A. (2009). Molecular and Cellular Aspects of Macrophage Aging. In T. Fulop, C. Franceschi, K. Hirokawa, & G. Pawelec (Eds.), *Handbook on Immunosenescence* (pp. 919-945): Springer Netherlands.

Seidler, S., Zimmermann, H. W., Bartneck, M., Trautwein, C., & Tacke, F. (2010). Age-dependent alterations of monocyte subsets and monocyte-related chemokine pathways in healthy adults. *BMC Immunol, 11*, 30. doi:10.1186/1471-2172-11-30

Seki, E., De Minicis, S., Gwak, G. Y., Kluwe, J., Inokuchi, S., Bursill, C. A., . . . Schwabe, R. F. (2009). CCR1 and CCR5 promote hepatic fibrosis in mice. *J Clin Invest, 119*(7), 1858-1870.

Seki, E., de Minicis, S., Inokuchi, S., Taura, K., Miyai, K., van Rooijen, N., . . . Brenner, D. A. (2009). CCR2 promotes hepatic fibrosis in mice. *Hepatology, 50*(1), 185-197. doi:10.1002/hep.22952

Sheedfar, F., Di Biase, S., Koonen, D., & Vinciguerra, M. (2013). Liver diseases and aging: friends or foes? *Aging Cell, 12*(6), 950-954. doi:10.1111/acel.12128

Sica, A., Erreni, M., Allavena, P., & Porta, C. (2015). Macrophage polarization in pathology. *Cell Mol Life Sci, 72*(21), 4111-4126. doi:10.1007/s00018-015-1995-y

Singh, P., Coskun, Z. Z., Goode, C., Dean, A., Thompson-Snipes, L., & Darlington, G. (2008). Lymphoid neogenesis and immune infiltration in aged liver. *Hepatology, 47*(5), 1680-1690. doi:10.1002/hep.22224

Solana, R., Tarazona, R., Gayoso, I., Lesur, O., Dupuis, G., & Fulop, T. (2012). Innate immunosenescence: effect of aging on cells and receptors of the innate immune system in humans. *Semin Immunol, 24*(5), 331-341. doi:10.1016/j.smim.2012.04.008

Solovjov, D. A., Pluskota, E., & Plow, E. F. (2005). Distinct roles for the alpha and beta subunits in the functions of integrin alphaMbeta2. *J Biol Chem, 280*(2), 1336-1345. doi:10.1074/jbc.M406968200

Song, J. J., Kim, S. S., Liu, Z., Madsen, J. C., Mathisen, D. J., Vacanti, J. P., & Ott, H. C. (2011). Enhanced in vivo function of bioartificial lungs in rats. *Ann Thorac Surg, 92*(3), 998-1005; discussion 1005-1006. doi:10.1016/j.athoracsur.2011.05.018

Spiller, K. L., Nassiri, S., Witherel, C. E., Anfang, R. R., Ng, J., Nakazawa, K. R., . . . Vunjak-Novakovic, G. (2015). Sequential delivery of immunomodulatory cytokines to facilitate the M1-to-M2 transition of macrophages and enhance vascularization of bone scaffolds. *Biomaterials, 37*, 194-207. doi:10.1016/j.biomaterials.2014.10.017

Spiro, R. G., & Bhoyroo, V. D. (1984). Occurrence of alpha-D-galactosyl residues in the thyroglobulins from several species. Localization in the saccharide chains of the complex carbohydrate units. *J Biol Chem, 259*(15), 9858-9866.

Stahl, E. C., & Brown, B. N. (2015). Cell Therapy Strategies to Combat Immunosenescence. *Organogenesis, 11*(4), 159-172. doi:10.1080/15476278.2015.1120046

Stahl, E. C., Haschak, M. J., Popovic, B., & Brown, B. N. (2018). Macrophages in the Aging Liver and Age-Related Liver Disease. *Front Immunol, 9*, 2795. doi:10.3389/fimmu.2018.02795

Steinmann, G. G., Klaus, B., & Muller-Hermelink, H. K. (1985). The involution of the ageing human thymic epithelium is independent of puberty. A morphometric study. *Scand J Immunol, 22*(5), 563-575.

Stephan, R. P., Reilly, C. R., & Witte, P. L. (1998). Impaired ability of bone marrow stromal cells to support B-lymphopoiesis with age. *Blood, 91*(1), 75-88.

Stone, K. R., Abdel-Motal, U. M., Walgenbach, A. W., Turek, T. J., & Galili, U. (2007). Replacement of human anterior cruciate ligaments with pig ligaments: a model for anti-non-gal antibody response in long-term xenotransplantation. *Transplantation, 83*(2), 211-219. doi:10.1097/01.tp.0000250598.29377.13

Stranks, A. J., Hansen, A. L., Panse, I., Mortensen, M., Ferguson, D. J., Puleston, D. J., . . . Simon, A. K. (2015). Autophagy Controls Acquisition of Aging Features in Macrophages. *J Innate Immun, 7*(4), 375-391. doi:10.1159/000370112

Suchy, D., Labuzek, K., Buldak, L., Szkudlapski, D., & Okopien, B. (2014). Comparison of chosen activation markers of human monocytes/macrophages isolated from the peripheral blood of young and elderly volunteers. *Pharmacol Rep, 66*(5), 759-765. doi:10.1016/j.pharep.2014.04.008

Sussman, E. M., Halpin, M. C., Muster, J., Moon, R. T., & Ratner, B. D. (2014). Porous implants modulate healing and induce shifts in local macrophage polarization in the foreign body reaction. *Ann Biomed Eng, 42*(7), 1508-1516. doi:10.1007/s10439-013-0933-0

Sutterwala, F. S., Haasken, S., & Cassel, S. L. (2014). Mechanism of NLRP3 inflammasome activation. *Ann N Y Acad Sci, 1319*, 82-95. doi:10.1111/nyas.12458

Swirski, F. K., Nahrendorf, M., Etzrodt, M., Wildgruber, M., Cortez-Retamozo, V., Panizzi, P., . . . Pittet, M. J. (2009). Identification of splenic reservoir monocytes and their deployment to inflammatory sites. *Science, 325*(5940), 612-616. doi:10.1126/science.1175202

Tacke, F. (2017). Targeting hepatic macrophages to treat liver diseases. *J Hepatol, 66*(6), 1300-1312. doi:10.1016/j.jhep.2017.02.026

Tacke, F., & Zimmermann, H. W. (2014). Macrophage heterogeneity in liver injury and fibrosis. *J Hepatol, 60*(5), 1090-1096. doi:10.1016/j.jhep.2013.12.025

Takano, M., Sugano, N., Mochizuki, S., Koshi, R. N., Narukawa, T. S., Sawamoto, Y., & Ito, K. (2012). Hepatocytes produce tumor necrosis factor-alpha and interleukin-6 in response to Porphyromonas gingivalis. *J Periodontal Res, 47*(1), 89-94. doi:10.1111/j.1600-0765.2011.01408.x

Takeuchi, O., & Akira, S. (2010). Pattern recognition receptors and inflammation. *Cell, 140*(6), 805-820. doi:10.1016/j.cell.2010.01.022

Tchkonia, T., Morbeck, D. E., Von Zglinicki, T., Van Deursen, J., Lustgarten, J., Scrable, H., . . . Kirkland, J. L. (2010). Fat tissue, aging, and cellular senescence. *Aging Cell, 9*(5), 667-684. doi:10.1111/j.1474-9726.2010.00608.x

Thall, A., & Galili, U. (1990). Distribution of Gal alpha 1----3Gal beta 1----4GlcNAc residues on secreted mammalian glycoproteins (thyroglobulin, fibrinogen, and immunoglobulin G) as measured by a sensitive solid-phase radioimmunoassay. *Biochemistry, 29*(16), 3959-3965.

Theurl, I., Hilgendorf, I., Nairz, M., Tymoszuk, P., Haschka, D., Asshoff, M., . . . Swirski, F. K. (2016). On-demand erythrocyte disposal and iron recycling requires transient macrophages in the liver. *Nat Med, 22*(8), 945-951. doi:10.1038/nm.4146

Thevaranjan, N., Puchta, A., Schulz, C., Naidoo, A., Szamosi, J. C., Verschoor, C. P., . . . Bowdish, D. M. E. (2017). Age-Associated Microbial Dysbiosis Promotes Intestinal Permeability, Systemic Inflammation, and Macrophage Dysfunction. *Cell Host Microbe, 21*(4), 455-466 e454. doi:10.1016/j.chom.2017.03.002

Thomson, A. W., & Knolle, P. A. (2010). Antigen-presenting cell function in the tolerogenic liver environment. *Nat Rev Immunol, 10*(11), 753-766. doi:10.1038/nri2858

Tietz, N. W., Shuey, D. F., & Wekstein, D. R. (1992). Laboratory values in fit aging individuals--sexagenarians through centenarians. *Clin Chem, 38*(6), 1167-1185.

Towbin, H., Rosenfelder, G., Wieslander, J., Avila, J. L., Rojas, M., Szarfman, A., . . . Timpl, R. (1987). Circulating antibodies to mouse laminin in Chagas disease, American cutaneous leishmaniasis, and normal individuals recognize terminal galactosyl(alpha 1-3)-galactose epitopes. *J Exp Med, 166*(2), 419-432.

Trepanowski, J. F., Canale, R. E., Marshall, K. E., Kabir, M. M., & Bloomer, R. J. (2011). Impact of caloric and dietary restriction regimens on markers of health and longevity in humans and animals: a summary of available findings. *Nutr J, 10*, 107. doi:10.1186/1475-2891-10-107

Tsou, C. L., Peters, W., Si, Y., Slaymaker, S., Aslanian, A. M., Weisberg, S. P., . . . Charo, I. F. (2007). Critical roles for CCR2 and MCP-3 in monocyte mobilization from bone marrow and recruitment to inflammatory sites. *J Clin Invest, 117*(4), 902-909. doi:10.1172/JCI29919

Urs, S., Smith, C., Campbell, B., Saxton, A. M., Taylor, J., Zhang, B., . . . Moustaid-Moussa, N. (2004). Gene expression profiling in human preadipocytes and adipocytes by microarray analysis. *J Nutr, 134*(4), 762-770. doi:10.1093/jn/134.4.762

van de Laar, L., Saelens, W., De Prijck, S., Martens, L., Scott, C. L., Van Isterdael, G., . . . Guilliams, M. (2016). Yolk Sac Macrophages, Fetal Liver, and Adult Monocytes Can Colonize an Empty Niche and Develop into Functional Tissue-Resident Macrophages. *Immunity, 44*(4), 755-768. doi:10.1016/j.immuni.2016.02.017

van der Geest, K. S. M., Abdulahad, W. H., Tete, S. M., Lorencetti, P. G., Horst, G., Bos, N. A., . . . Boots, A. M. H. (2014). Aging disturbs the balance between effector and regulatory CD4+T cells. *Experimental Gerontology, 60*, 190-196. doi:10.1016/j.exger.2014.11.005

van Duin, D., Mohanty, S., Thomas, V., Ginter, S., Montgomery, R. R., Fikrig, E., . . . Shaw, A. C. (2007). Age-associated defect in human TLR-1/2 function. *J Immunol, 178*(2), 970-975.

van Furth, R., Cohn, Z. A., Hirsch, J. G., Humphrey, J. H., Spector, W. G., & Langevoort, H. L. (1972). The mononuclear phagocyte system: a new classification of macrophages, monocytes, and their precursor cells. *Bull World Health Organ, 46*(6), 845-852.

Verma, S., Tachtatzis, P., Penrhyn-Lowe, S., Scarpini, C., Jurk, D., Von Zglinicki, T., . . . Alexander, G. J. (2012). Sustained telomere length in hepatocytes and cholangiocytes with increasing age in normal liver. *Hepatology, 56*(4), 1510-1520. doi:10.1002/hep.25787

von Leden, R. E., Khayrullina, G., Moritz, K. E., & Byrnes, K. R. (2017). Age exacerbates microglial activation, oxidative stress, inflammatory and NOX2 gene expression, and delays functional recovery in a middle-aged rodent model of spinal cord injury. *J Neuroinflammation, 14*(1), 161. doi:10.1186/s12974-017-0933-3

Wakabayashi, H., Nishiyama, Y., Ushiyama, T., Maeba, T., & Maeta, H. (2002). Evaluation of the effect of age on functioning hepatocyte mass and liver blood flow using liver scintigraphy in preoperative estimations for surgical patients: comparison with CT volumetry. *J Surg Res, 106*(2), 246-253.

Wan, J., Benkdane, M., Teixeira-Clerc, F., Bonnafous, S., Louvet, A., Lafdil, F., . . . Pavoine, C. (2014). M2 Kupffer cells promote M1 Kupffer cell apoptosis: a protective mechanism against alcoholic and nonalcoholic fatty liver disease. *Hepatology, 59*(1), 130-142. doi:10.1002/hep.26607

Wang, G. L., Salisbury, E., Shi, X., Timchenko, L., Medrano, E. E., & Timchenko, N. A. (2008). HDAC1 cooperates with C/EBPalpha in the inhibition of liver proliferation in old mice. *J Biol Chem, 283*(38), 26169-26178. doi:10.1074/jbc.M803544200

Wang, J., & Kubes, P. (2016). A Reservoir of Mature Cavity Macrophages that Can Rapidly Invade Visceral Organs to Affect Tissue Repair. *Cell, 165*(3), 668-678. doi:10.1016/j.cell.2016.03.009

Wang, K., Yao, Y., Zhu, X., Zhang, K., Zhou, F., & Zhu, L. (2017). Amyloid beta induces NLRP3 inflammasome activation in retinal pigment epithelial cells via NADPH oxidase- and mitochondria-dependent ROS production. *J Biochem Mol Toxicol, 31*(6). doi:10.1002/jbt.21887

Wang, L. D., & Wagers, A. J. (2011). Dynamic niches in the origination and differentiation of haematopoietic stem cells. *Nat Rev Mol Cell Biol, 12*(10), 643-655. doi:10.1038/nrm3184

Wang, Y., Wehling-Henricks, M., Samengo, G., & Tidball, J. G. (2015). Increases of M2a macrophages and fibrosis in aging muscle are influenced by bone marrow aging and negatively regulated by muscle-derived nitric oxide. *Aging Cell, 14*(4), 678-688. doi:10.1111/acel.12350

Weng, N. P., Akbar, A. N., & Goronzy, J. (2009). CD28(-) T cells: their role in the age-associated decline of immune function. *Trends Immunol, 30*(7), 306-312. doi:10.1016/j.it.2009.03.013

Wikby, A., Johansson, B., Olsson, J., Lofgren, S., Nilsson, B. O., & Ferguson, F. (2002). Expansions of peripheral blood CD8 T-lymphocyte subpopulations and an association with cytomegalovirus seropositivity in the elderly: the Swedish NONA immune study. *Exp Gerontol, 37*(2-3), 445-453.

Wilhite, T., Ezzelarab, C., Hara, H., Long, C., Ayares, D., Cooper, D. K., & Ezzelarab, M. (2012). The effect of Gal expression on pig cells on the human T-cell xenoresponse. *Xenotransplantation, 19*(1), 56-63. doi:10.1111/j.1399-3089.2011.00691.x

Williams, G. C. (1957). Pleiotropy, Natural Selection, and the Evolution of Senescence. *Evolution, 11*(4), 398-411.

Winkler, S., & Rosen-Wolff, A. (2015). Caspase-1: an integral regulator of innate immunity. *Semin Immunopathol, 37*(4), 419-427. doi:10.1007/s00281-015-0494-4

Wong, C. K., Smith, C. A., Sakamoto, K., Kaminski, N., Koff, J. L., & Goldstein, D. R. (2017). Aging Impairs Alveolar Macrophage Phagocytosis and Increases Influenza-Induced Mortality in Mice. *J Immunol, 199*(3), 1060-1068. doi:10.4049/jimmunol.1700397

Wong, R. J., Aguilar, M., Cheung, R., Perumpail, R. B., Harrison, S. A., Younossi, Z. M., & Ahmed, A. (2015). Nonalcoholic steatohepatitis is the second leading etiology of liver disease among adults awaiting liver transplantation in the United States. *Gastroenterology, 148*(3), 547-555. doi:10.1053/j.gastro.2014.11.039

Wynn, T. A., & Vannella, K. M. (2016). Macrophages in Tissue Repair, Regeneration, and Fibrosis. *Immunity, 44*(3), 450-462. doi:10.1016/j.immuni.2016.02.015

Yamada, K., Yazawa, K., Shimizu, A., Iwanaga, T., Hisashi, Y., Nuhn, M., . . . Sachs, D. H. (2005). Marked prolongation of porcine renal xenograft survival in baboons through the use of alpha1,3-galactosyltransferase gene-knockout donors and the cotransplantation of vascularized thymic tissue. *Nat Med, 11*(1), 32-34. doi:10.1038/nm1172

Yeh, P., Ezzelarab, M., Bovin, N., Hara, H., Long, C., Tomiyama, K., . . . Cooper, D. K. (2010). Investigation of potential carbohydrate antigen targets for human and baboon antibodies. *Xenotransplantation, 17*(3), 197-206. doi:10.1111/j.1399-3089.2010.00579.x

Yeung, O. W., Lo, C. M., Ling, C. C., Qi, X., Geng, W., Li, C. X., . . . Man, K. (2015). Alternatively activated (M2) macrophages promote tumour growth and invasiveness in hepatocellular carcinoma. *J Hepatol, 62*(3), 607-616. doi:10.1016/j.jhep.2014.10.029

Yona, S., Kim, K. W., Wolf, Y., Mildner, A., Varol, D., Breker, M., . . . Jung, S. (2013). Fate mapping reveals origins and dynamics of monocytes and tissue macrophages under homeostasis. *Immunity, 38*(1), 79-91. doi:10.1016/j.immuni.2012.12.001

Younossi, Z. M., Koenig, A. B., Abdelatif, D., Fazel, Y., Henry, L., & Wymer, M. (2016). Global epidemiology of nonalcoholic fatty liver disease-Meta-analytic assessment of prevalence, incidence, and outcomes. *Hepatology, 64*(1), 73-84. doi:10.1002/hep.28431

Zeeh, J., & Platt, D. (2002). The Aging Liver. *Gerontology, 48*(3), 121-127.

Zeng, Z., Surewaard, B. G., Wong, C. H., Geoghegan, J. A., Jenne, C. N., & Kubes, P. (2016). CRIg Functions as a Macrophage Pattern Recognition Receptor to Directly Bind and Capture Blood-Borne Gram-Positive Bacteria. *Cell Host Microbe, 20*(1), 99-106. doi:10.1016/j.chom.2016.06.002

Zhang, X., Han, J., Man, K., Li, X., Du, J., Chu, E. S., . . . Yu, J. (2016). CXC chemokine receptor 3 promotes steatohepatitis in mice through mediating inflammatory cytokines, macrophages and autophagy. *J Hepatol, 64*(1), 160-170. doi:10.1016/j.jhep.2015.09.005

Zhao, L., Lim, S. Y., Gordon-Weeks, A. N., Tapmeier, T. T., Im, J. H., Cao, Y., . . . Muschel, R. J. (2013). Recruitment of a myeloid cell subset (CD11b/Gr1 mid) via CCL2/CCR2 promotes the development of colorectal cancer liver metastasis. *Hepatology, 57*(2), 829-839. doi:10.1002/hep.26094

Zhou, Z., Xu, M. J., & Gao, B. (2016). Hepatocytes: a key cell type for innate immunity. *Cell Mol Immunol, 13*(3), 301-315. doi:10.1038/cmi.2015.97

Zissel, G., Schlaak, M., & Muller-Quernheim, J. (1999). Age-related decrease in accessory cell function of human alveolar macrophages. *J Investig Med, 47*(1), 51-56.